Technische Universität München

Fakultät für Medizin

Neuronal glutamate promotes pancreatic cancer cell migration through neuro-cancer synapses that fuel the GRIN2D-EZH2-E2F1-RB pathway

Lei Ren

Vollständiger Abdruck der von der Fakultät für Medizin der Technischen Universität München zur Erlangung des akademischen Grades eines

Doktors der Medizin

genehmigten Dissertation.

Vorsitzender: Prof. Dr. Lars Mägdefessel

Prüfer der Dissertation:

1. Prof. Dr. Dr. Ihsan Ekin Demir
2. Prof. Dr. Hana Algül

Die Dissertation wurden am 12.01.2022 bei der Technischen Universität München eingereicht und durch die Fakultät für Medizin am 12.07.2022 angenommen.

Table of Contents

1.0 Introduction

1.1 Pancreatic cancer

Pancreatic ductal adenocarcinoma (PDAC), which is also known as pancreatic cancer (PCa), is one of the deadliest common malignancies with a poor outcome[1]. PCa is currently the seventh leading cause of tumor-associated death worldwide[2] and the fourth most common cause in the United States[3] and Germany[4,5], with over 100,000 deaths per year in Europe alone, and is predicted to become the second leading cause of tumor-associated mortality worldwide by 2030[2,6]. Although PDAC-associated morbidity does not rank highly in cancer epidemiology[6], the 5-year overall survival (OS) rate is abysmal at only 9%[3], and in 2018, PDAC caused approximately 432,242 deaths[2], which is almost the highest number found among all cancers[7]. Worldwide, 458,918 new cases of PCa were diagnosed in 2018[8], and the American Cancer Society estimates that 60,430 adults (31,950 men and 28,480 women) in the United States will develop PCa and 48,220 people will die due to PCa in 2021[9]. Furthermore, 355,317 new patients with PCa are estimated to be diagnosed by 2040[8]. Most patients with PDAC exhibit locally advanced or distal metastasis by the time of diagnosis due to the lack of early atypical symptoms at early stages[1], and only a limited number (20% -30%)[10-12] of patients can undergo radical resection at early stages. As a result, obtaining an understanding of the molecular mechanism of local malignant carcinogenesis and distant metastasis is critical, and new treatment strategies are urgently needed.

PDAC originates from pancreatic exocrine cells and accounts for more than 90% of pancreatic neoplasms[13]. At present, the neoplastic precursor lesions of PDAC include pancreatic intraepithelial neoplasia (PanIN), intraductal papillary mucinous neoplasm (IPMN) and mucinous cystic neoplasm (MCN)[14]. As the most common and representative pancreatic precursor lesion, PanIN is found in 82% of invasive pancreatic ductal adenocarcinomas[15],

which indicates that the overwhelming majority of invasive ductal adenocarcinomas evolve through PanIN and can acquire clonal genetic and epigenetic alterations during this process[16]. The genetic alterations in PDAC have been thoroughly characterized[14], and four major mutated driver genes have been identified: the KRAS oncogene[17] and the tumor-suppressor genes CDKN2A[18], TP53[19], and SMAD4[20]. Constant signal transduction of the KRAS oncogene and loss of tumor suppressor genes (CDKN2A, TP53, and SMAD4) results in continuous and uncontrollable cell proliferation, survival and carcinogenesis and promotes the progression of PanIN evolving into PDAC at the primary site[21-25].

Variable risk factors, including being overweight or obese[26], type 2 diabetes[27,28] and history of alcohol and tobacco intake,[29] are well recognized to be associated with the development of PCa[30]. The progression of PanIN, which is a precancerous precursor to the evolution of PCa, has been correlated with fatty infiltration of the pancreas[31]. Obesity-related malignancies, including PCa, exhibit a disproportionate increase among patients aged 25-49 years in the USA[32]. Analogously, the relative carcinogenic risk of developing PCa within one year of a diagnosis of diabetes (5.4-fold) is higher than that among patients with long-term diabetes (1.5-fold)[28], which implies that the onset of diabetes might be a vital risk factor for PCa. Although the genetic uniqueness of tobacco-related PCa compared with other tobacco-related cancers has not been elucidated, the rate of developing PCa among smokers is approximately twice as high as that among nonsmokers[33], and the relative risk among heavy drinkers is also higher than that among individuals with no history of drinking alcohol or among light drinkers ; thus, and tobacco and alcohol are regarded as risk factors for PCa[29]. A healthy lifestyle (which incorporates limited alcohol consumption, never smoking, a standard weight, and regular physical activity) markedly decreases the risk of PCa[34,35]. The typical symptoms of PCa do not usually develop until the tumor is at a locally advanced stage, and these symptoms include abdominal pain that radiates to the back, weight loss or loss of appetite,

jaundice, light-colored stools and dark-colored urine, skin pruritus, diabetes (new diagnosis or uncontrollable diabetes), ascites, nausea, and vomiting. Among these, the most common symptom is weight loss, as has been observed in up to 92% of patients with pancreatic head cancer and almost 100% of pancreatic body and tail cancer cases[36]. Abdominal pain that radiates to the back, which is well known as "mixed type" pain and comprises neuropathic and nociceptive pain[36], is the second most common symptom.

PDAC has the lowest 5-year survival rate[37] and an increasing morbidity among all solid tumors. As such, PDCA is a growing global health problem, and improving the dismal 5-year survival offered by the currently available treatments is a challenge to pancreatologists. This fact highlights the urgent need to develop novel therapeutic strategies to combat this deadly cancer. At present, multidisciplinary combined sequential therapy has become a hot spot in cancer treatment, and PDAC is no exception. The traditionally recommended strategy for any cancer is upfront surgical resection followed by systemic chemotherapy with or without radiation. However, in the multidisciplinary therapy setting, neoadjuvant treatment (NAT) has been of recent interest as an alternative to surgical resection for patients with PDAC. The increasing amount of data demonstrates that NAT for locally advanced PCa (LAPC) and borderline resectable PCa (BRPC) has oncological benefits for not only the biological behavior of the cancer itself but also for creating the opportunity for R0 radical resection, which illustrates the clear role of NAT in the treatment of patients with PDAC. Radical resection remains the preferred method for the treatment of nonmetastatic PDAC, and the other methods include pancreaticoduodenectomy (Whipple procedure), distal pancreatectomy and total pancreatectomy[38]. Therefore, the only method for decreasing cancer-related death remains dependent on early diagnosis and surgical resection combined with systemic chemotherapy, which currently offers the only hope of a cure or long-term survival for patients with PDAC [39,40].

To date, remarkable advantages with respect to the overall survival and R0 resection rate have been observed for patients with PDAC who were administered NAT, and the increase in the use of neoadjuvant immunotherapy in cancer treatment and the obvious advantages of this treatment make NAT a novel regimen for PDAC. However, the optimal drug regimens, the timing of surgery in regard to therapy and whether additional radiotherapy combined with traditional NAT is warranted for relevant patients remain to be defined[41]. Evidence from unremitting research on the mechanism of carcinogenesis and distant metastasis will furnish support and encouragement for the future development of therapeutic strategies that improve the prognosis of PCa.

1.2 Neural invasion (NI) in PCa

As the most common adverse histological characteristic of PCa related to a deteriorated prognosis and enhanced cancer aggressiveness[42-45], NI has been defined as tumorous neuroinvasion by environmental neoplastic cells and/or infiltration into the spaces of the epineurium, perineurium, or endoneurium[44,46], particularly infiltration of the intrapancreatic and extrapancreatic nerves by PCa cells[47]. In these nerves, cancer cells can damage the nerve sheaths during the frequent interactions between PCa cells and nerves and keep the remaining nerves stimulated by inflammatory cells and cancer cells[48,49]. NI appears to occur in up to 100% of patients with PCa and is correlated with local recurrence and neuropathic pain sensation in PCa[43,50 46,51]. The severity of NI has been identified as a pivotal and independent prognostic factor regarding the overall survival of patients with PDAC[50,52-57]. Indeed, the overall survival of patients without NI is two years longer than that of patients with NI[58]. Therefore, understanding the mechanisms of the NI of PCa is absolutely indispensable.

The normal pancreas is innervated by a complex network of two groups of afferent fibers. The first group consists of sensory nerve fiber branches from the dorsal root ganglion (DRG) and the abdominal vagus nerve, and the second group consists of sympathetic nerve fibers derived from the splanchnic nerves, which run through the celiac plexus and reach the lower thoracic segments of the spinal cord via the splanchnic nerves[50,59]. The latter group is well known for stimulating visceral pain. Most nerve afferents mediating pancreatic pain belong to the splanchnic nerves that pass through the coeliac ganglion and enter the thoracic DRG[60,61]. The DRG is found at a hypersensitive state that is subject to modulation from the brainstem over descending facilitation. It has been reported that nerve growth factors (NGFs), as the pathogenetic factors for pain generation, can activate neurogenic inflammation by syncretizing with tropomyosin receptor kinase A (TrkA) and neurotrophin receptor p75 (P75NTR)[48,49], which are related to the incidence of NI[62] and are overexpressed only in PDAC cells and nearby nerves but typically absent in the normal exocrine pancreas[62,63]. Several studies have shown that the nervous system is involved in all stages of PDAC evolution. The normal neural architecture of the pancreas in PCa is transformed into hyperinnervation, and this effect is accompanied by substantial neural hypertrophy[50,64-66]. Neuroglial cells such as Schwann cells emerge around mouse and human PanIN, i.e., during early carcinogenesis[67,68]. The ablation of sensory neurons via neonatal capsaicin injection can impede NI, postpone PanIN development and extend survival in a mouse PDAC model[69]. Moreover, signaling molecules derived from neurons and/or from PCa cells or from the frequent interactions between neurons and cancer cells are indispensable for NI[70]. The neural affinity for PCa is increased by an enhanced level of transforming growth factor-α (TGFα) in neurons near the pancreas and elevated expression of epidermal growth factor receptor (EGFR) in PCa cells[43]. The treatment of DRG neurons with extracts derived from human PDAC tissue and cell lines significantly increases the neuronal branching capacity of DRG neurons[71].

In brief, PCa cells exhibit a strong propensity for NI, the severity of which has been identified as a pivotal and independent prognostic factor for the overall survival of patients with PDAC[50,52-57,72]. NI is also related to advanced cancer recurrence and metastasis and neuropathic pain[73]; the latter is the typical symptom of PCa and clearly reduces a patient's quality of life. Nerve invasion-targeted therapeutic methods are an underlying and compellent strategy for patients with PCa because these strategies can not only prevent cancer invasion and progression but also improve neuropathic pain and thereby a patient's quality of life. Nevertheless, there remains no effective targeted strategy for NI[74].

1.3 L-glutamate and glutamatergic receptors

L-glutamate, the most abundant excitatory neurotransmitter in DRG neurons, is considered a strategic participant in conveying uninjurious irritation as well as nociceptive or neuropathic pain. The L-glutamate concentration in the neuronal cytoplasm is 1–10 mM, whereas that in synaptic vesicles is approximately 100 mM[75], and the estimated intracellular L-glutamate concentration in pancreatic β cells if 1–7 mM[76]. Previous studies have detected the synthetic mechanism and critical mitochondrial enzyme glutaminase (GLS) involved in L-glutamate generation in DRG neurons, particularly small and medium-sized DRG neurons, which exhibit the highest amounts of L-glutamate estimated by immunohistochemistry[77-79]. Furthermore, GLS exhibits enzymatic activity not only in DRG neurons but also in dorsal roots and the sciatic and trigeminal nerves[77].

However, as the ligand and the major physiological agonist for two classes of glutamatergic receptors of either G protein-coupled or ion channels[80,81], L-glutamate has long been associated with cancer[81]. The role of L-glutamate in promoting cancer growth and invasion was first demonstrated in glioma[82]. Subsequently, an increasing number of cancer cells have been demonstrated to secrete L-glutamate[83,84], but the mechanisms and functions

of secreted L-glutamate in cancer cells remain elusive. The tumor-promoting effects of L-glutamate have been attributed to signal transduction through G-protein-coupled L-glutamate receptors[85] or ionotropic receptors (AMPA receptors)[86].

Glutamatergic receptors are classified into two predominant types, namely, metabotropic L-glutamate (mGlu) and ionotropic L-glutamate (iGlu) receptors, which can be endogenously stimulated by L-glutamate. mGlu receptors belong to the superfamily of cell surface G-coupled receptor proteins (GPCRs) composed of seven transmembrane domains[87] and have been subdivided into three major groups, namely, Group I (distinguished by mGlu1 and mGlu5), Group II (mGlu2 and mGlu3) and Group III (mGlu4, mGlu6, mGlu7, and mGlu8), according to the homology of their molecular sequence structure, G-protein coupling, pharmacological and physiological characteristics and ligand selectivity[87]. In line with their electrophysiological properties, sequence homologies and affinity for selective agonists, ionotropic receptors are distinguished into three major subtypes: N-methyl-D-aspartate receptors (NMDARs), α-amino-3-hydroxy-5-methyl-4-isoxazole propionic acid (AMPA) receptors and kainate receptors. NMDARs and AMPA receptors, which participate in synaptic plasticity and transmission, long-term enhancement or inhibition and excitotoxicity, are the dominating ionotropic glutamatergic receptors involved in glutamatergic neurotransmission[88]. Compared with L-glutamate AMPA and kainate receptors, activated NMDARs can induce longer downstream depolarizing responses[89]. The homo or heteromers of AMPA and kainate receptors are assembled from four and five subunits, including GluA1-4 and GluK1-5, respectively[89]. Functional heterotetrameric NMDARs are composed of two obligatory glycine-binding GluN1 subunits and two modulatory L-glutamate-binding GluN2A/2B/2C/2D or glycine-binding GluN3A/3B subunits in some cases[90,91], which are necessary for the opening of ion channels. This fact implies the existence of unique NMDARs among the glutamatergic receptor family due to the requirement for NMDAR activation based on simultaneous binding with L-glutamate and the

coagonist glycine[92,93]. Another peculiarity of NMDARs is that extracellular Mg2+ can block this ion pore, and this blockage could be conquered by mediating depolarization from the activation of AMPA and kainate receptors[92]. The prosurvival and synaptic plasticity pathways are mainly mediated by synaptic NMDARs, whereas L-glutamate excitotoxicity is mostly responsible for extrasynaptic NMDARs[94,95].

The opening kinetics of NMDARs depends on the subunit composition and has a profound impact on downstream signaling pathways. GluN2-containing subunits direct sufficient glutamatergic neurotransmission in a few neurological diseases[96-98]. As the main regulators of the "switch" (open/close) of NMDAR activation[99], the GluN2 subunit is the most commonly considered critical determinant of NMDAR functional heterogeneity[89,96,100-108]. At the embryonic development and synaptic levels, both GluN2B subunits are mainly restricted to the forebrain, and GluN2D subunits mostly found in the mid-brain are widely present in the embryonic brain of rodents[101,102,109]. The expression of the GluN2A subunit is observed from birth and gradually increases, and this increase is accompanied by the evolution from GluN2B-containing NMDARs into GluN2A-containing NMDARs in the central nervous system[100]. GluN2C is scarce[110-112], and its expression begins from the second postnatal week and is mainly concentrated in the cerebellum and the olfactory bulb, which can also undergo developmental switching from GLuN2B-type NMDAR. The GluN2B level is markedly decreased in adults[101] but remains higher than that of GluN2A[113]. GluN2A- and GluN2B-type NMDARs are regarded as the major subunits of functional NMDARs in neurons[106]. GluN2A-type NMDARs mainly reside in synapses and are preferentially responsible for cell survival, whereas GluN2B-containing NMDARs are mainly located in extrasynapses and mediate cell death[114]. Compared with GluN2A- and GluN2B-containing NMDARs, the GluN2C and GluN2D types exhibit relatively slow inactivation dynamics and low signal-channel conductance[89] and display lower affinity for Mg2+ blockade[101,115 116]. These findings have led to the focus on

GluN2A- and/or GluN2B-containing receptors in most previous studies. Moreover, the properties and functions of GluN2D encoded by GRIN2D (located at 19q13.1-qter and containing 1,336 amino acids) have been largely understudied[113]. Based on these unique features, GluN2D-type NMDARs exhibit a stronger affinity for L-glutamate[117-119]. These unique features and biophysical attributes enable GluN2D-containing NMDARs to represent an unparalleled and striking potential target among the GRIN gene family[120].

1.4 Glutamate-NMDAR signaling pathway

1.4.1 Glutamate-NMDAR signaling pathway at the synapse level

The structure of an excitatory synapse comprising presynaptic and postsynaptic neurons communicates through the neurotransmitter L-glutamate[121] (Figure 1), which is trafficked into presynaptic vesicles for exocytosis during synaptic activity by three isoforms of vesicular L-glutamate transporter (vGlut) proteins, vGlut1, vGlut2 and vGlut2[122-125]. Notably, vGlut1 is present mainly in medium- and large-sized DRG neurons, whereas vGlut2 and vGlut3 are preferentially found in small- and medium-sized DRG neurons[126-128]. Unlike vGlut3, which primarily marks neurons that were initially identified as nonglutamatergic[122,129-132], vGlut1 and vGlut2 are more specifically found in glutamatergic neurons[122,129,133]. Currently, vGlut2 is the most universally considered molecular marker for excitatory glutamatergic neurons[122,134,135]. Li *et al*[80]. revealed that the vGlut2 gene is transcriptionally upregulated in cancer cells and that the combination of higher expression levels of GluN2B and vGlut2 indicates a poor prognosis in cancer patients. Synaptobrevin (Syb)/vesicle-associated membrane proteins (VAMPs), which are components of soluble N-ethylmaleimide-sensitive fusion attachment protein receptor (SNARE) complexes and essential for neurotransmitter release, are localized in

synaptic vesicles at nerve terminals[136,137]. Syb1/VAMP1 predominantly localizes in the spinal cord, such as motor neurons and nerve terminals of the neuromuscular junction (NMJ), whereas Syb2/VAMP2 is primarily found in central synapses in the brain[138]. Syb 1, which is an essential membrane component of synaptic vesicles, is involved in exocytosis by bringing synaptic vesicles and the target presynaptic membrane to close proximity and allows their fusion[139-141].

After crossing the synaptic cleft, L-glutamate binds to the ligand-binding domain of GluN2 subunits with the help of postsynaptic density protein 95 (PSD-95), which is the first member to be identified as the main and most abundant scaffold protein in the membrane-associated guanylate kinase (MAGUK) family[142-145]. It has been well established that PSD-95 can anchor and stabilize the surface expression of GluN2-containing NMDARs[146-149] and regulates the interactions between NMDARs and downstream signaling molecules to propagate L-glutamate responses intracellularly by specifically binding its PDZ domains to the C-terminus of GluN2[150]. One study[151,152] revealed the coexpression and strong colocalization between GluN2-containing NMDARs and PSD-95 at the cell surface and at intracellular sites.

1.4.2 Hypothesis

Pancreatic cancer cells can migrate along nerves after they establish intimate contacts with Schwann cells and axons during NI[153-155], but the mechanism of NI is unclear. An increasing number of reports have confirmed that the expression of NMDAR has also been found in various human cancer cell lines[156], such as human small-cell lung cancer[157], ovarian cancer[80], breast cancer[80,158] and prostate cancer[80,159]. Compared with normal tissues, the NMDAR level is elevated in a variety of human cancer tissues of patients with a worsened

prognosis[80]. Immunohistochemistry has demonstrated that all invasive adenocarcinoma and pancreatic neuroendocrine tumors express GluN1 and GluN2B proteins, which are the membrane components of PCa cell lines[160], and human tissue microarrays (TMAs) have shown higher expression of GluN2B in PDAC[80]. Based on the approximately 100% prevalence of NI in PCa and due above-mentioned release of L-glutamate, the autocrine secretion of the excitatory neurotransmitter L-glutamate from an increasing number of cancer cells stimulates NMDAR activity to induce tumor invasion and growth by enhancing GluN2-mediated glutamate-NMDAR signaling[80,161]. Nevertheless, the autocrine secretion of L-glutamate is not sufficient to explain the specific induction of GluN2-NMDAR signaling[161]. Recent studies have shown that the central nervous system[162], glioma cells[162,163] or metastatic breast cancer cells[161] can form pseudotripartite synapses with neuron synapses to fuel themselves with L-glutamate in a manner similar to that found with an excitatory synapse structure (Figure 1).

We hypothesized that this glutamate-NMDA axis and pseudotripartite synapses may also be involved in the frequent interaction of PCa cells with peripheral neurons during NI.

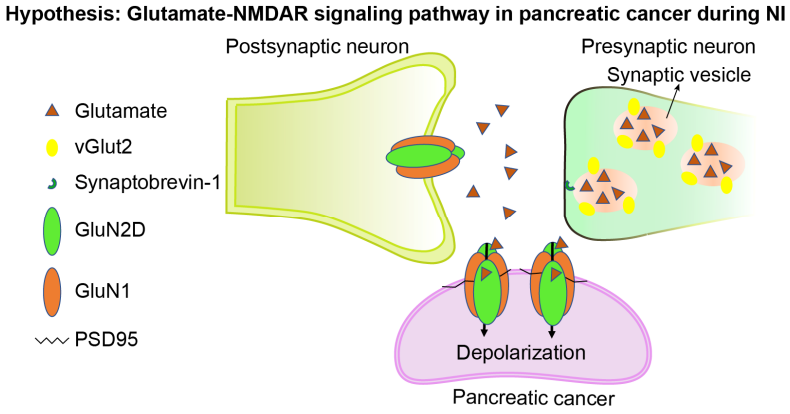

Figure 1. Hypothesis of pseudo-tripartite synapses established by pancreatic cancer cells and intrapancreatic neuronal endings. The tripartite synapse composed of pre- and post-synaptic neurons (above) and pancreatic cancer cells (below) provide the fuel of L-glutamate ligand, activating GluN2D-NMDAR signaling to stimulate tumor growth in vivo.

2.0 Aims of the present study

Glutamate, which is mainly present in DRG neurons, might stimulate NMDAR activity in cancer cells to induce tumor invasion and growth through the glutamate-NMDAR signaling pathway. Indeed, a somewhat similar mechanism has been detected in glioma cells and metastatic breast cancer cells, which can form pseudotripartite synapses with neuron synapses to fuel themselves with L-glutamate. However, this glutamate-NMDAR axis and pseudotripartite synapses might also be involved in the frequent interaction of PCa cells with peripheral neurons. This phenomenon has not yet been analyzed in NI in PCa. GluN2D-containing NMDARs present an unparalleled and striking potential target among the GRIN gene family due to their unique features and biophysical attributes. Furthermore, only a few studies have provided evidence regarding GluN2D-mediated glutamate-NMDAR signaling in NI in PCa. Here, we sought to ascertain whether GluN2D-containing NMDARs and their ligand, L-glutamate, might be involved in neuroinvasion and/or invasive growth in PCa. To investigate the regulation and mechanistic functions of GluN2D-mediated glutamate-NMDAR signaling in PCa, the potential translational relevance to PCa appears to be particularly substantial.

Therefore, the first aim of the present study was to investigate the target genes of glutamatergic receptors that might be involved in NI in PCa. For this purpose, a bioinformatics analysis of PCa tissues and cells from The Cancer Genome Atlas (TCGA) and Cancer Cell Line Encyclopedia (CCLE), respectively, was performed. Glutamatergic receptor-associated genes were compared between PCa and normal pancreas tissues, and these comparisons included the relevant clinical biological characteristics; the distribution of the expression of these genes in neuroinvasive and non-neuroinvasive cancer cells was confirmed by real-time PCR.

The second aim of the study was to illustrate the correlation between L-glutamate and GluN2D (encoded by GRIN2D). For this purpose, cancer cells were treated with different

concentrations of L-glutamate, and the expression levels of GluN2D-containing NMDARs in neuroinvasive and non-neuroinvasive PDAC cells were then verified by real-time PCR and western blotting. We subsequently sought to elucidate GluN2D-mediated phenotypic features of these two types of PCa cells. To this end, PCa cells were pretreated with receptor antagonist or siRNA interference and then stimulated or chemoattracted with L-glutamate or DRG-conditioned medium (CM). The proliferation, migration and invasion of the cells were determined through cell viability, wound healing and Transwell assays, respectively.

The third aim of the study was to investigate the L-glutamate level of DRG neurons and cancer cells and to ascertain the potential signaling molecules involved in the glutamate-NMDAR signaling pathway. For this purpose, the correlation of the signaling molecules belonging to the glutamate-NMDAR signaling pathway in PCa tissues was checked by bioinformatic analysis and further confirmed by immunohistochemistry. Western blotting was performed in PCa cells, which included monocultured cells, cells cocultured with DRG neurons and cells pretreated with GRIN2D siRNA and GluN2D antagonist and then stimulated with L-glutamate.

3.0 Materials and Methods

3.1 Materials

3.1.1 List of the antibodies

Primary antibodies

Antibody	Catalogue number	Application	Source
Rabbit anti-vGlut-2 Ab	135403	WB(1:1000),IHC(1:200), ICC(1:400)	synaptic systems
Rabbit anti-PSD95 Ab	ab18258	WB(1:1000),IHC(1:250), ICC(1:250)	abcam
Rabbit anti-synaptobrevin-1 Ab	104002	WB(1:1000), IHC(1:200), ICC(1:200)	synaptic systems
Rabbit anti-GluN1	PA3-102	WB(1:1000), IHC(1:200), ICC(1:200)	Thermo Fisher
Rabbit anti-GluN2D Ab	PA5-101608	WB(1:1000), IHC(1:200), ICC(1:200)	Thermo Fisher
Rabbit anti-PGP9.5 Ab	Z5116	IF(1:200)	Dako Deutschland GmbH
Rabbit anti-S100 mAb (EP1576Y)	Ab52642	, IHC(1:200)	Abcam
Mouse anti-Cytokeratin Pan Ab	MA5-13203	ICC(1:200), IF(1:200)	Thermo Fisher
Mouse anti-GAPDH Ab	SC-32233	WB(1:1000)	Santa Cruz Biotechnology
Mouse anti-Beta-Tubulin Ab	sc-5274	WB(1:1000)	Santa Cruz Biotechnology
Ezh2 (D2C9) XP® Rabbit mAb	5246s	WB(1:1000), ICC(1:200), ChIP (1:100)	Cell signaling
Tri-Methyl-Histone H3 (Lys27) (C36B11) Rabbit mAb	9733s	WB(1:1000)	Cell signaling
Acetyl-Histone H3 (Lys27) (D5E4) XP® Rabbit mAb	8173s	WB(1:1000)	Cell signaling
Anti-E2F-1 Antibody	05-379	WB(1:1000)	Upstate
Anti-E2F-1 Antibody	3742s	ChIP (1:100)	Cell signaling
Retinoblastoma (Rb) antibody	554136	WB(1:1000)	BD Pharmingen™
cyclin D1 antibody	sc-8396	WB(1:1000)	Santa Cruz

CDKN2A / p16INK4a antibody	sc-1207	WB(1:1000)	Santa Cruz
CDK4	sc-23896	WB(1:1000)	Santa Cruz
Phospho-Rb (Ser807/811) (D20B12) XP® Rabbit mAb	8516S	WB(1:1000)	Cell signaling
Phospho-Rb (Ser780) (D59B7) Rabbit mAb	8180S	WB(1:1000)	Cell signaling

Secondary antibodies

Antibody	**Catalogue number**	**Application**	**Source**
Alexa Fluor goat anti-mouse IgG 594	1830459	IF(1:200)	Thermo Fisher Scientific
Horseradish peroxidase - Labelled Polymer Goat Anti-Mouse Ab	K4000	IHC	Dako Deutschland GmbH
Alexa Fluor goat anti-rabbit IgG 488	1885240	IF(1:200)	Thermo Fisher Scientific
Horseradish peroxidase - Labelled Polymer Goat Anti-Rabbit Ab	K4003	IHC	Dako Deutschland GmbH
ECL anti-mouse IgG peroxidase-linked antibody	NA931V	WB(1:2500)	GE Healthcare Life Sciences
ECL anti-rabbit IgG peroxidase-linked antibody	NA9340V	WB(1:2500)	GE Healthcare Life Sciences

3.1.2 Chemicals and Reagents

Chemical/Reagent	**Product number**	**Source**
Albumin Fraction V (BSA)	T844.3	Carl Roth GmbH
Ammonium persulfate (APS)	9592.1	Carl Roth GmbH
Citric acid (Monohydrate)	3958.4	Carl Roth GmbH
B-27 Supplement (50x)	1116531	Gibco
BCA protein assay	23225	Thermo Fisher Scientific

ECL Plus Western Blotting substrate	32132	Thermo Fisher Scientific
Extracellular matrix (ECM) gel	E1270	Sigma-Aldrich Chemie GmbH
Glycine	3908.3	Carl Roth GmbH
Collagenase type II	LS004176	Worthington Biochemicals
EGF	17005042	Invitrogen
Ethanol 70%	7078027	Otto Fischer GmbH
Ethanol 96%	7138032	Otto Fischer GmbH
Ethanol absolute	7127114	Otto Fischer GmbH
Ethanol absolute	64-17-5	Merck KGaA
Dulbecco's Phosphate Buffered Saline	D8537	Sigma
Fetal Bovine Serum	F7524	Sigma-Aldrich Chemie GmbH
GluN2D NMDAR antagonist UBP145	HB4717	Hellobio
formaldehyde		Carl Roth GmbH
HEPES solution	H0887	Sigma-Aldrich Chemie GmbH
Fluorescence Mounting Medium	S3023	Dako Deutschland GmbH
KAPA SYBR® FAST Kit for LightCycler® 480	KK4611	Sigma (Rothe)
Hank’s BSS	H15-010	PAA
Methanol	4627.5	Carl Roth GmbH
Nuclease-Free water	2004098	Invitrogen
13mm round coverslip	1-6284	Neolab
hydrogen peroxide 30 %	9681.1	Carl Roth GmbH
Keratinocyte SFM	17005042	Invitrogen
L-Glutamine solution	G7513	Sigma-Aldrich Chemie GmbH
Matrigel	356231	CORNING

DAPI	ab228549	Abcam
L-glutamate	ab120049	Abcam
Natriumchlorid (NaCl)	3957.2	Carl Roth GmbH
Milk	T145.3	Carl Roth GmbH
Crystal Violet	C0775	Sigma-Aldrich
Normal goat serum	50062Z	Life technologies
Neurobasal medium	21103	Gibco
KPL Biotinylated antibody goat anti-mouse IgG	10247762	Sera Care
Minimum Essential medium Eagle (MEM) media	M2279	Sigma-Aldrich Chemie GmbH
Mitomycin C	M4287	Sigma-Aldrich
RIPA buffer	R0278	Sigma-Aldrich Chemie GmbH
KPL Streptavidin/Phosphatase Reagent	140375	Sera Care
Penicillin-Streptomycin	P0781	Sigma-Aldrich Chemie GmbH
PBS Dulbecco	L182-50	Biochrom GmbH
Roticlear	A538.1	Carl Roth GmbH
Rotiphorese Gel 30	3029.1	Carl Roth GmbH
phosphatase inhibitor	4906837001	Sigma-Aldrich Chemie GmbH
protease inhibitor	4693159001	Sigma-Aldrich Chemie GmbH
SDS, ultra-pure	2326.2	Carl Roth GmbH
LDS sample buffer (4X)	2197595	Invitrogen
Sample Reducing Agent (10X)	2032941	Invitrogen
Dulbecco′s Modified Eagle′s Medium (500 ml)	D5671-500ML	Sigma
Dulbecco′s Modified Eagle′s Medium	D5796-500ML	Sigma

RPMI-1640 Medium	R8758	Sigma-Aldrich Chemie GmbH
Transfer Membrane 0.2 µm	ISEQ00010	Merck Millipore
Tris base	T1503	Sigma-Aldrich Chemie GmbH
TEMED	2367.3	Carl Roth GmbH
Super Signal West Pico PLUS Chemiluminescent Substrate	34577	Thermo Fisher Scientific
Culture-insert 2 well	81176	Ibidi
Triton X 100	3051.2	Carl Roth GmbH
Trypsin-EDTA solution	T3924	Sigma-Aldrich Chemie GmbH
Tris-HCl	T3253	Sigma-Aldrich Chemie GmbH
Cell Culture Insert (8 µm)	353097	FALCON
ε-aminocaproic acid	7260	Sigma-Aldrich Chemie GmbH
Opti-MEM™ I Reduced Serum Medium	31985070	Thermo Fisher Scientific
Tween 20	9127.2	Carl Roth GmbH
VectaMount Permanent Mounting Medium	H-5000	Vector
Lipofectamine™ RNAiMAX Transfection Reagent	13778075	Thermo Fisher Scientific

3.1.3 Buffers and Solutions

Immunohistochemistry

10x Tris Buffered Saline (TBS)

Distilled Water	800 mL
NaCl	85 g
Tris base	24.2 g
Adjust pH to 7.4 with	5 M HCl

Constant volume with distilled water to	1000 mL

20x Citrate buffer

Citric acid (Monohydrate)	21 g
Distilled Water	300 mL
Adjust pH to 7.4 with	5 M NaOH
Constant volume with distilled water to	500 mL

Washing Buffer (1x TBST)

10x TBS	100 mL
Tween 20	1 mL
Constant volume with distilled water to	1000 mL

Washing Buffer (1x PBST)

PBS	9.55 g
Tween 20	1 mL
Constant volume with distilled water to	1000 mL

Western Blotting

Electrophoresis buffer (10x)

Tris base	30.3 g
Glycine	144 g
SDS	10g
Constant volume with distilled water to	1000 mL

Lower Tris buffer (4x)

Tris-HCl	181.5 g
SDS	4 g

Check pH 8.8	
Constant volume with distilled water to	1000 mL

Upper Tris buffer (4x)

Tris-HCl	60.5 g
SDS	4 g
Check pH 6.8	
Constant volume with distilled water to	1000 mL

10% APS

APS	10 g
Constant volume with distilled water to	100 mL

Anode buffer I

Tris base	36.3 g
Methanol	200 mL
Constant volume with distilled water to	1000 mL

Anode buffer II

Tris base	3.03 g
Methanol	200 mL
Constant volume with distilled water to	1000 mL

Cathode buffer

Tris base	3.03 g
Methanol	200 mL
ε-aminocaproic acid	5.24 g
Constant volume with distilled water to	1000 mL

Washing Buffer (1x TBST)

10x TBS	100 mL
Tween 20	1 mL
Constant volume with distilled water to	1000 mL

Blocking Buffer (1x TBST)

Dry milk or BSA	0.5 g
Washing buffer	10 mL

3.1.4 Kits

L-glutamate assay Kit (MAK004)	Sigma-Aldrich Chemie GmbH
siPOOL-5 Kit (2146 – EZH2 human))	SiTOOLs BIOTECH
siPOOL-5 Kit (2906 - Grin2d human)	SiTOOLs BIOTECH
siPOOL-5 Kit (1869 – E2F-1 human)	SiTOOLs BIOTECH
RNeasy plus mini Kit (250)	QIAGEN
High-Capacity cDNA Reverse Transcription Kit	Thermo Fisher Scientific
RQ1 RNase-Free DNase (M6101)	Promega
HistoMark RED Phosphatase Substrate Kit (5510-0036)	Insight Biotechnology
Pierce™ Magnetic ChIP Kit (26157)	Thermo Fisher Scientific
NE-PER™ Nuclear and Cytoplasmic Extraction Reagents (78835)	Thermo Fisher Scientific
Pacific Blue™ Annexin V/SYTOX™ AADvanced™ Apoptosis Kit, for flow cytometry (A35136)	Thermo Fisher Scientific

3.1.5 Laboratory equipment

Accumax	Sigma-Aldrich Chemie GmbH
PH-meter	BECKMAN (Washington, DC, USA)
Balance	SCAL TEC SBC 52
Microscopes	Olympus IX50 inverse microscope and Zeiss Axioplan 2
Centrifuge	Eppendorf
Water bath	Lauda ecocline RE 104, MEDAX
Refrigerator 4℃	
Freezer -20℃	
Freezer -80℃	Heraeus
Shaker	IKA-Shaker MTS 4
Glass coverslips	Plano
Power supple	Bio RAD MODLL 200/2.0
Magnetic mixer	IKA-COMBIMAG RET
Vortex Mixer	
Stereomicroscope	Zeiss Stemi 2000
Tissue embedding machine	Leica
Tissue processor	Leica
Imaging software	Olympus analysis software and Zeiss KS300 program
Microtome	Leica JUNG RM2055
X-ray films	Hyperfilm, Amersham Bioscience
Photometer	Thermo-Labsystem Opsys MR

3.2 Methods

3.2.1 Cell culture

PCa cell lines such as Su.86.86, Panc-1 and Capan-1 were purchased from American Type Culture Collection (ATCC), and T3M4 was a kind gift from Dr. Metzgar (Durham, North Carolina, USA). According to the supplier's recommendations, all PCa cell lines were maintained in DMEM (Sigma) with 10% FCS and 4.0 mM L-glutamine. Mouse primary DRG neurons were cultured in neurobasal medium with 10% FCS, 2% B27 (Gibco) and 0.5 mM L-glutamine. All cells were routinely confirmed to be negative for mycoplasma and cultured at 37ºC in a humidified atmosphere consisting of 95% air and 5% CO2. For the L-glutamate and DRG CM treatment experiment, $3x10^5$ PCa cells were seeded into a 6-well plate in DMEM with 10% FCS and 4.0 mM L-glutamine. Forty-eight hours later, the cells were washed with Dulbecco's phosphate-buffered saline. The cells were starved overnight in glutamine- and serum-free medium, stimulated with different concentrations of L-glutamate and glycine or DRG CM for 48 hours, and harvested for western blotting and quantitative real-time PCR assays.

3.2.2 Isolation of primary DRG neurons and coculture with cancer cells

Primary DRG neurons were isolated as described previously[164] from the lumbar spinal region of 3- to 14-day-old newborn C57BL/6 mice after anterior laminectomy, and the neurons were maintained in a Petri dish with serum-free MEM placed on ice. After removing the roots under microscopy, the DRG neurons were collected into microtubes, and after collagenase type II (100 µl of 10X collagenase + 900 µl of Hanks' BSS), the microtubes were incubated for 30 minutes at 37ºC in an atmosphere with 5% CO2 to digest the DRG. Syringe needles were then used to mince the DRG. Primary DRG neurons ($4x10^5$) were seeded in 13-mm glass coverslips preplaced in 24-well plates after sterilization with 70% ethanol or one well of 6-well

plates precoated with poly-D-lysine (Sigma, P6407). Once the primary neurons reached ~95% confluence (7~10 days after seeding), cancer cells were added to the primary neuron culture. After coculturing for 2 days, the cells were harvested in 6-well plates for western blotting and real-time PCR, and immunocytochemical staining was performed in 24-well plates.

3.2.3 Treatment of the supernatant of DRG neurons

The obtained primary DRG neurons were seeded in 10-cm plates precoated with poly-D-lysine hydrobromide (4 μg/mm^2) and cultured in neurobasal medium with 10% FCS, 2% B27 (Gibco) and 0.5 mM L-glutamine. Once the primary neurons reached 70-80% confluence, the fresh and serum-free medium was changed, and 48 hours later, the supernatants were collected, centrifuged and stored at -80°C for measurement of the level of L-glutamate. The cells were seeded in 6-well plates and serum-starved overnight; the cells in the control group were then treated with L-glutamate-free DMEM medium, and the cells in the experimental group were treated with the concentration of L-glutamate in the DRG neuron supernatant for 48 hours. Harvested cells were used for western blotting and real-time PCR.

3.2.4 Western blotting

Cells were washed three times with precooled DPBS, lysed for 15 minutes on ice in RIPA lysis buffer containing protease inhibitor (EDTA-free) and phosphatase inhibitor (PhosSTOP), scrubbed and sonicated to remove the cell debris, and the total protein concentrations were detected using a BCA protein assay kit. Twenty micrograms of protein in the sample was diluted to the same volume with loading dye (4X LDS sample buffer and 10X Sample Reducing Agent) and distilled water, boiled for 5 minutes at 95°C and cooled on ice. The proteins were electrophoretically fractionated by 10% SDS–PAGE and then transferred to nitrocellulose membranes. The membranes were blocked with 5% BSA in TBST buffer for 1 hour, incubated with the primary antibody overnight at 4ºC, washed with TBST buffer, and incubated with the

secondary antibodies for 1 hour at room temperature. Visualization of the membrane was then performed with ECL Plus western blotting substrate. ImageJ was used to measure the density of the target bands.

3.2.5 Immunohistochemical and immunofluorescent staining

Harvested human tissues were fixed in 4% paraformaldehyde overnight and embedded in paraffin, and 3-μm paraffin sections were prepared using a microtome. The sections were deparaffinized three times with Roticlear® and rehydrated in different concentrations of ethanol. Antigen retrieval was performed with citrate buffer (pH 6.0) and heat for 20 minutes. After treatment with 3% hydrogen peroxide in methanol, the sections were blocked with 10% normal goat serum for 1 hour at room temperature, incubated with the primary antibody overnight at 4ºC, washed three times with TBST and then incubated with the secondary antibody (Dako) for 1 hour at room temperature. Dako Liquid DAB and Substrate Chromogen System were used for the color reaction. In the immunofluorescence analysis, Alexa Fluor goat IgG was used as the secondary antibody.

For double staining, the cells were first incubated with anti S100 antibody overnight at 4ºC. On the following day, color reactions were performed using the DAB and Substrate Chromogen System and then blocked with 10% normal goat serum, and the cells were then incubated with the other primary antibody overnight 4ºC. On the third day, the cells were incubated with KPL biotinylated antibody for 1 hour, and KPL Streptavidin/Phosphatase Reagent and HistoMark RED Phosphatase Substrate were then used for color reactions.

3.2.6 Immunocytochemical staining

For immunocytochemical staining, the cells were washed three times with TBST, fixed with 4% paraformaldehyde for 15 minutes, blocked with 10% normal goat serum for 1 hour, and then incubated with the primary antibody overnight at 4ºC. Afterward, the coverslips were

incubated with Alexa Fluor goat IgG secondary antibody and DAPI for 1 hour at room temperature. After washing, 13-mm coverslips were removed from the 24-well plates and mounted on slides with fluorescence mounting medium.

3.2.7 Cell proliferation assay

Cell viability assays were performed in a 96-well plate. The cells were starved in medium without serum and glutamine overnight, and 5000 cells/well were seeded in triplicate and grown for 24 hours at 37°C in a humidified atmosphere with 5% CO_2. The cells were then exposed to L-glutamate at concentrations of 0, 0.125, 0.25, 0.5, 0.75, 1.0, 1.25, 1.5, 2.5, 5.0, 7.5, and 10.0 µM or 0.2 µM glycine[89] and the GluN2D antagonist UBP145 at concentrations of 0, 0.01, 0.1, 1.0, 10.0, 100, 500, and 1000 µM for 48 hours. Ten microliters of 3-(4,5-dimethyl-2-thiazolyl)-2,5-diphenyl-2H-tetrazolium bromide (MTT, 5 µg/µl in PBS) was added to the wells, and the plate was incubated for 4 hours at 37°C in the presence of 5% CO_2. After incubation for 15 minutes on a shaker wrapped in aluminum foil, the medium from each well was removed, 100 µl of DMSO was added to each well to dissolve the MTT, and the absorbance at a wavelength of 570 nm was measured by spectrophotometry.

3.2.8 Cell invasion assay

Cell invasion assays were performed in Transwell chamber with an 8-µm membrane and 24-well plates. The upper side of the membrane was coated with 60 µl of Matrigel (1:3, 3.33 mg/ml). The cells were starved overnight in glutamine- and serum-free medium, resuspended in FCS-free and trypsin-free medium and counted; subsequently, 50000 cells were seeded into the upper compartment with 100 µl of FCS-free medium, and the lower compartments were filled with 700 µl of medium containing 10% FCS and 0.5 µM L-glutamate and DRG CM. For the cell invasion assay with UBP145, the cells were pretreated for 30 minutes with UBP145 and then seeded; DMSO (1:10.000) was used as an appropriate control. Twenty-four hours

after treatment, the cells were gently scraped twice to remove the soaking media and Matrigel from the upper side of the porous polycarbonate membrane using cotton swabs. The invaded cells were fixed with ice-cold MeOH for 10 minutes at room temperature, stained with crystal violet for 30 minutes, imaged, and then merged in glacial acetic acid with shaking for 5 minutes. The absorbance at a wavelength of 570 nm was measured by spectrophotometry.

3.2.9 Cell migration assay

The cells (10^6) were starved overnight in glutamine- and serum-free medium, seeded into each well of the Culture-Insert 2 Well (ibidi) and incubated at 37°C for 24 hours with and 5% CO2 to obtain a confluent cell layer. After treatment with mitomycin C for at least 2 hours, the Culture-Insert 2 Well was gently removed with sterile tweezers. For the cell migration assay with UBP145, the cells were treated for 30 minutes with UBP145 after removal of the Culture-Insert 2 Well, and DMSO (1:10.000) was used as an appropriate control. The fresh medium was then changed to 0.5 µl of L-glutamate or DRG CM containing 0.5 µM L-glutamate, and images were obtained after 24 hours.

3.2.10 RNA isolation and reverse transcription

The isolate of RNA was performed with the RNeasy plus mini kit (Qiagen) according to the recommended procedure. After three washes with DPBS, an appropriate volume of RLT Plus Buffer was added to harvest the cell lysates, and the lysates were transferred to a 2-ml collection tube containing a gDNA Eliminator spin column. The column was discarded, and the flow-through was retained. The same volume of 70% ethanol was aspirated to the flow-through and transferred into a 2-ml collection tube containing an RNeasy Mini spin column. The column was retained, and the flow-through was discarded. Subsequently, 700 µl of RW1 buffer and 500 µl of RPE buffer were sequentially added and centrifuged, and the latter step (RPE buffer) were repeated twice. The spin column membrane was allowed to dry, 30 µl of RNase-free

water was then added directly to the membrane, and the membrane was centrifuged to elute the RNA.

According to the procedures provided with RQ1 RNase-Free DNase, the DNase digestion reaction reagent (1–8 μl of RNA in water, 1 μl of RQ1 RNase-Free DNase 10X Reaction Buffer, and 1 U/μg RQ1 RNase-Free DNase) was added, and the sample was incubated at 37°C for 30 minutes. Subsequently, 1 μl of RQ1 DNase Stop Solution was aspirated to terminate the reaction, and the sample was incubated at 65°C for 10 minutes to inactivate the DNase. Based on the protocols of the High-Capacity cDNA Reverse Transcription Kits, 10 μl of 2X RT master mix was added for the reverse transcription reactions, and the thermal cycler was programmed as follows: 25°C for 10 minutes → 37°C for 120 minutes → 85°C for 5 minutes → 4°C.

3.2.11 Quantitative real-time polymerase chain reaction (QRT-PCR)

All real-time PCRs were performed in triplicate using a mixture of reagents and a LightCycler 480. The reactions included 5 μl of diluted cDNA samples, 10 μl of SYBR green, 1 μl of forward primer, 1 μl of reverse primer and 3 μl pf nuclease-free water. The samples were denatured by incubation at 95°C for 5 minutes and amplified by 45 cycles of 95°C for 15 seconds and 60°C for 45 seconds. The results were normalized to the human and mouse housekeeping gene GAPDH. The primer sequences are shown in Tables 1-3.

Table 1. Homo sapiens primer sequence used for QRT-PCR analysis

Gene Name	Sense (5'→3')	Antisense (5'→3')
GRIN1	TGGCTTCTGCATAGACCTGCTCAT	TTGTTGCTGTTGTTTACCCGCTCC
GRIN2A	CACAAGCTGGTCATTGCCTG	AGCTTGCTTTCAGCTCCACC
GRIN2B	AGGTCCATCAGCAAGAAGCC	TGACGGTGTGGGTTGAGATG
GRIN2C	GACGAGATCAGCAGGGTAGC	ACAGTGGCAGGCAGAGAATC
GRIN2D	GGGTTGGGAAGGAAAGCAGT	ACCAAATCCTCTCCGGCTTG
DLGAP1	GTTGGGAGCAGGAACATGGA	TGTGGAACCCTGAGATGTGC
GRIA1	CTGTGAATCAGAACGCCTCA	TCACTTGTCCTCCACTGCTG

GRIA2	GGAGCCAAGGACTCTGGAAG	CACCAGCATTGCCAAACCAA
GRIA3	CACTGAGATGAAGAGGCGGG	GTGACTACTGCCAAACTCCCA
GRIA4	TGGTGTCAGTGTGGTCTTGTTCCT	ATGCCAAATTCATTGGGAGGCTGG
GRIK1	ATTGACTCCAAAGGTTACGGAGTGGG	GCAGCTTCCCTTCTTCTTGGAGTTGA
GRIK2	GAACATGCAGCGATTGCTAA	TGGGTTCGGGTAGAAATGAG
GRIK3	GGCCCTAATGTCACCGACTCTCTG	TCGAACCGGTCATTCCCGTATAGC
GRIK4	GCATGGACAGCCACCTCTAT	GTGGTTCCCCTTCAGCATTA
GRIK5	ATCAACCGGAAGGCAGACC	CCATGTGCACTCGGTAGAGG
GRM1	ATCCACTGCAACCCATCCAG	AGCTCCTTCCTCCTGTAGCA
GRM2	TCAACGAGGCCAAGTTCATTG	GGCTGACTGACACGCACATG
GRM3	CACTGGGCAGAAACCTTATCG	CCCTGGTTGCATATTCTTCATTT
GRM4	TGCCAAGATACGCCAAGCTA	TACCCTCTCCCACCTCCTTG
GRM5	GAGCAGATCAGCAGTGTGGT	CGTGGGCAACTGGATCTCTT
GRM6	CACAAGGTTTCTCTCCTTCCAGA	ACTGTATGCACACACCGAGT
GRM7	ACTGACATCAGCACTGCCAA	ATTCTAAAGAGCCAGGGCGG
GRM8	GAGAACTCCCGTTCCTGTCC	AGGGCTTCAATCTGGTCAGC

Table 2. Mouse primer sequence used for QRT-PCR analysis

Gene Name	Sense (5'→3')	Antisense (5'→3')
GRIN1	AACCTGCAGCAGTACCATCC	GCAGCAGGACTCATCAGTGT
GRIN2A	TCCGCCTTTCCGATTTGGG	GCGTCATAGATGAAAGCGTCC
GRIN2B	CTGTGTGAGAGGAAATCTCGG	GAAATGTATTCGGATGCCAGC
GRIN2C	TCGGAGAGCTGTAGCAGTTG	TTGGGGAAATCCCTAATGGGTC
GRIN2D	AAGATGCTGTTGCTGCTGGC	AGAAGACCAGCGCCACGTT
DLGAP1	CCCAGGATGAATGGTCAGGG	TGTAGCTACCACTGCGCATC
GRIA1	TTCATTCGGTGCTGGCTGTA	AAAGCCGCATGTTCCTGTGA
GRIA2	GCCTTGCGACACCATGAAAG	CGAGTCCTTGGCTCCACATT
GRIA3	ATGAGCAAGGCCTCTTGGAC	AGCACTGGTCTTGTCCTTGG
GRIA4	AAGGCTATGGTGTAGCGACG	TCAAGGCACTCGTCTTGTCC
GRIK1	TTGTTCTGGCTGCAGGACTC	GGAGTTGGTCGGATGGGTTT
GRIK2	GCAAAGAGGCCAGTGCTCTA	GTCTGGATGGTATGGTGGCA
GRIK3	CCGCAAGTCTGATAGGACCC	TCCACTGGCCTTTGTCATCC
GRIK4	GAAGGTCTTACCGGCCACAT	CTCAGCCAACTCCTTGAGCA
GRIK5	CGTCCATCTCCCACCTTGTC	AAAGCCCAGGATGTTGGAGG
GRM1	ATCACTACCTGCTTCGCAGTG	GAGAATTCTGGCTGCCTCTTCTT
GRM2	ATGAGACCTGTCAATGGGCG	AGCCTACCTTCTGGTAGCGA
GRM3	CCACTGTTGCCTCTGAAGGT	GCGATGCAGATGTTGCGTAG
GRM4	GCTTCCTGCCGTTGACTTACA	GCCGTGAGCGGAAGTTTCAT
GRM5	CATCCTAGCCAAACCGGAGA	TTTCCATTGGAGCTTAGGGTT

GRM6	TCATCCCTCCCCAGAATCCTT	CTGCTCCTGGACTGAGCCAA
GRM7	AAATGTAGACCCAAACAGCCC	AGAATAATTCAAGGTCTTCCTCCTC
GRM8	CTGATATGGAGCTGCGGGT	TCCAACAGATCCTCCGTTCA

Table 3. EZH2, E2F-1, CDKN2A and CDK4 primer sequence

Gene Name	Sense (5'→3')	Antisense (5'→3')
EZH2 (human)	ATCTGAGAAGGGACCGGTTT	GCTGCTTCCACTCTTGGTTT
E2F-1 (E2F1)(human)	CGGCGCATCTATGACATCAC	GTCAACCCCTCAAGCCGTC
CDKN2A (human)	CCGCTTCTGCCTTTTCACTG	CCCCTGAGCTTCCCTAGTTC
CDK4 (human)	TGGCTGAAATTGGTGTCGGT	CACGAACTGTGCTGATGGGA
GAPDH (human)	TGTTGCCATCAATGACCCCTT	CTCCACGACGTACTCAGCG
GAPDH (mouse)	AATGTGTCCGTCGTGGATCTG	CAACCTGGTCCTCAGTGTAGC

3.2.12 Measurement of the L-glutamate concentration

The L-glutamate level assay was performed in duplicate. Following the protocol recommended by the manufacturer of the L-glutamate Assay Kit (Sigma, MAK004-1KT), after the mono-/coculture of cancer cells and DRG, the supernatants from the mono-/coculture group and DRG CM were collected, and the cells were washed three times with PBS, homogenized in L-glutamate assay buffer and then centrifuged to remove insoluble cell debris. All the samples were deproteinized and filtered through a 10-kDa MWCO spin filter. Fifty microliters of each sample, including a blank sample, and 100 μl of reaction mixes according to the experimental scheme were coincubated in 96-well plates for 30 minutes at 37°C, and the absorbance at 450 nm was then measured.

3.2.13 Chromatin Immunoprecipitation (ChIP)

The Pierce Magnetic ChIP Kit was purchased from Thermo Fisher, and ChIP experiments were performed according to the manufacturer's instructions. SU86.86 cells were incubated with 1% paraformaldehyde for 10 minutes, mixed with a final concentration of 1X glycine solution and incubated for 5 minutes for DNA-protein cross-linking. The cells were lysed with

membrane extraction buffer, MNase digestion buffer, MNase (ChIP grade), and MNase stop solution for the collection of nuclei and sonicated with six 20-second pulses at a power setting of 3 watts to produce 200-300 bp chromatin fragments. The lysates were then immunoprecipitated with ChIP Grade Protein A/G Magnetic Beads conjugated with target-specific antibody (anti-EZH2 / anti-E2F1) (ChIP-grade) and normal rabbit IgG and anti-RNA polymerase II antibody (binding to the GAPDH promoter) as the negative and positive controls, respectively. The precipitated DNA fragments were analyzed by qRT–PCR. The relative primer sequences are shown in Table 4.

Table 4. Human primer sequence used for ChIP-PCR analysis

Gene Name	Sense (5'→3')	Antisense (5'→3')
EZH2-GRIN2D-Primer1	TTAACGTCACCAGATGGGGC	CAGTCTGGGTCAGGGGTTTC
EZH2-GRIN2D-Primer2	CTCGAGTCCGAGGTATGACG	ACTGCTTTCCTTCCCAACCC
E2F1-EZH2 Primer1	CGTGTGTTCAGCGAAAGAAC	ATCGCCATCGCTTTTATTTG
E2F1-EZH2 Primer2	GACAACCAGAGCGAAACTCC	GGAAGCCAAGTTTGAACCAG
E2F1-EZH2 Primer3	CGCCGTCTCTTTGTTCTTTC	GTTCCCGCCACCTATCCT
16q22 (control quality)	CTACTCACTTATCCATCCAGGCTAC	ATTTCACACACTCAGACATCAAG

3.2.14 siRNA transfection

siRNA oligonucleotides for GRIN2D (NM_000836), EZH2 (NM_001203247, NM_001203248, NM_001203249, NM_004456, NM_152998), and E2F1 (NM_005225) were purchased from siTOOLs Biotech (Munich, Germany). According to the manufacturer's instructions, Lipofectamine™ RNAiMAX Transfection Reagent was used for siRNA transfections, and siPOOL reverse transfection was performed with a final siRNA concentration of 2 nM. According to the manufacturer's reverse transfection protocol, diluted

siPOOL and diluted RNAiMax were well mixed at a ratio of 1:1 by vortexing and then incubated for 5 minutes at room temperature. Transfection mix was transferred to the bottom of the cell culture plate or dish, and the cell suspension was then added to the transfection reaction. Forty-eight hours after transfection, the efficacy of the silencing was simultaneously analyzed by real-time PCR and western blotting. For evaluating the effect of GRIN2D RNAi on cell migration and invasion, cancer cells were reseeded 48 hours after siRNA transfection and grown for an additional 24-48 hours for phenotypic experiments.

3.2.15 Bioinformatics analysis

To verify the transcriptional levels of glutamatergic receptors in human PCa cells, which were classified into four types according to their core components described below, the gene expression levels were normalized with a housekeeping gene (HKG), and the geometric mean of the ranks (rank product) of the per-sample gene expression and the across-sample mean expression of each gene were calculated.

- NMDAR: GRIN1, GRIN2A, GRIN2B, GRIN2C, GRIN2D, DLGAP1.
- AMPAR: GRIA1, GRIA2, GRIA3, GRIA4
- Kainate: GRIK1, GRIK2, GRIK3, GRIK4, GRIK5
- Metabotropic: GRM1, GRM2, GRM3, GRM4, GRM5, GRM6, GRM7, GRM8.

For differential expression analysis of the unpaired samples, we analyzed 171 human normal pancreas and 179 human PCa tissues, performed UCSC XENA unified processing of TCGA and GTEx RNA-seq data in TPM (transcripts per million reads) format by the Toil process[165], and extracted the corresponding normal and PCa tissue data from TCGA and GTEx. For the molecular correlation analysis, RNA-seq data from TCGA PCa project level 3 in HTSeq-FPKM (Fragments Per Kilobase per Million) format were used. The RNA-seq data in FPKM format were converted into TPM format, and log2 conversion was performed to compare the expression levels between the samples. The Mann–Whitney U test (Wilcoxon

rank-sum test) and Spearman’s correlation analysis were performed using the ggplot2 (version 3.3.3) R package.

3.2.16 Flow cytometry analysis

According to the manufacturer's instructions, harvested cancer cells and wash with cold 1xPBS, centrifuged and discarded the supernatant and re-suspended the cells in 100µl of 1x AnnexinV buffer, added 3µl of AnnexinV and 0.7 µl of Sytox, incubated for 30 minutes at room temperature and avoided from light, after incubation add 200µl of 1x AnnexinV buffer and keep samples on ice, proceed immediately with FACS analysis.

3.2.17 Statistical analysis

GraphPad Prism 8 Software (GraphPad, San Diego, California, USA) was used to perform all statistical analyses and generate the graphs. The data are expressed as the means ± SDs from three repeated and independent experiments. An unpaired Student’s t test was used to assess the significance of the difference between two groups. A p value less than 0.05 was considered to indicate significance.

4.0 Results

4.1 Glutamatergic receptor expression in PCa

To more accurately evaluate L-glutamate-mediated signaling in human PCa, we assessed the expression level of all glutamatergic receptors in human PCa profiled by TCGA through bioinformatic analyses. Encouraged by the finding that the expression level of GRIN2D was far higher than that of other glutamatergic receptors in human PCa (Figure 2a), we focused on NMDAR components. Compared with the levels found in the normal pancreas, we found elevated expression levels of GRIN1, GRIN2A, and GRIN2D in PCa (Figure 2b), and only the GRIN2D level was significantly associated with the T and N stage of the TNM status (Figure 2c-d) and with the histologic grade of PCa (Figure 2e). To further study the broader correlation between GRIN2D and cancers, we evaluated the expression of GRIN2D genes across multiple human cancer types and found that the GRIN2D level in most cancers was higher than that in normal tissue (Figure 2f).

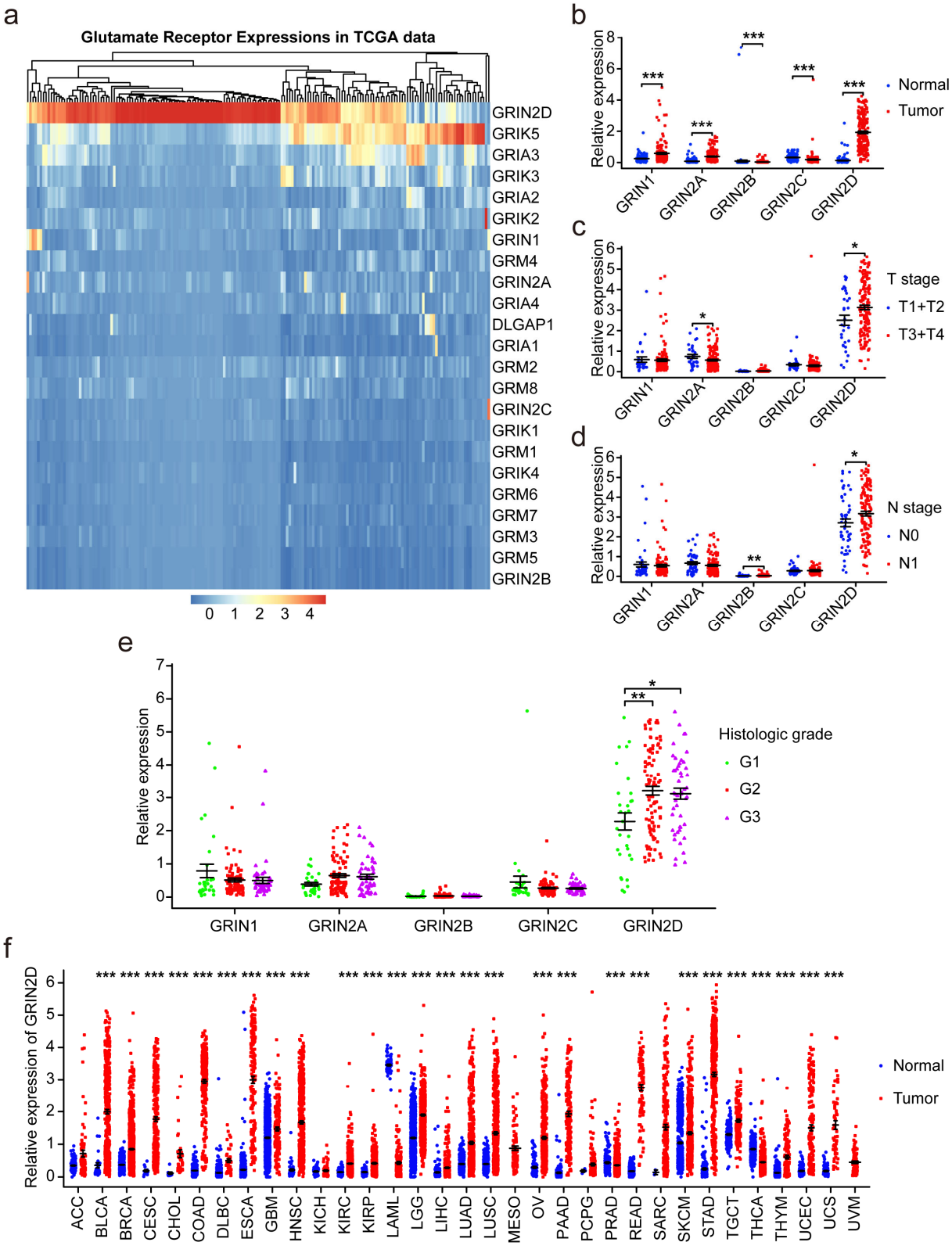

Figure 2. Association of the Glutamatergic receptors (Especially NMDAR) with human pancreatic cancer. (a) mRNA expression of 23 Glutamatergic receptor-associated genes in 177 pancreatic cancer patients from The Cancer Genome Atlas (TCGA). Samples were sorted by Glutamatergic receptor Z-scores of normalized expression values of all 23 genes. (b) Dot comparison of mRNA expression of GRIN1, GRIN2A, GRIN2B, GRIN2C, GRIN2D (from left to right) in Pancreatic

cancer and normal pancreas. P-values were computed using Wilcoxon rank sum test. (c, d, and e) Dot comparison of mRNA expression of GRIN1, GRIN2A, GRIN2B, GRIN2C, GRIN2D (from left to right) in Pancreatic cancer was associated with the T and N stage of the TNM status and the histologic grade. P-values were computed using Wilcoxon rank-sum test. (f) Dot comparison of mRNA expression of GRIN2D across multiple human cancer types. P-values were computed using Wilcoxon rank-sum test.

Because heterotetrameric NMDARs consist of two obligatory GluN1 subunits (encoded by GRIN1) and two modulatory GluN2 subunits (GluN2A/2B/2C/2D; encoded by GRIN2A/2B/2C/2D), which are considered the major determinants of NMDAR functional heterogeneity, the coexpression levels of GRIN1 and GRIN2D in human PCa showed a particularly significant correlation (Figure 3a and 3b).

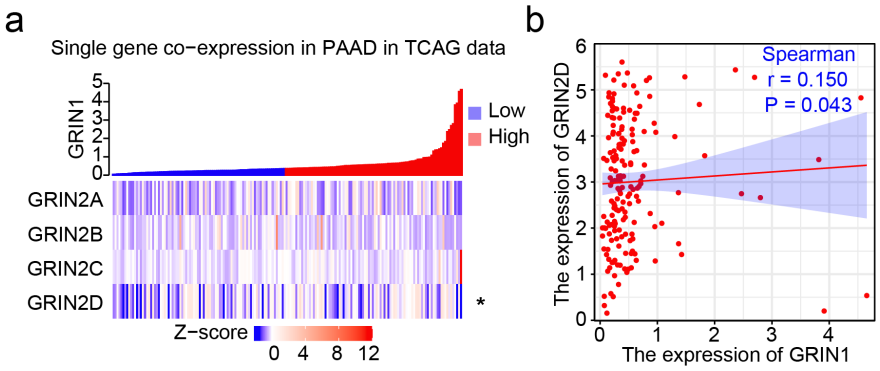

Figure 3. Association of the Glutamatergic receptors (Especially NMDAR) with human pancreatic cancer. (a) Comparison of mRNA co-expression of GRIN1 and GRIN2 (2A/2B/2C/2D) in human pancreatic cancer. P-values were computed using Spearman. (b) Comparison of mRNA co-expression of GRIN1 and GRIN2D in human pancreatic cancer. P-values were computed using Spearman.

4.2 Expression of NMDAR signaling components in PCa cells

Encouraged by the GRIN2D level in human PCa in TCGA obtained from the comparison of TCGA data, we found that GRIN1 and GRIN2D exhibited the highest expression among all glutamatergic receptors in 41 PCa cells derived from the Cancer Cell Line Encyclopedia (CCLE) data (Figure 4a and 4b).

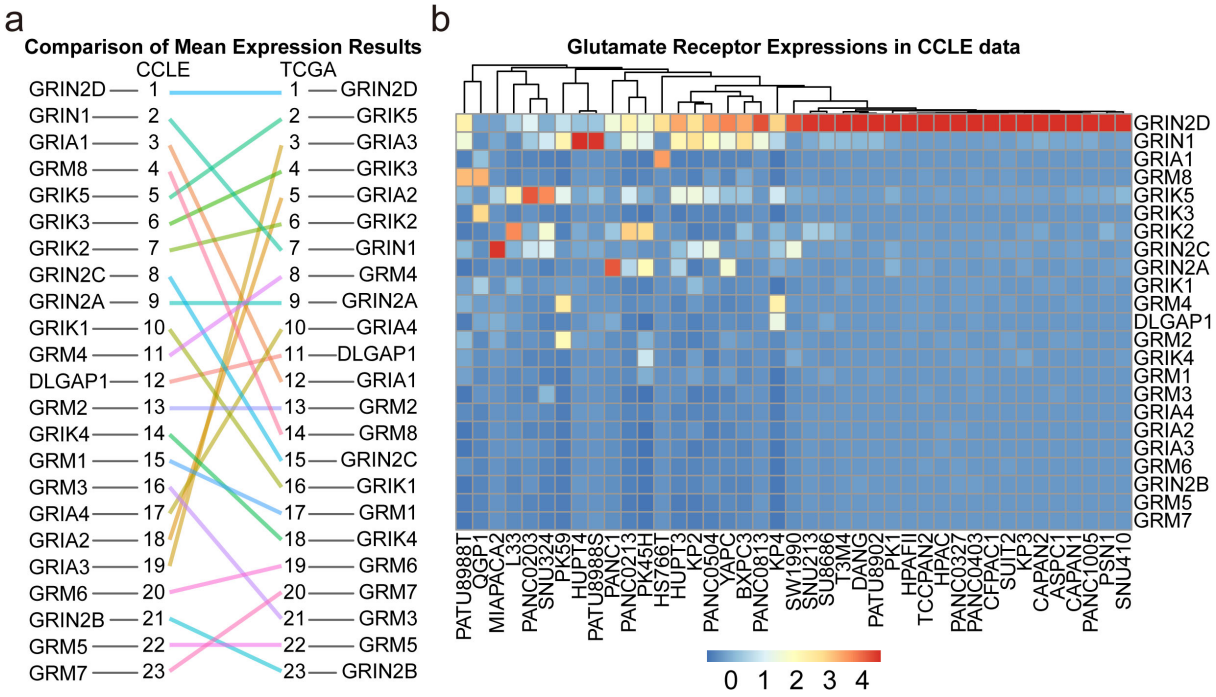

Figure 4. Expression of Glutamatergic receptor components in pancreatic cancer cells. (a) Comparison of the mean expression of Glutamatergic receptors between the TCGA and CCLE data. (b) mRNA expression of 23 Glutamatergic receptor-associated genes in 41 pancreatic cancer cells from CCLE data. Samples were sorted by Glutamatergic receptor Z-scores of normalized expression values of all 23 genes.

Quantitative real-time PCR was performed to analyze the expression levels of 23 glutamatergic receptors in neuro-affinity cells (SU.86.86 and T3M4) and non-neuro-affinity cells (Panc-1 and Capan-1) of PCa[67,68]. Consistent with TCGA and CCLE data, GRIN2D exhibited the highest expression level (Figure 5a-5d), particularly among NMDAR subtypes (Figure 5e). Because the neuroinvasive ability of TPAC cancer cells can be reproduced by a 3D migration assay[166], compared with the non-neuroinvasive KPC cell line, 23 glutamatergic receptor levels measured in these three kinds of mouse PCa cell lines showed that the GRIN2D gene exhibited the highest (Figure 6b and 6d) or second-highest expression (Figure 6c) by quantitative real-time PCR, and these results were generally consistent with mouse CCLE data, which showed that GRIN2D exhibited the highest expression among the GRIN gene family (Figure 6a).

All the above-described data prompted us to focus on the relationship of the NMDAR signaling pathway with the GRIN2D receptor in PCa to understand its biological role in NI.

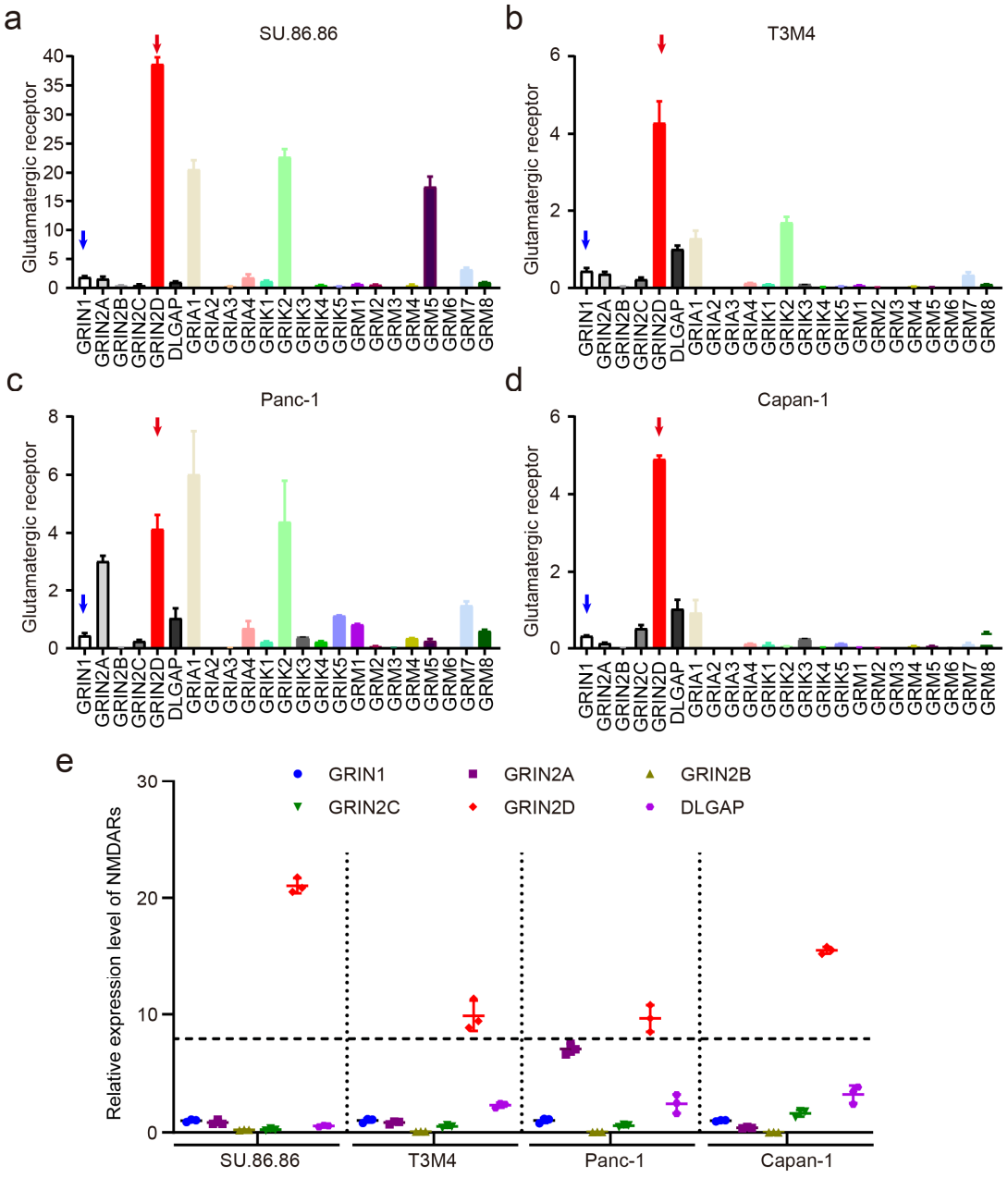

Figure 5. Expression of NMDAR signaling components in human pancreatic cancer cells. (a, b, c, and d) The relative expression of 23 L-glutamate receptor genes were respectively demonstrated in SU.86.86, T3M4, Panc-1, and Capan-1 by quantitative real-time PCR. (e) Measurement distribution of NMDRA components in SU.86.86, T3M4, Panc-1, and Capan-1.

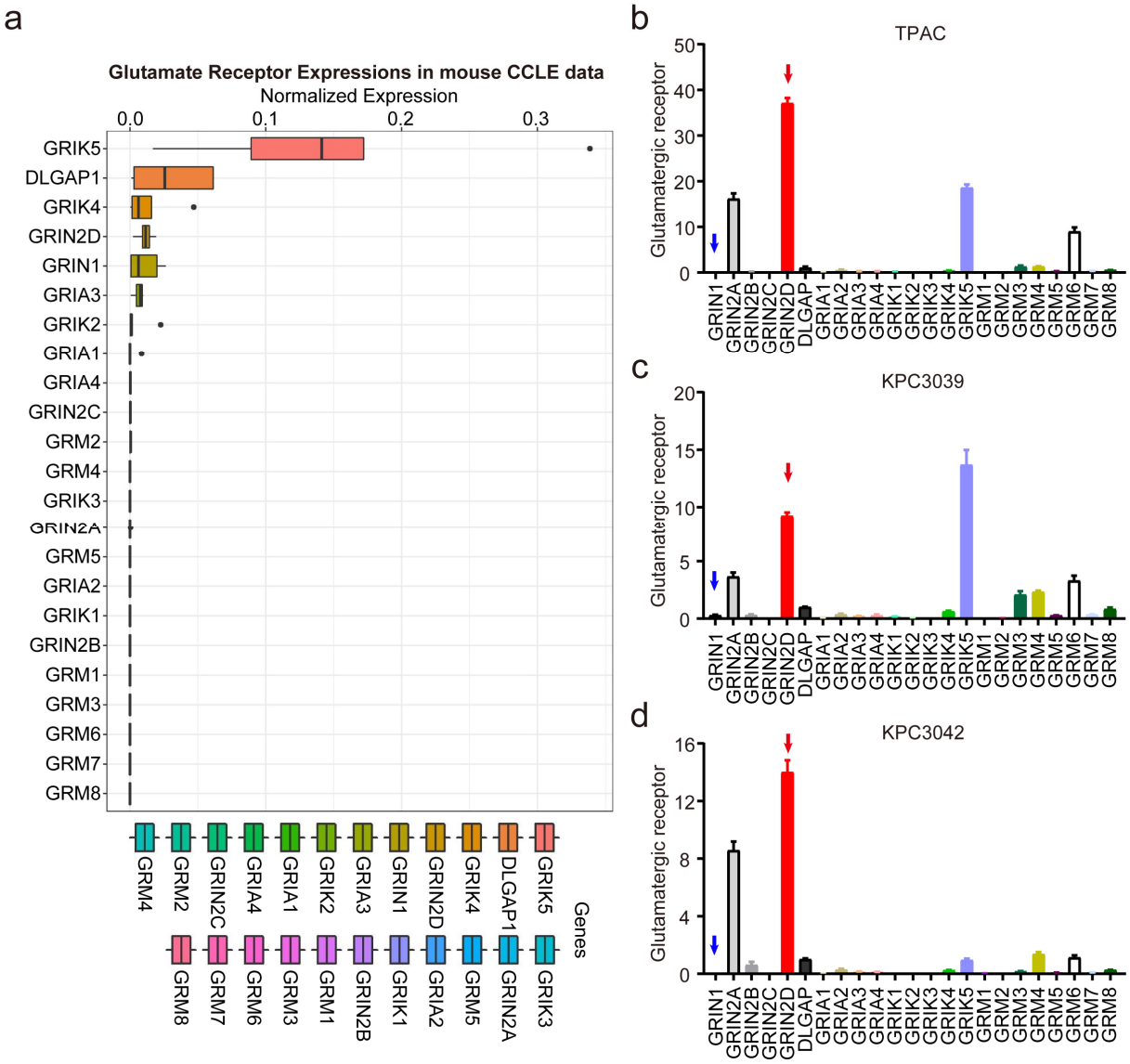

Figure 6. Expression of NMDAR signaling components in mouse pancreatic cancer cells. (a) Boxplot expression of 23 Glutamatergic receptor-associated genes in mouse cell line data from CCLE. Samples were sorted by Glutamatergic receptor Z-scores of normalized expression values of all 23 genes. (b) Measurement distribution of 23 L-glutamate receptor genes were respectively demonstrated in TPAC, KPC3039, and KPC3042 by quantitative real-time PCR.

4.3 Activation of GluN2D-containing NMDAR in human PCa cells by L-glutamate

GRIN2D is the L-glutamate-binding receptor of NMDAR, and we explored whether GRIN2D expression can be activated by L-glutamate. The L-glutamate EC50 demonstrated over 5-6-fold higher potency for L-glutamate (EC50=0.2-0.4 μM) at GluN2D receptors than GluN2A- and GluN2B-containing NMDARs[89,120]. To confirm the variation of the GluN2D level

in PCa cells induced by L-glutamate, the PCa cells were treated with different concentrations of L-glutamate that ranged from 0 μM to 10 μM and 0.2 μM glycine. Compared with the control group, we found that the treatment with increasing concentration of L-glutamate resulted in the gradual upregulation followed by downregulation in the neuro-affinity cell lines (SU.86.86 and T3M4) by real-time PCR (Figure 7a and 7b) and western blotting (Figure 7c and 7d). The GRIN1 level showed variation corresponding with the changes in GRIN2D expression.

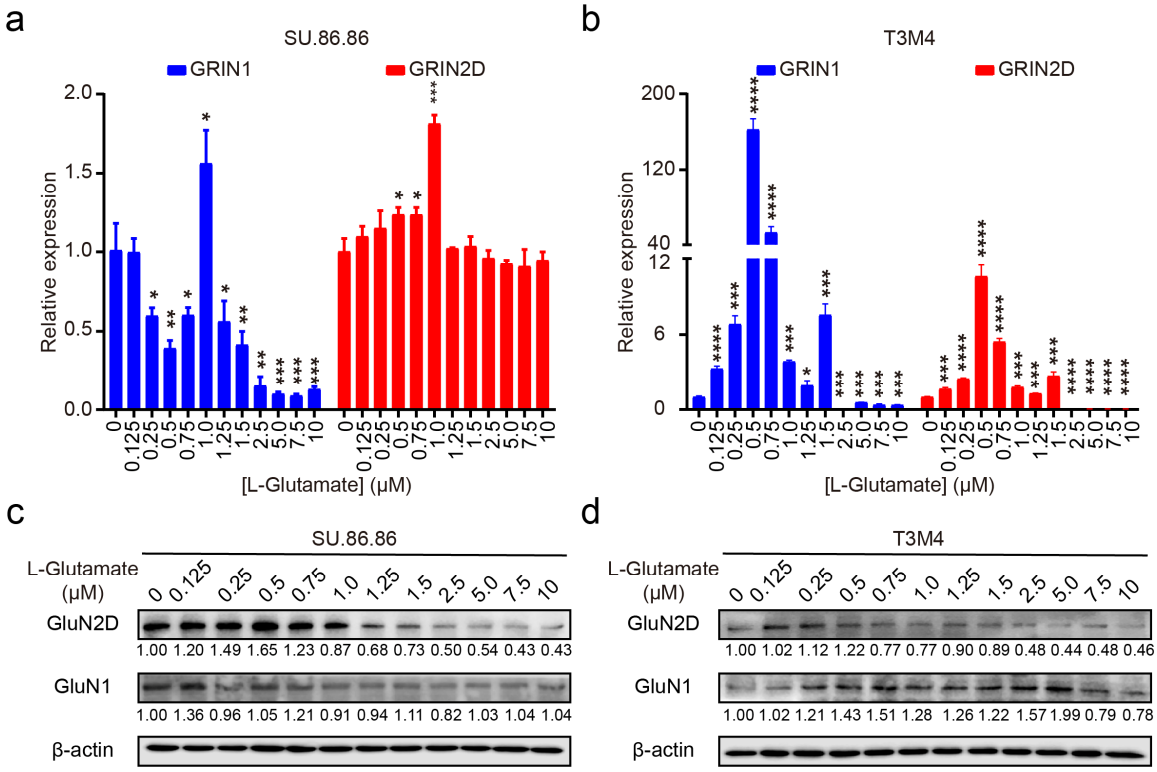

Figure 7. GluN2D-containing NMDAR activation in SU.86.86 and T3M4. The relative expressions of GRIN1 (encoded GluN1) and GRIN2D (encoded GluN2D) were measured in SU.86.86 and T3M4 by quantitative real-time PCR and western blotting after treating with different concentrations of L-glutamate for 48 hours.

Unlike the results found for the neuro-affinity cell lines, GRIN2D expression was gradually downregulated or not significantly changed in the non-neuro-affinity cell lines (Panc-1, Capan-1) compared with the control group by treatment with increasing concentrations of L-glutamate, as demonstrated by real-time PCR (Figure 8a and 8b) and western blotting (Figure 8c and 8d).

The GRIN1 levels presented variations corresponding to with the changes in GRIN2D expression.

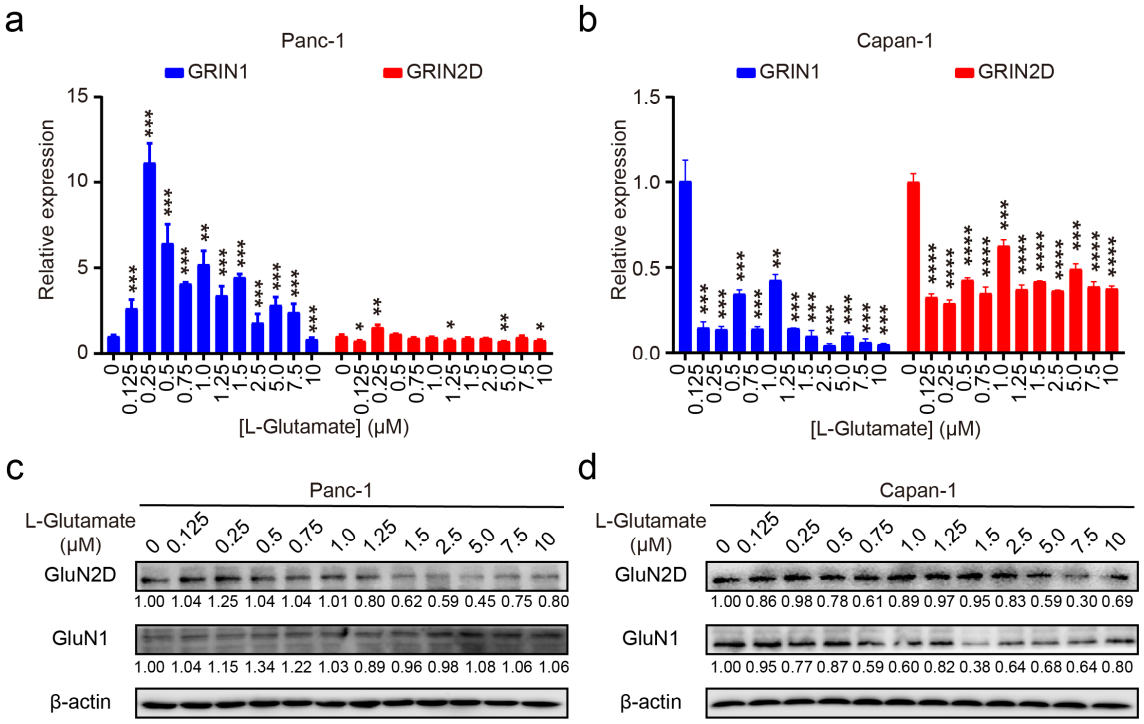

Figure 8. GluN2D-containing NMDAR activation in Panc-1 and Capan-1. The relative expressions of GRIN1 (encoded GluN1) and GRIN2D (encoded GluN2D) were measured in Panc-1 and Capan-1 by quantitative real-time PCR and western blotting after treating with different concentrations of L-glutamate for 48 hours. n = 3 independent experiments.

Consistently, compared with the results found for the control group, increased levels of GRIN2D expression were found after treatment with L-glutamate in the murine, neuro-affinity TPAC cancer cell line by real-time PCR (Figure 9a) and western blotting (Figure 9b). In contrast, GRIN2D expression was downregulated or not significantly changed in the non-neuro-affinity cell lines (KPC3039 and KPC3042) compared with the control group, as demonstrated by real-time PCR (Figure 9c and 9d) and western blotting (Figure 9e and 9f). The GRIN1 levels showed corresponding changes in these three types of mouse cell lines.

Together, the above-described results demonstrate that the activation of L-glutamate with an excess concentration can upregulate the expression of GluN2D-NMDAR signaling in neuro-affinity cancer cells (SU.86.86, T3M4, and TPAC) compared with the results found for

the control group, and this finding was accompanied by further increases in the L-glutamate concentrations. In addition, the GRIN2D levels were reduced or inhibited by negative feedback. Nonetheless, the GRIN2D levels were lower in the non-neuro-affinity cancer cells (Panc-1, Capan-1, KPC3039, and KPC3042) than in the control cells.

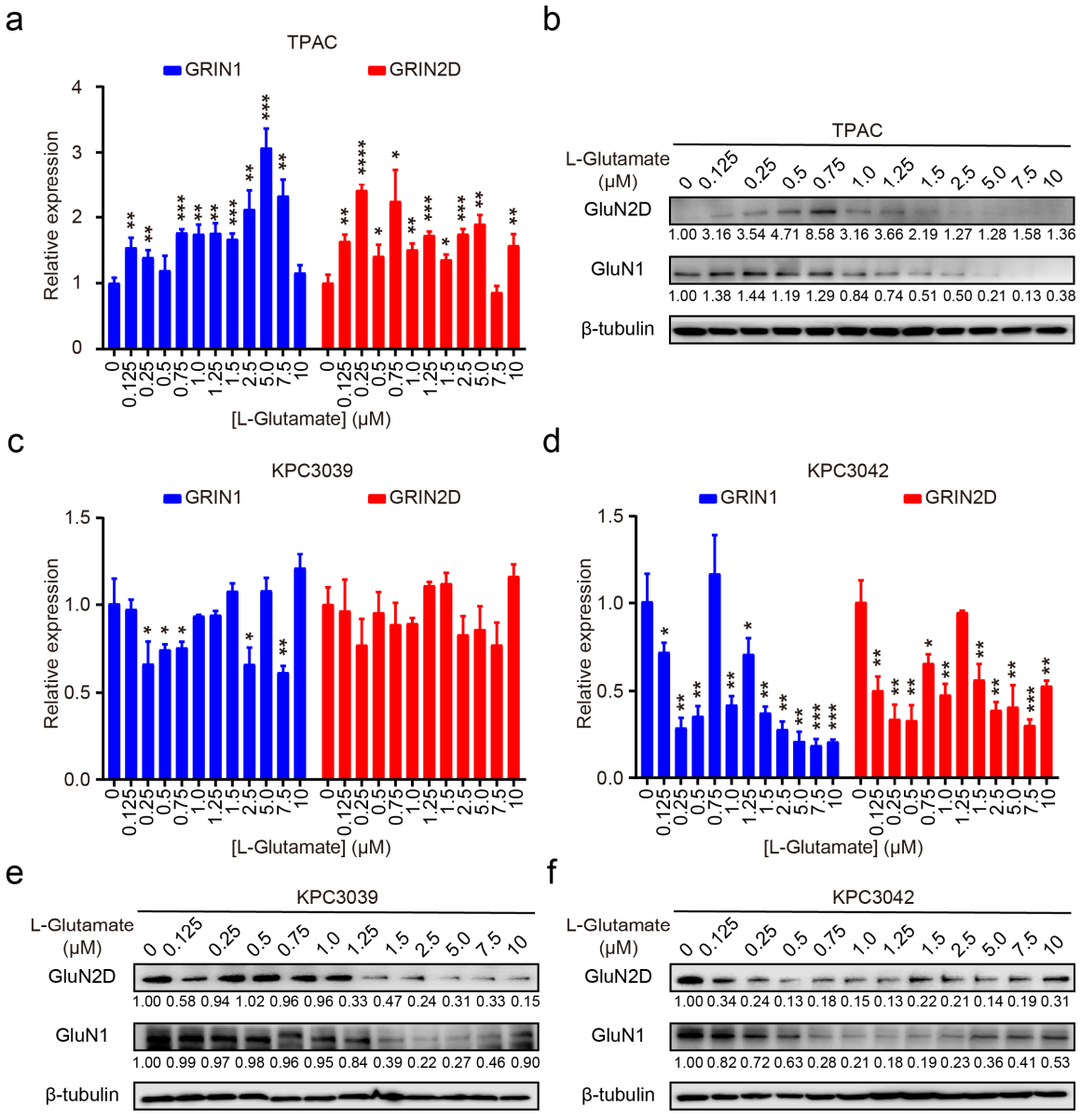

Figure 9. GluN2D-containing NMDAR activation in mouse cell lines. The relative expressions of GRIN1 (encoded GluN1) and GRIN2D (encoded GluN2D) were measured in TPAC, KPC3039, KPC3042 by quantitative real-time PCR and western blotting after treating with different concentrations of L-glutamate for 48 hours. n = 3 independent experiments.

In brief, L-glutamate upregulated the GluN2D levels in pancreatic neuroinvasive cancer cells, and these phenomena were not observed in non-neuro-affinity PCa cell lines. This finding might imply that low L-glutamate concentrations can be involved in NI mediated by GluN2D-NMDAR signaling in PCa.

4.4 Phenotypic functions of the GRIN2D gene (encoding GluN2D) in PCa

Compared with that in non-neuroinvasive PCa cells, increasing L-glutamate concentrations could elevate the expression and/or tend to present the upregulated influence tendency on GluN2D levels in neuroinvasive PCa cells, and this finding broadly encouraged us to further investigate the phenotypic function of GRIN2D in PCa cells. Based on the above-described results and the EC50 of L-glutamate, we first performed cell viability assays of PCa cells (human: SU.86.86, T3M4, Panc-1, and Capan-1; mouse cell lines: TPAC, KPC3039, KPC3042) treated with different concentrations of L-glutamate. The results revealed that different concentrations of L-glutamate had no effect on either human (Figure 10a) or mouse PCa cell growth (Figure 10b).

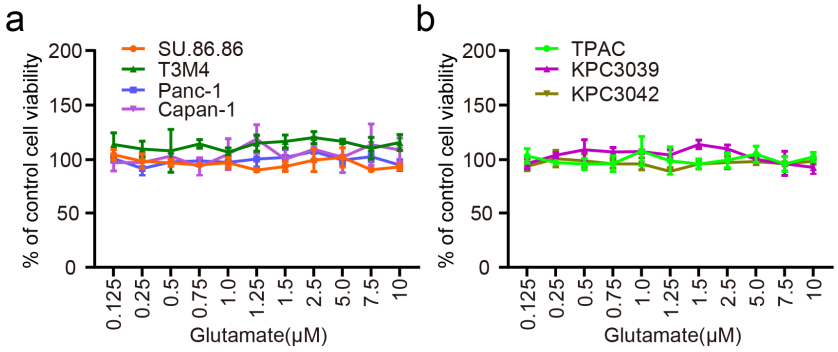

Figure 10. Cell proliferation was stimulated by different concentrations of L-glutamate in pancreatic cancer. Cell viability assays were performed in cancer cells (Human: SU.86.86, T3M4, Panc-1, and Capan-1; Mouse cell lines: TPAC, KPC3039, KPC3042) treated with different concentrations of L-glutamate (Range from 0 μM to 10 μM).

4.4.1 L-glutamate induces the migration and invasion of PCa cells

We subsequently performed cell migration and invasion assays (Figure 11) of these cancer cells. The results confirmed that 0.5 µM L-glutamate and DRG CM (containing 0.5 µM L-glutamate) significantly increased the migratory (Figure 12a) and invasive (Figure 12b) capabilities of human SU.86.86 and T3M4 cell lines but did not promote the migration of Panc-1 and Capan-1 cells (Figure 12a). In contrast, L-glutamate and DRG CM decreased the invasive capability of Panc-1 and Capan-1 cells, respectively (Figure 12b).

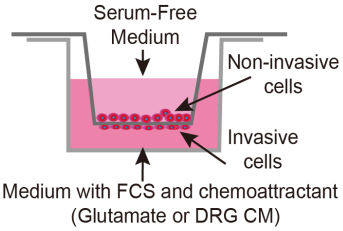

Figure 11. Schematic illustration of cell invasion for the cancer cells. Matrigel cell invasion through the 8 µm pore-size membrane transwell chamber placed in 24-well plates was performed in cancer cells (Human: SU.86.86, T3M4, Panc-1, and Capan-1; Mouse cell lines: TPAC, KPC3039, KPC3042). The upper compartment: FCS -free medium; for the GluN2D antagonist UBP145, pre-treatment of the cancer cells was performed for 30 minutes with UBP145 before seeding. DMSO (1:10.000) was negative control. The lower compartment: medium containing 0.5 µM of L-glutamate, or DRG CM prediluted to contain 0.5 µM of L-glutamate.

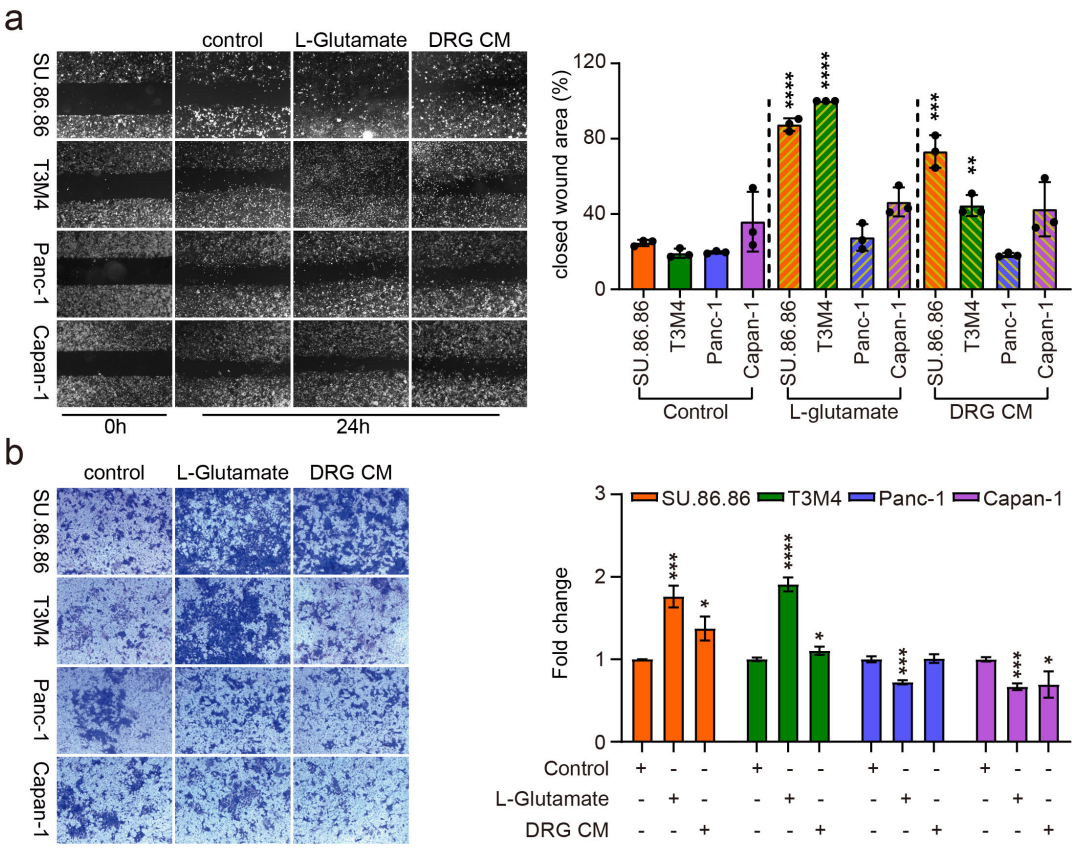

Figure 12. Cell migration and invasion in human pancreatic cancer cells. (a) Typical cell migration was measured in the Culture-Insert 2 Well; quantification of closed wound area of wound healing assay. (b) Representative stainings with crystal violet of invaded cells on the lower side of the 8 µm pore-size porous polycarbonate membrane under a phase-contrast microscope (20X); quantification of the invaded cells. Values were mean ± SD from triplicate independent experiments. P-value was determined by unpaired t-test.

We repeated these phenotypic experiments with murine neural and non-neuroinvasive PCa cells. Our results revealed that 0.5 µM L-glutamate and DRG CM (containing 0.5 µM L-glutamate) can also boost phenotypic functions, including migration and invasion, in TPAC but not KPC cell lines (Figure 13a and 13b), and L-glutamate even reduced the invasion capability of KPC3042 cells (Figure 13b).

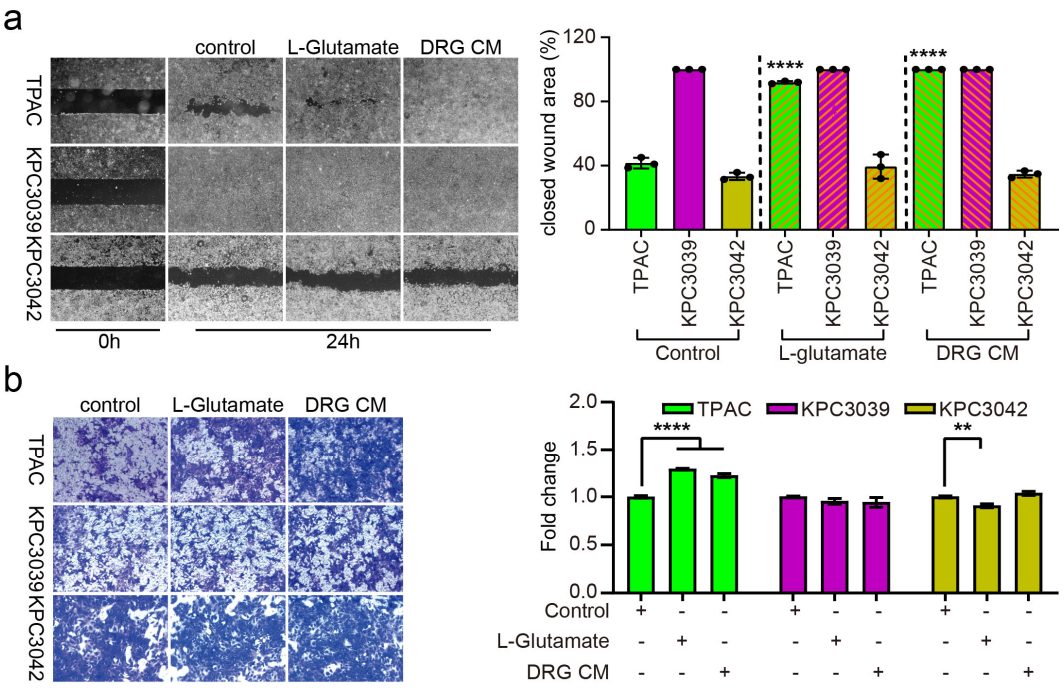

Figure 13. Cell migration and invasion in mouse pancreatic cancer cells. (a) Typical cell migration was measured in the Culture-Insert 2 Well; quantification of closed wound area of wound healing assay. (b) Representative stainings with crystal violet of invaded cells on the lower side of the 8 µm pore-size porous polycarbonate membrane under a phase-contrast microscope (20X); quantification of the invaded cells. Values were mean ± SD from triplicate independent experiments. P-value was determined by unpaired t-test.

4.4.2 The GluN2D antagonist UBP145 controls the migrative and invasive phenotype of PCa cells

To confirm that L-glutamate varied the phenotype of PCa cells based on the functions of the NMDAR receptor subtype GluN2D, we pretreated the cancer cells with the GluN2D antagonist UBP145 and conducted further cell phenotypic experiments. We first verified the maximal nontoxic and reliable concentration of UBP45 for PCa cells through cell proliferation assays (Figure 14a and 14b), and the results demonstrated that 10 μM was the highest nontoxic concentration of UBP145 for the pretreatment of cancer cells[167].

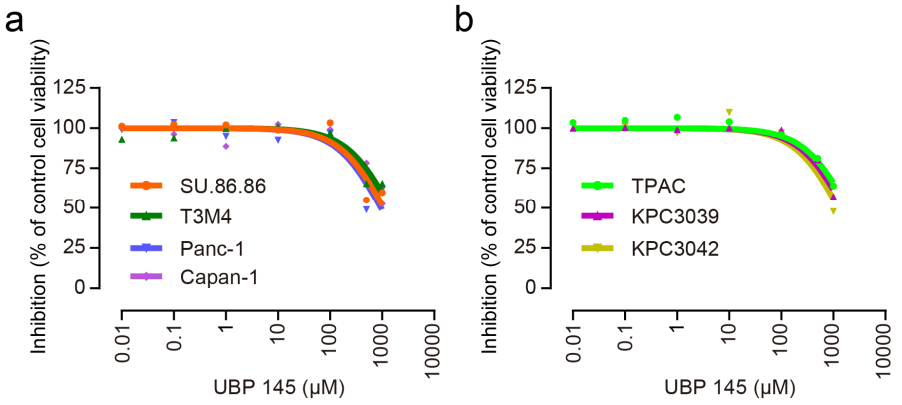

Figure 14. Cancer cell proliferation was inhibited by GluN2D antagonist UBP145. Dose–response-inhibition of GluN2D antagonist UBP145 to the cell viability was calculated by cell viability in cancer cells.

In identical cell phenotyping experiments, we pretreated cancer cells with 10 μM UBP145 for 30 minutes[167] and then cultured or chemoattracted the cells by changing the fresh medium with L-glutamate or DRG CM. The comparison of the pretreatment groups revealed that UBP145 exerted no effect on the migration and invasion of cancer cells with the exception of a slight inhibitory effect on the invasion of T3M4 cells (Figure 15b). Compared with the results found for cancer cells that were not pretreated with UBP145, we found that the previous migratory and invasive phenotypes stimulated or chemoattracted by L-glutamate and DRG CM were completely reversed in the neuroinvasive cancer cell lines SU.86.86, T3M4, and TPAC

(Figure 15a and 15b and Figure 16a and 16b). Moreover, the migrative and invasive cell phenotypes of the Panc-1 and Capan-1 cell lines pretreatment with UBP145 exhibited no notable variation from those of the non-pretreated cells (Figure 15). In contrast, the invasive capability of KPC3039 cells was decreased after the pretreatment (Figure 16b), and the effects of the L-glutamate and DRG CM treatments on the migratory capacity of these cells were different (Figure 16a).

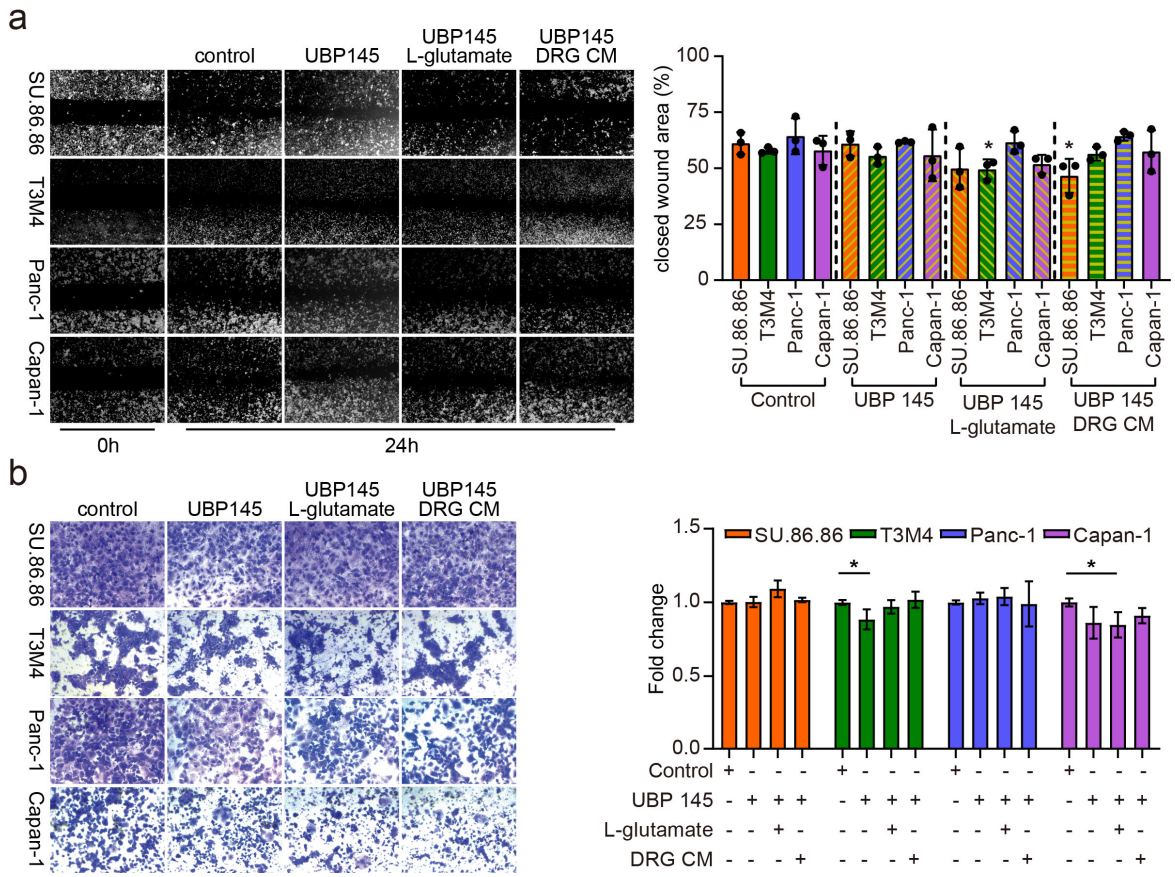

Figure 15. Cell migration and invasion after inhibition by UBP145 in human pancreatic cancer cells. (a) Typical cell migration was measured in the Culture-Insert 2 Well; Quantification of closed wound area of wound healing assay. (b) Representative stainings with crystal violet of invaded cells; quantification of the invaded cells. Treated cancer cells by UBP145 for 30 minutes and DMSO (1:10.000) as appropriate control in UBP145 experiments. Values are mean ± SD from triplicate independent experiments. P-value was determined by unpaired t-test.

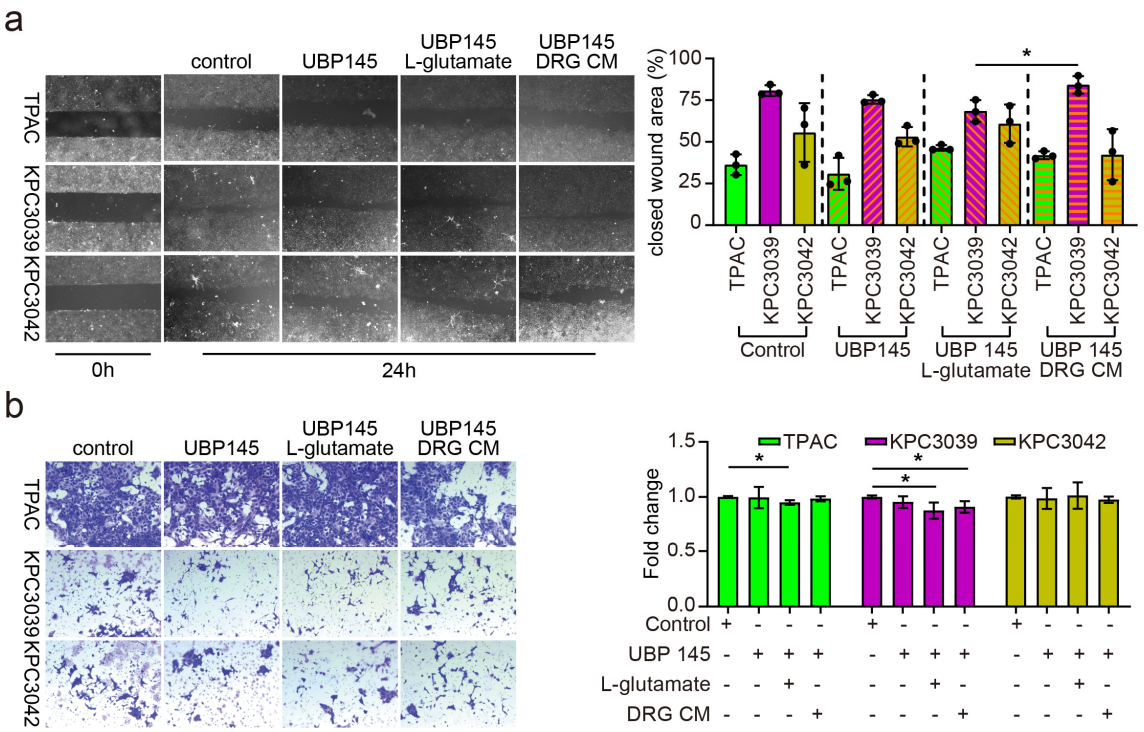

Figure 16. Cell migration and invasion after inhibition by UBP145 in mouse pancreatic cancer cells. (a) Typical cell migration was measured in the Culture-Insert 2 Well; Quantification of closed wound area of wound healing assay. (b) Representative staining with crystal violet of invaded cells; quantification of the invaded cells. Treated cancer cells by UBP145 for 30 minutes and DMSO (1:10.000) as appropriate control in UBP145 experiments. Values are mean ± SD from triplicate independent experiments. P-value was determined by unpaired t-test.

4.4.3 The silencing of GluN2D receptors decreases the invasion and migration of PCa cells

To further determine the phenotypic function of GluN2D-containing receptors at the gene level, we selected one neuroinvasive (SU.86.86) and one non-neuroinvasive cancer cell (Capan-1), which manifested typical phenotypic features in pharmacological inhibition via the GluN2D antagonist. We measured the efficacy of GRIN2D siRNA transfection on SU.86.86 and Capan-1 cells by RT–PCR and western blotting after transfection (Figure 17a and 17b) and reseeded the cells to perform further phenotypic experiments. We found that chemoattraction by L-glutamate and DRG CM exerted no effects on the migration and invasion of SU.86.86 and Capan-1 cancer cells in which GluN2D receptor expression was suppressed, which is

consistent with the results obtained with pharmacological inhibition using UBP145 (Figure 17c and 17d).

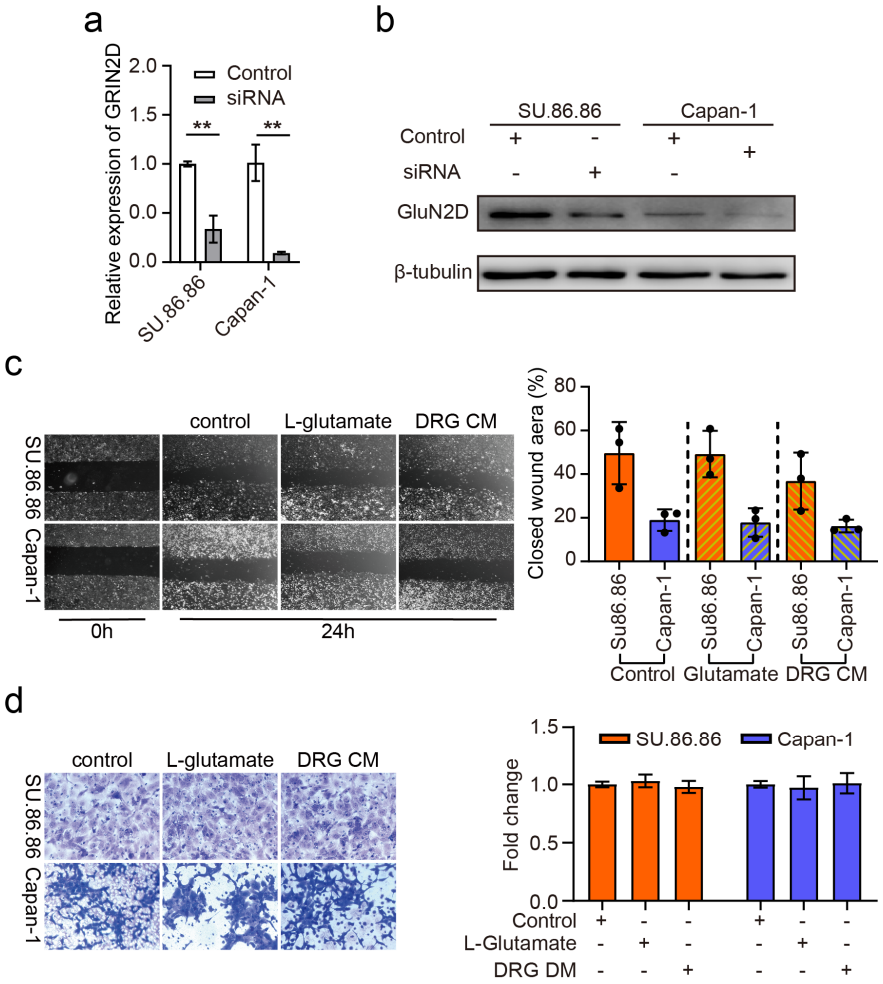

Figure 17. Cell migration and invasion after GRIN2D siRNA interfering. (a and b) Efficacy of GRIN2D siRNA on SU.86.86 and Capan-1 were analyzed by RT-PCR and western blotting after GRIN2D siRNA transfection for 48 hours. The final concentration of the negative control and the specific oligonucleotides was 2 nM. For the assessment of the effect of GRIN2D on cell migration and proliferation, cancer cells were reseeded after GRIN2D siRNA transfection for 48 hours: (c) Typical cell migration was measured in the Culture-Insert 2 Well; Quantification of closed wound area of wound healing assay. (d) Representative staining with crystal violet of invaded cells; quantification of the invaded cells. Values are mean ± SD from triplicate independent experiments. P-value was determined by unpaired t-test.

Based on the abovementioned findings, L-glutamate can promote the migration and invasion of pancreatic neuroinvasive cancer cells, and this promotion can be prohibited by antagonization of or interference with the GluN2D receptor subtype. These results further

revealed one certain contact between GluN2D receptor subtypes and PCa nerve invasion, which supported our hypothesis.

4.5 Activation of GluN2D-NMDAR signaling in PCa tissues with NI

According to our hypothesis, this glutamate-NMDAR axis might be involved in PCa tissues, approximately 100% of which reportedly exhibit NI. The above-described results, which confirmed significant variations in phenotypic features mediated by GluN2D in neuroinvasive cancer cells, prompted us to further ascertain the levels of signal-transduction molecules belonging to the glutamate-NMDAR signaling pathway in PCa, which is the pathway mainly detected at the synaptic level. We analyzed the correlations between the signal-transduction molecules belonging to the abovementioned axis and human PCa tissues, which revealed higher levels of GRIN2D, GRIN1 and PSD-95 (encoded by SAP90 or DLG4[168]) in PCa tissues than in normal pancreatic tissues (Figure 18).

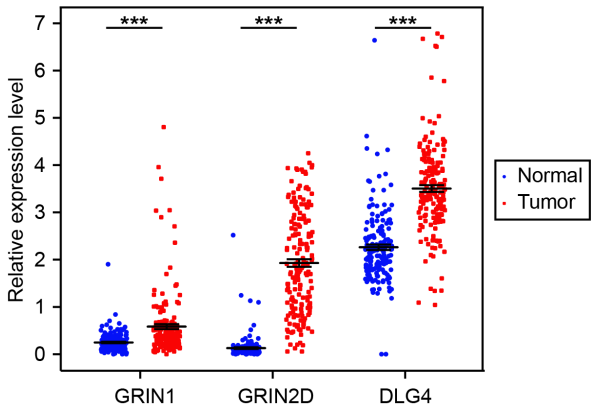

Figure 18. The correlations between the signal-transduction molecules and human pancreatic cancer tissues. Dot comparison of mRNA expression of GRIN1, GRIN2D, and PSD95 (encoded by SAP90 or DLG4) in pancreatic cancer and normal pancreas. P-values were computed using Wilcoxon rank sum test.

To further clarify the expression levels of these signal-transduction molecules in cancer cells with or without NI in PCa tissues, PCa tissues from 20 patients were analyzed by immunostaining. The presence of NI was analyzed through double immunostaining with the

cancer cell marker PanCK and the neural marker S100 (Figure 19-1#). We then assessed the levels of GluN1, GluN2D, and PSD-95 (revealed by the percentage of GluN2D-, GluN1-, and PSD-95-positive cancer cells) in PCa cells that had been selected from specific localizations. GluN2D-mediated NMDAR signaling, including both subunits (GluN2D and GluN1) and PSD-95, was significantly upregulated in PCa cells with NI compared with PCa cells without NI (Figure 19-2#,3#,4#).

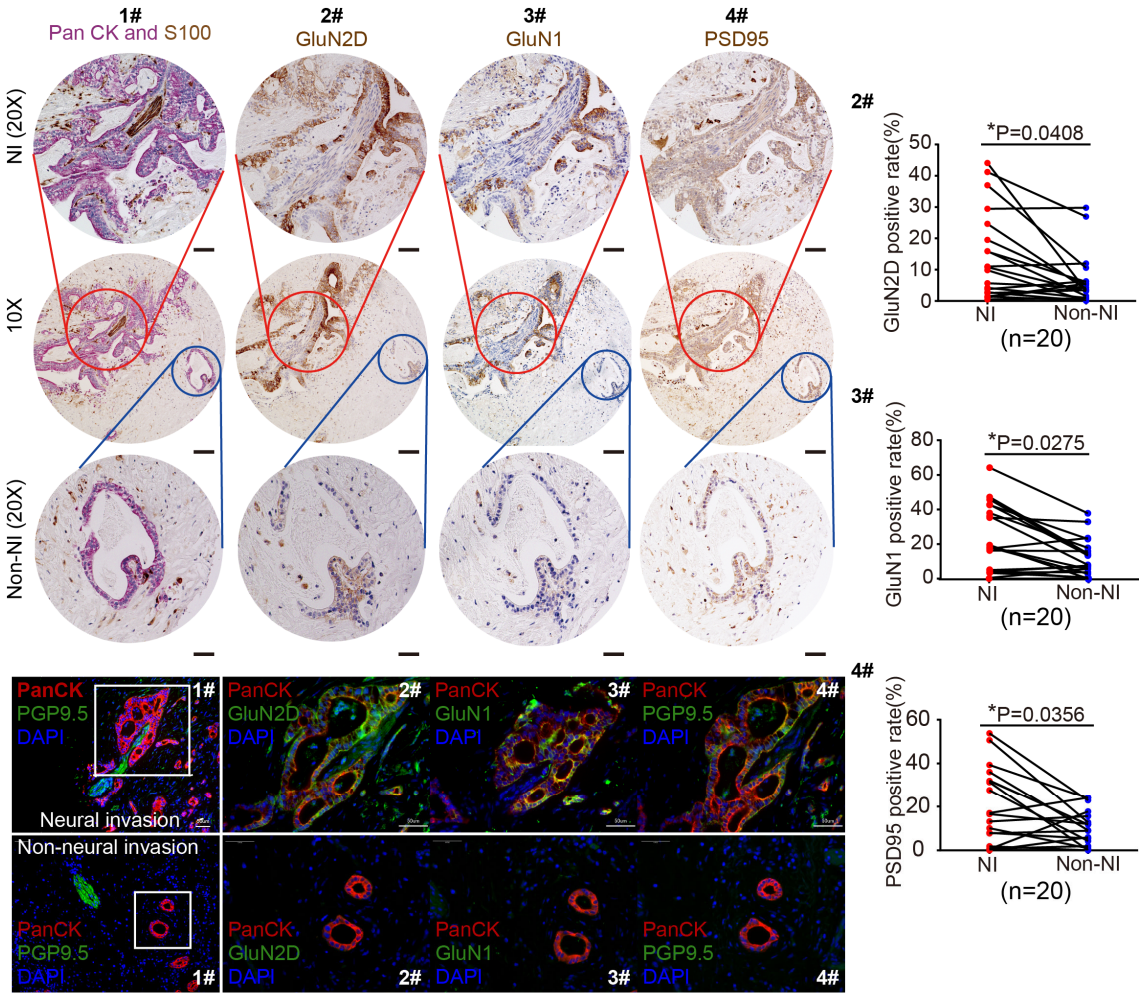

Figure 19. GluN2D-NMDAR signaling was highly activated in human pancreatic cancer tissues with neural invasion. (1#) Location of cancer cells whether with neural invasion or not by double staining with Pan CK and S100; Immunohistochemical staining of GluN2D (2#), GluN1 (3#), and PSD95 (4#) in 20 human pancreatic cancers. Results are expressed as mean ± SD. P-value was determined by unpaired t-test. Scale bar: 50μm.

We also immunostained the nerves of these PCa tissues with the presynaptic vesicle marker Syb 1 and the vesicular transport protein vGlut2 (for L-glutamate loading into synaptic

vesicles) using the same staining methods to first localize the nerves (Figure 20 a1). Consistent with the finding of active NMDAR signaling, including PSD-95, the immunostaining results revealed significantly higher levels of secreted Syb 1 and vGlut2 in nerves with invaded cancer cells comparison with those found in nerves without invading cancer cells (Figure 20 a2#,3# and b,c).

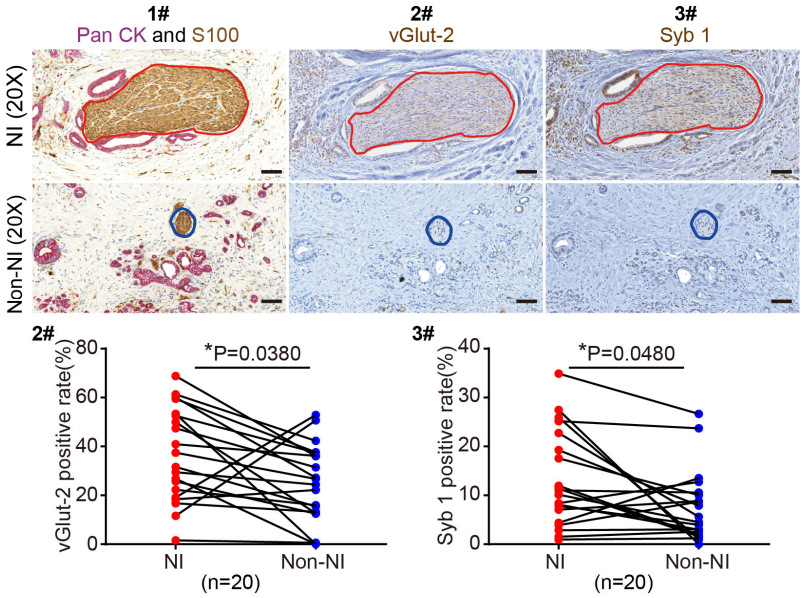

Figure 20. GluN2D-NMDAR signaling was highly activated in human pancreatic cancer tissues with neural invasion. (1#) Location of neurons whether invaded cancer cells or not by double staining with Pan CK and S100. Immunohistochemical staining of vGlut2 (2#) and Syb 1 (3#) in the nerves of 20 human pancreatic cancers. Results are expressed as mean ± SD. P-value was determined by unpaired t-test. Scale bar: 50μm.

4.6 GluN2D mediated Glutamate-NMDAR signaling in PCa cells is activated by DRG CM or coculture with neurons

The increased levels of GluN2D-mediated glutamate-NMDAR signaling molecules in neuroinvasive human PCa tissues broadly encouraged us to further investigate GRIN2D-mediated glutamate-NMDAR signaling in PCa cells.

4.6.1 Activation of GluN2D-NMDAR signaling by DRG CM

Based on our hypothesis, we treated PCa cell lines for 48 h with DRG CM, in which the L-glutamate concentration was prediluted to 0.5 μM after measurement of the secreted L-glutamate level. Compared with the results found for the untreated group, our real-time PCR and western blotting results confirmed increased expression of GRIN1 and GRIN2D in the neuroinvasive cancer cell lines SU.86.86, T3M4, and TPAC after DRG CM treatment, whereas a decrease or no significant change was detected in non-neuroinvasive cancer cells (Panc-1, Capan-1, KPC3039, and KPC3042). PSD-95, as a member of the MAGUK class of proteins at synapses[142,169,170], can anchor and cluster the trafficking and localization of L-glutamate NMDAR receptors[170-172] and then stabilize cell-surface NMDARs and inhibit their internalization[173-175]. Our western blotting results revealed that the expression of PSD-95 generally exhibited the same changes as GluN1 and GluN2D (Figure 21a-b and Figure 22a-b).

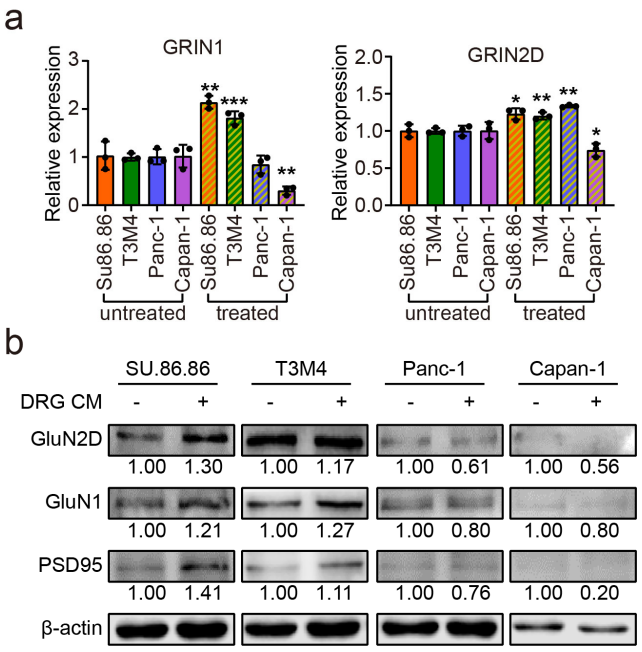

Figure 21. GluN2D-NMDAR signaling in pancreatic cancer cells was enhanced by the DRG conditioned medium. The relative expression levels of GRIN1 (encoded GluN1) and GRIN2D (encoded GluN2D) were performed in SU.86.86, T3M4, Panc-1 and Capan-1 by quantitative real-time

PCR (a) and western blotting (b) after treating for 48 hours with DRG conditioned medium, which was measured the secreted L-glutamate level and prediluted L-glutamate concentration to 0.5 μM. P-value was determined by unpaired t-test. n = 3 independent experiments.

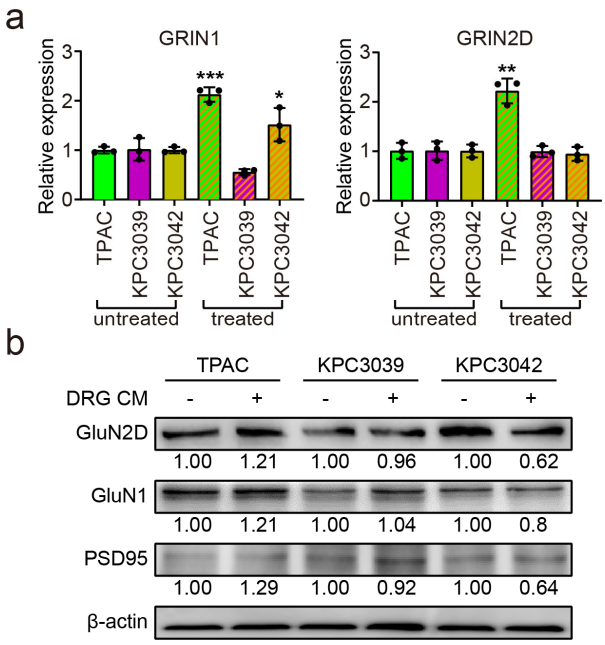

Figure 22. GluN2D-NMDAR signaling in pancreatic cancer cells was enhanced by the DRG conditioned medium. The relative expression levels of GRIN1 (encoded GluN1) and GRIN2D (encoded GluN2D) were performed in TPAC, KPC3039, and KPC3042 by quantitative real-time PCR (a) and western blotting (b) after treating for 48 hours with DRG conditioned medium, which was measured the secreted L-glutamate level and prediluted to contain 0.5 μM of L-glutamate. P-value was determined by unpaired t-test. n = 3 independent experiments.

4.6.2 Variation in the secretion of L-glutamate between cancer cells and DRG

As the ionotropic L-glutamate receptor, GRIN2D can be activated by L-glutamate, which is the most abundant excitatory neurotransmitter in DRG neurons and the ligand and major physiological agonist of NMDAR[80,81,176,177]. L-glutamate has long been associated with cancer[81]. To investigate the L-glutamate levels in cancer cells and DRG neurons, we first established monoculture and cocultures of cancer cells and DRG neurons (Figure 23a), and 48 hours later, cell lysates and supernatants were collected from the monocultures of the cancer cells and DRG neurons and from the coculture of cancer cells and DRG neurons to measure the L-glutamate levels.

Our results for the human cell lines revealed that the secreted L-glutamate concentrations in the supernatant and cell lysates from the cocultures of the neuroinvasive human cancer cells SU.86.86 and T3M4 were higher than those obtained with the monocultures of DRG neurons and SU.86.86 and T3M4 cells. However, compared with the results obtained with the monoculture of DRG neurons, the L-glutamate level in the supernatant and cell lysates of the Panc-1 coculture was notably reduced and increased, respectively (Figure 23b). Here, Our results especially found the elevated L-glutamate level in the cell lysates from the coculture of neuroinvasive cancer cells and DRG was significantly higher than the sum of the levels found with the two corresponding monocultures, not simple sum of these two corresponding monocultures.

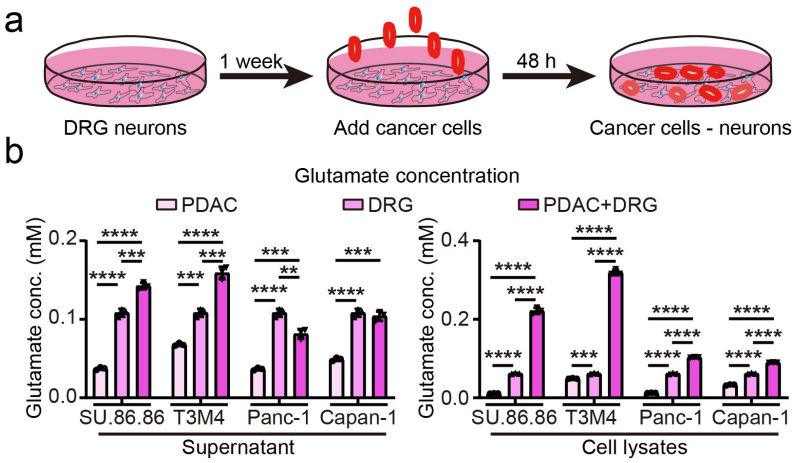

Figure 23. Secretion variation of L-glutamate between cancer cells and DRG. (a) Schematic illustration of cancer cell–primary DRG neuron co-culture system and experimental design. (b) Secreted L-glutamate levels in DRG conditioned medium, supernatant and cell lysates of monoculture cancer cells (Human PDAC cell lines: SU.86.86, T3M4, Panc-1, Capan-1) and cocultured cancer cell-DRG after culturing for 48 hours; no starve treatment before the experiments. P-value was determined by unpaired t-test. n = 3 independent experiments.

Based on the above-described findings, the elevated L-glutamate levels in the cocultures of neuroinvasive cancer cells and DRG neurons might predict the presence of pseudotripartite synapses because the L-glutamate levels in the cocultures were not simply as high as of two monocultures.

4.6.3 Activation of GluN2D-NMDAR signaling by direct contact with DRG neurons

Furthermore, to investigate the influences of the GluN2D levels after the direct contact of cancer cells with DRG neurons, we cocultured cancer cells and DRG neurons, as illustrated in Figure 23a, and in contrast to the previous experiments, the cells were starved overnight before the coculture. Similar results of elevated levels of GRIN2D (encoding GluN2D) were observed in the neuroinvasive cancer cells SU.86.86, T3M4, and TPAC after coculture with DRG neurons for 48 hours, as determined by real-time PCR and western blotting; however, the decreasing or without significant changes were presented in non-neuroinvasive cancer cells (Panc-1, Capan-1, KPC3039, and KPC3042) (Figure 24a-24b and Figure 25a-25b). Nevertheless, the levels of GRIN1 (encoding GluN1) exhibited reductions or no significant changes accompanied by the changes in GRIN2D (encoding GluN2D) only in Panc-1 and Capan-1 cells. Decreased GluN1 levels but increased GRIN1 gene levels were found in the KPC3039 and KPC3042 cocultures (Figure 24b and Figure 25b). Western blotting revealed that the variations in the PSD-95 levels were similar to those found for GluN2D (Figure 25).

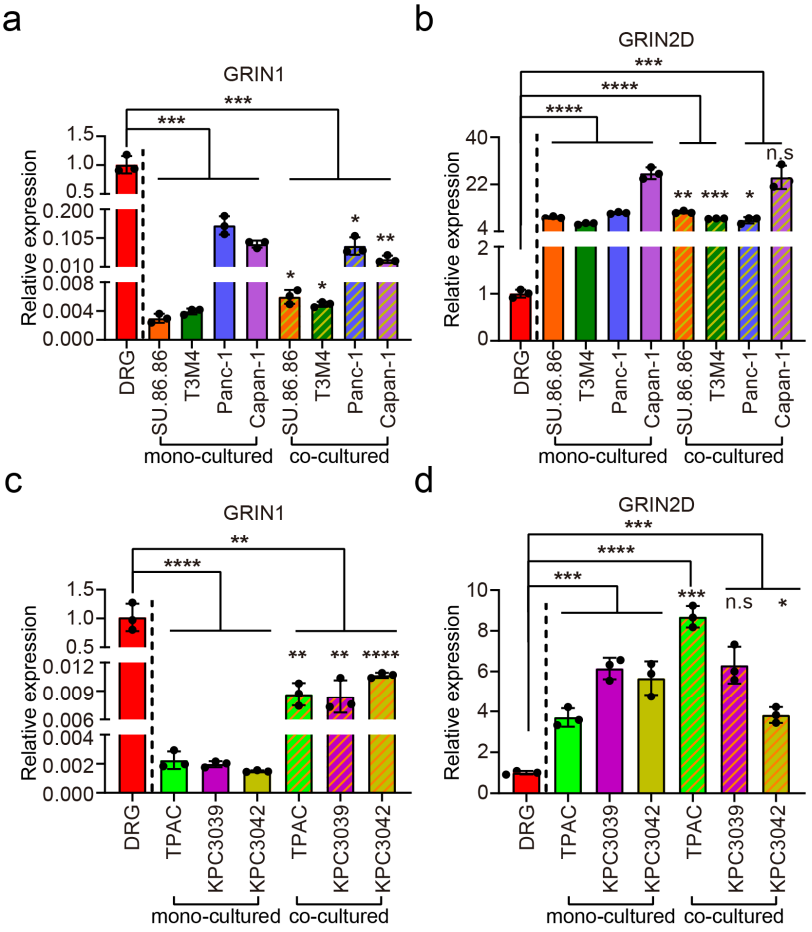

Figure 24. GluN2D-NMDAR signaling in pancreatic cancer cells was activated in co-culture with neurons. The relative expression levels of GRIN1 and GRIN2D were performed in pancreatic cancer cell lines by quantitative real-time PCR after directly coculturing with DRG neurons - a: SU.86.86, T3M4, Panc-1, and Capan-1; b: TPAC, KPC3039, KPC3042. P-value was determined by unpaired t-test. n = 3 independent experiments.

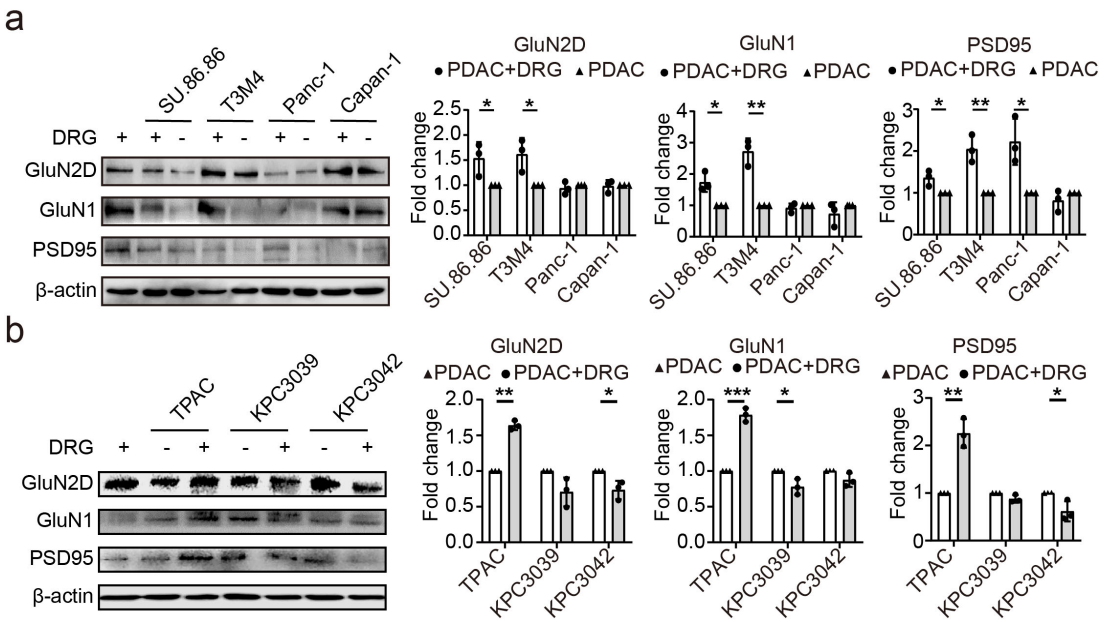

Figure 25. GluN2D-NMDAR signaling in pancreatic cancer cells was activated in co-culture with neurons. The relative expression levels of GluN1, GluN2D and PSD95 were performed in pancreatic cancer cell lines by western blotting after directly coculturing with DRG neurons - a: SU.86.86, T3M4, Panc-1, and Capan-1; b: TPAC, KPC3039, KPC3042. P-value was determined by unpaired t-test. n = 3 independent experiments.

To further confirm the activation of GluN2D-NMDAR signaling at the cancer cell level in PCa tissues, we confirmed that the expression levels of vGlut-2 and Syb 1, as hypothetical signal-transduction molecules, were basically consistent with those found for GuN2D in human PCa cell lines with the exception of Syb 1 in the Su.86.86 cell line (Figure 26).

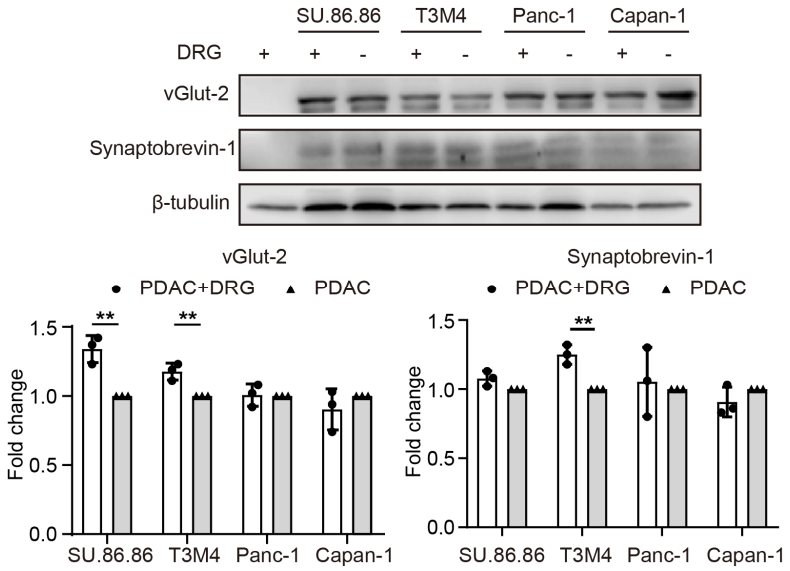

Figure 26. GluN2D-NMDAR signaling in pancreatic cancer cells was activated in co-culture with neurons. The relative expression levels of vGlut-2 and Synaptobrevin-1 were performed in pancreatic cancer cell lines by western blotting after directly coculturing with DRG neurons in SU.86.86, T3M4, Panc-1, and Capan-1. P-value was determined by unpaired t-test. n = 3 independent experiments.

In view of the typical phenotypic characteristics caused by gene-level interference by GRIN2D siRNA and protein-level pharmacological antagonism of the GluN2D antagonist UBP145, we selected SU.86.86 and Capan-1 for the subsequent experiments. Initially, we verified that L-glutamate exerts no significant effect on the senescence of these two cell lines via FACS (Figure 27).

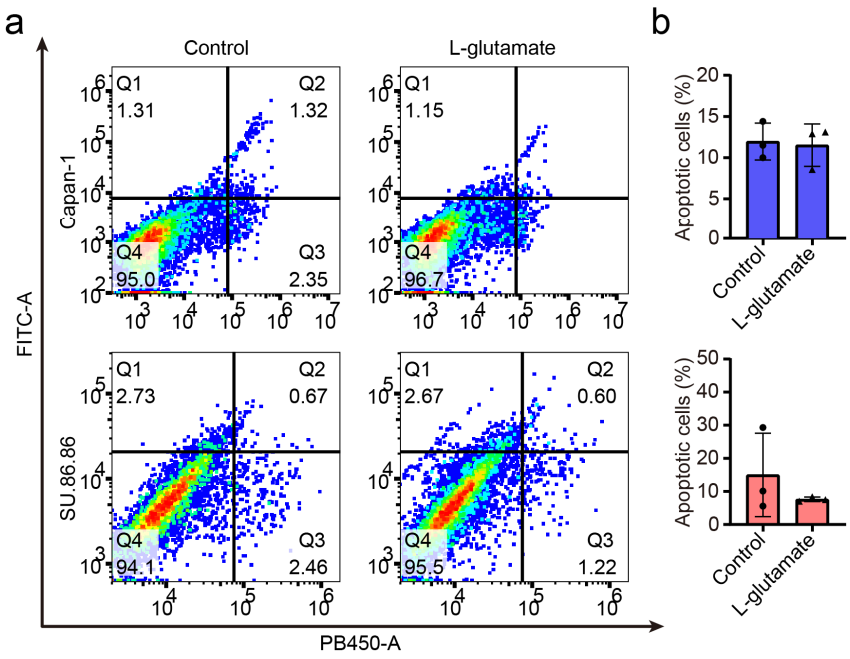

Figure 27. Cell apoptosis in pancreatic cancer cells were not involved in L-glutamate treatment. a. Representative dot-plot diagrams and summary data of flow cytometry; b. Apoptotic cell percentage in SU.86.86 and Capan-1. Values were presented as mean ± SD from triplicate independent experiments. P-value was determined by unpaired t-test.

Then, we cocultured SU.86.86 and Capan-1 cells with DRG to perform immunocytochemical staining and then found that the expression levels of signal-transduction molecules belonging to the glutamate-NMDAR axis (GRIN2D, GRIN1, and PSD-95) in SU86.86 cells in direct contact with DRG neurons and those of Syb 1 and vGlut-2 on axons were notably higher than those found with the SU.86.86 monocultures. However, these alterations were not observed between the Capan-1 cell monocultures and cocultures (Figure 28).

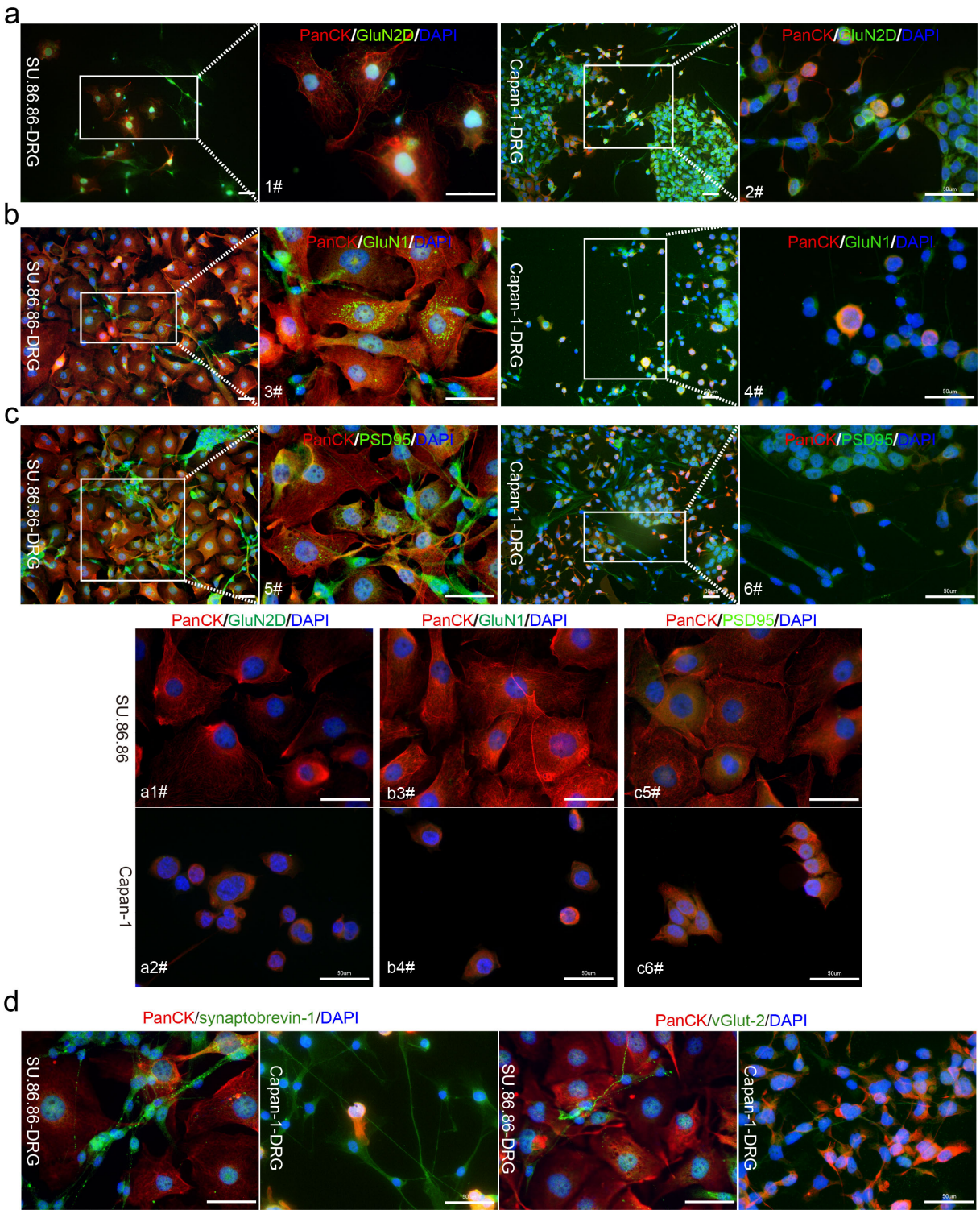

Figure 28. GluN2D-NMDAR signaling was highly activated in neuroinvasive cancer cell. After coculturing with DRG, the expression levels of transduction molecules of the L-glutamate-NMDAR signaling pathway were prominently up-regulated in neuroinvasive SU.86.86 cancer cell in comparison to the non-neuroinvasive Capan-1 cancer cell such as GluN2D (a), GluN1 (b), PSD95 (c), vGlut-2 and synaptobrevin-1 (d). Scale bar: 50μm

To further investigate the influence of GluN2D on GluN2D-NMDAR signaling activation, a western blotting analysis was performed, and the results showed that the levels of GluN2D, GluN1, and PSD-95 were synchronously downregulated in the SU.86.86 cell line after GRIN2D siRNA transfection but not in Capan-1 cells, which showed that the expression levels of GluN1 and PSD-95 appear to be unrelated to the level of GluN2D. It should be noted that these two types of cell lines were chemically stimulated in fresh medium containing 0.5 μl of L-glutamate (Figure 29).

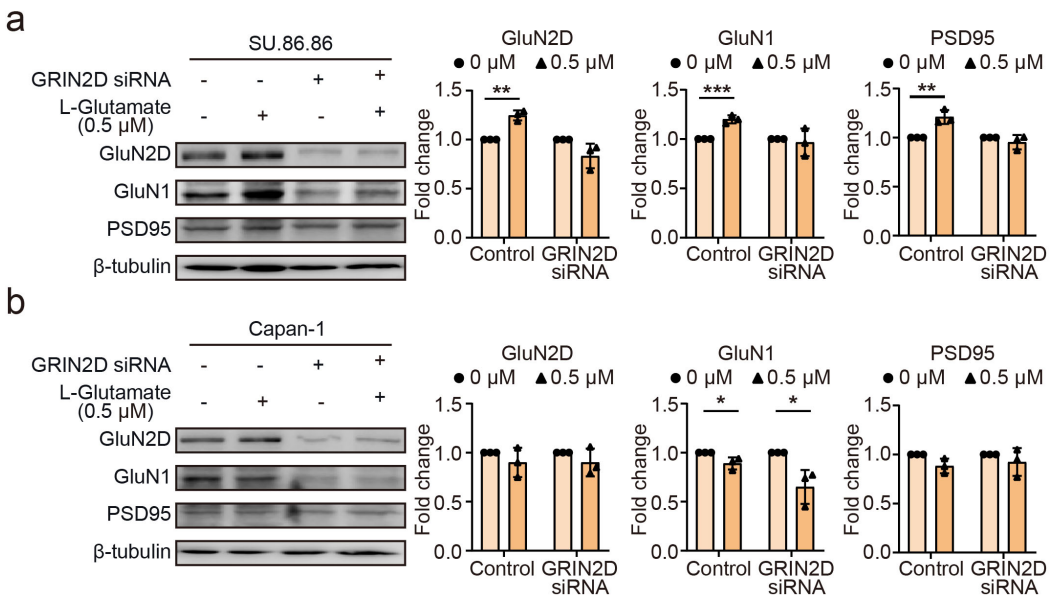

Figure 29. GluN2D-NMDAR signaling in pancreatic cancer cells after GRIN2D siRNA transfection was activated by L-glutamate. The relative expression levels of GluN1, GluN2D and PSD95 were performed in SU.86.86 (a) and Capan-1 (b) after GRIN2D siRNA transfection by western blotting. P-value was determined by unpaired t-test. n = 3 independent experiments.

4.7 EZH2 is a transcription factor (TF) that mediates GRIN2D expression through the E2F-1-Rb signaling pathway

4.7.1 EZH2 is the TF that regulates GRIN2D expression

After searching the ARCHS4 database (https://maayanlab.cloud/archs4/gene/GRIN2D), we found enhancer of zeste homolog 2 (EZH2), which is the enzymatic catalytic subunit of polycomb repressive complex 2 (PRC2), to be the most likely relevant TF regulating GRIN2D expression in human cells. We also found that only two subtypes of GRIN1 and GRIN2D in NMDAR are coexpressed and positively correlated with the TF EZH2 in PCa by TCGA through bioinformatic analyses (Figure 30a and 30b). We performed western blotting and demonstrated that GluN2D and EZH2 exhibited synchronous variation at the protein level after treatment with L-glutamate in both human and mouse PCa cell lines, and this finding revealed that L-glutamate can synchronously increase the GluN2D and EZH2 levels in neuroinvasive PCa cell lines but not in non-neuroinvasive PCa cell lines (Figure 30c-1# for human cell lines and 30c-2# for mouse cell lines). To clarify the upstream TF, we conducted chromatin immunoprecipitation (ChIP) PCR assays. The results revealed that EZH2 directly bound to the GRIN2D promoter in the SU.86.86 cell line and that treatment with 0.5 μM L-glutamate increased the enrichment of EZH2 on the GRIN2D promoter, the expression of which was also upregulated by 0.5 μM L-glutamate (Figure 30d), two pairs of primers were performed to search the EZH2 binding sites located at GRIN2D promoter from hTFtarget dataset (Figure 30e).

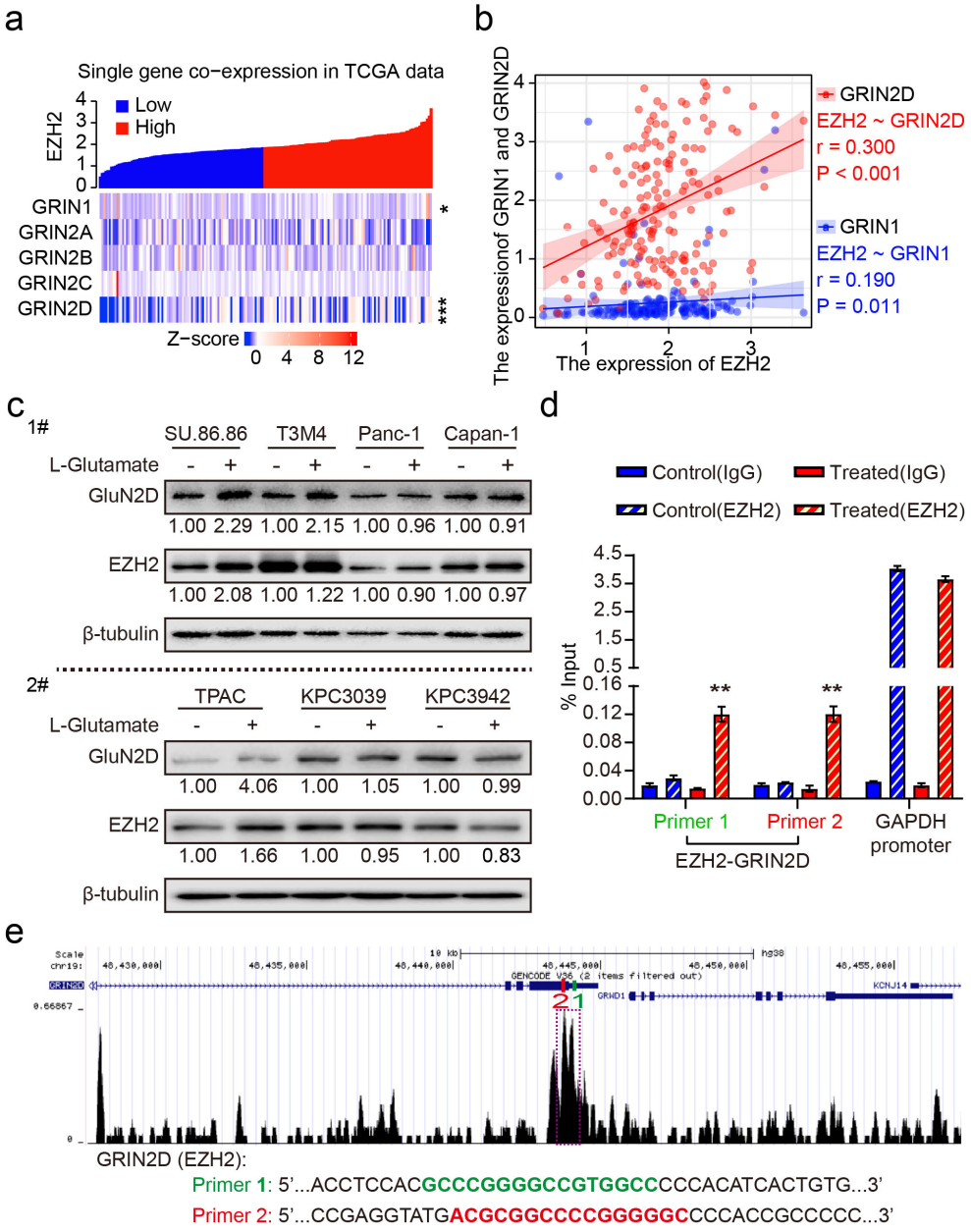

Figure 30. EZH2 as the transcription factor regulating GRIN2D expression. (a) Comparison of mRNA co-expression of EZH2 and NMDRA subtypes (GRIN1 and GRIN2 (2A/2B/2C/2D)) in human pancreatic cancer. P-values were computed using Spearman. (b) Comparison of mRNA co-expression among EZH2 and GRIN1 and GRIN2D in human pancreatic cancer. P-values were computed using Spearman. (c) The relative expression levels of GluN2D and EZH2 in pancreatic cancer cells were performed by western blotting after treating with L-glutamate, which include SU.86.86, T3M4, Panc-1, and Capan-1; TPAC, KPC3039, KPC3042. (d) ChIP-PCR assays showed EZH2 binding to the GRIN2D gene promoter after treating with L-glutamate in SU86.86 cell lines, IgG was used as a negative control, GAPDH was used as a positive control which was bound by Anti-RNA Polymerase II Antibody from the manufacturer's instructions. (e) The binding site of EZH2 to GRIN2D gene. P-value was determined by unpaired t-test. n = 3 independent experiments.

To further confirm the connection between EZH2 and L-glutamate in PCa cells, we used the SU.86.86 and Capan-1 cell lines for experiments, treated these cells with 0.5 μM L-glutamate and CM (containing 0.5 μM L-glutamate) and then performed immunocytochemistry staining. We found that EZH2, which is mainly expressed in the nucleus, was upregulated by L-glutamate and CM in SU.86.86 cells but not Capan-1 cells (Figure 31).

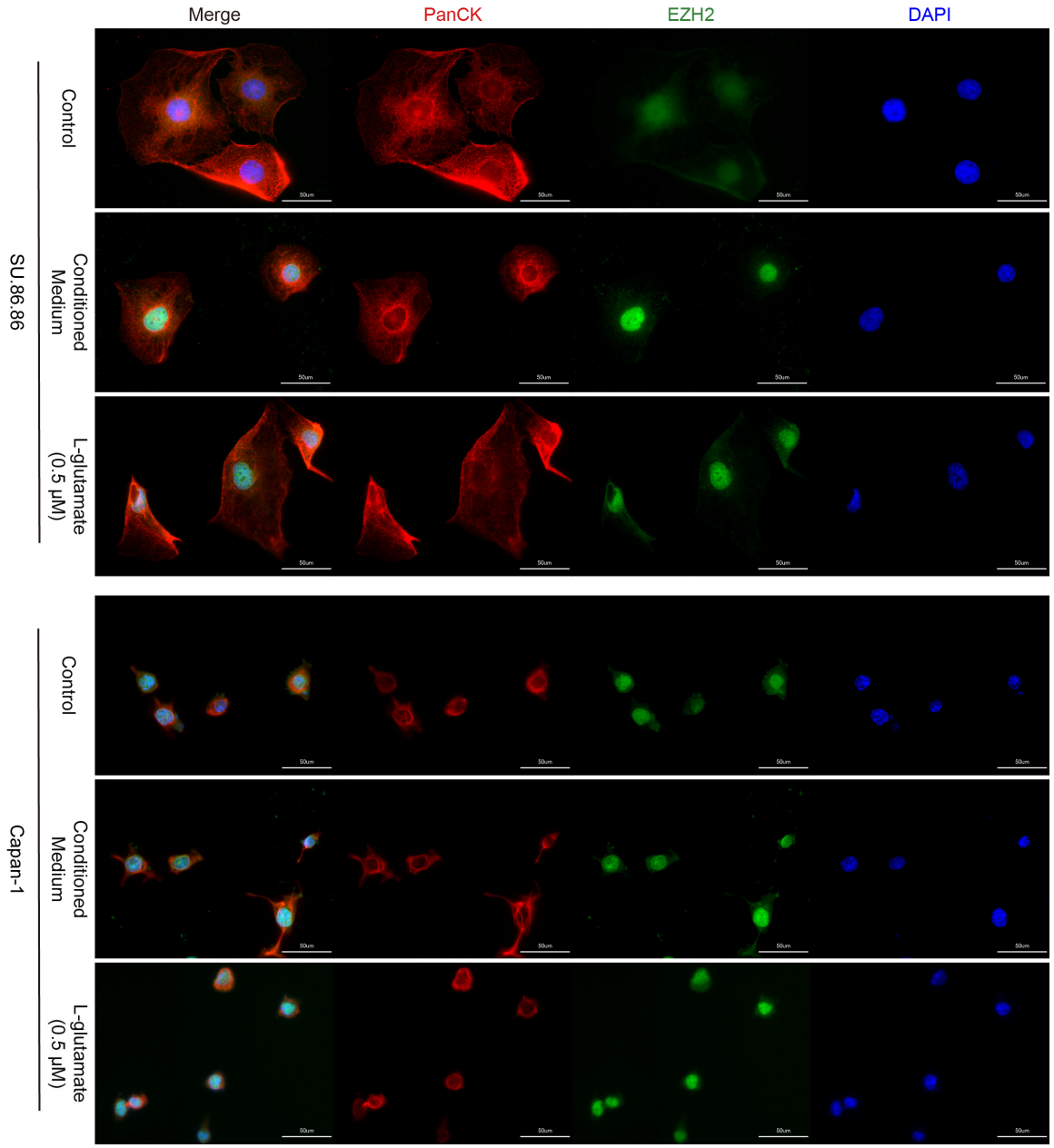

Figure 31. EZH2 as the transcription factor for GRIN2D expression is regulated by L-glutamate . Compared to the non-neuroinvasive Capan-1 cell lines, EZH2 as the transcription factor for GRIN2D is upregulated by L-glutamate in neuroinvasive SU.86.86 cell lines, which is the ligand of GluN2D. Scale bar: 50μm.

After checking the EZH2 transfection efficacy in SU.86.86 cells via PCR and western blotting (Figure 32a), SU.86.86 cells were subjected to EZH2 siRNA transfection and then treated with 0.5 μM L-glutamate and DRG CM. As demonstrated by PCR and western blotting, the GRIN2D levels were significantly lower in the EZH2 siRNA-transfected group than in the non-transfected group, and this finding was obtained with both the L-glutamate and DRG CM treatments (Figure 32b and c).

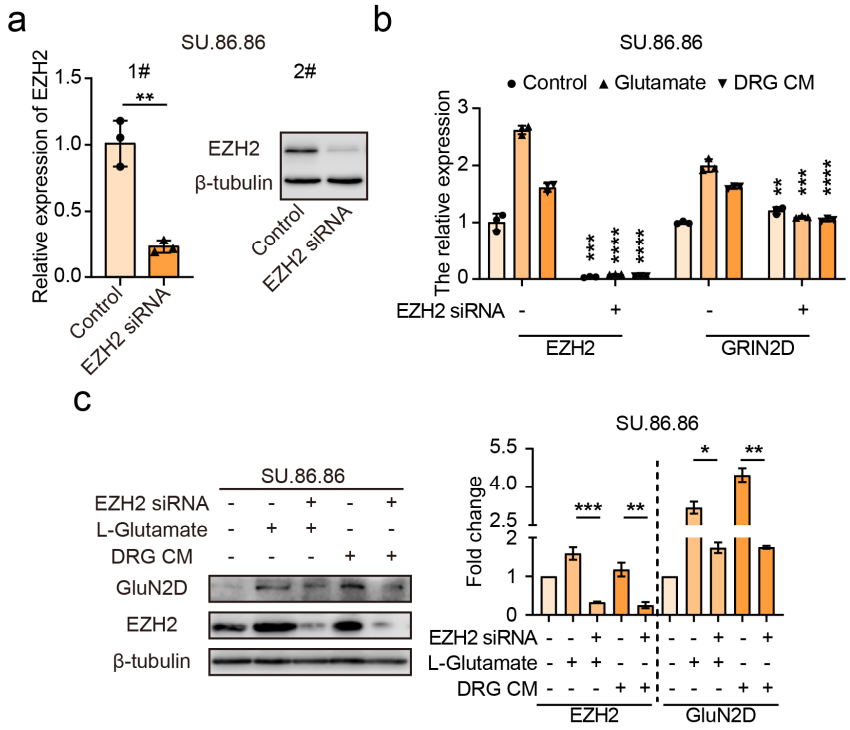

Figure 32. GRIN2D expression levels were down-regulated after EZH2 siRNA transfection. (a) The efficacy of EZH2 siRNA transfection in SU.86.86 via PCR (1#) and western blotting (2#). (b) and (c)The relative expression levels of GluN2D and EZH2 in SU.86.86 after EZH2 siRNA transfection (PCR and western blotting) in L-glutamate (0.5 μM) and DRG CM group. P-value was determined by unpaired t-test. n = 3 independent experiments.

4.7.2 EZH2 mediates GRIN2D expression through the E2F-1-Rb signaling pathway

EZH2 can suppress gene transcription by catalyzing the trimethylation of histone 3 lysine 27 (H3K27me3) and can also be involved in facilitating cell proliferation by inhibiting cyclin-dependent kinase (CDK) inhibitors, particularly CDKN2A (p16INK4a, p14ARF), which is the canonical target and tumor-suppressor gene, as mentioned above[178,179]. Moreover, p16INK4a silencing to reinstate tumorigenesis requires H3K27 trimethylation at an early epigenetic phase[180], and high levels of H3K27 trimethylation were found at the P16INK4a promoter, which led to a corresponding reduction in the p16INK4A levels[181]. CDK4, as the major oncogenic driver and regulator among the cyclin-dependent kinase family[182], plays a pivotal and essential role in normal cell proliferation as a G1 serine/threonine kinase[183] by driving the progression of cells into the DNA synthetic (S) phase of the cell division cycle[184]. After binding with the regulatory cyclin subunit cyclin D1, activated CDK4-cyclin D1 complexes phosphorylate and repress the tumor-suppressor protein retinoblastoma (RB); Rb phosphorylation can result in release of the TF E2F-1, which can strongly bind to dephosphorylated RB; and the activation of E2F-1 further regulates the cell cycle transition from the G1 phase to the S phase[185]. Blocking the interaction between CDK4 and RB can decrease the phosphorylation of RB. Furthermore, dephosphorylated RB suppressed E2F-1 activity after binding with E2F-1 and thereby maintains cell cycle arrest in cancer cells. However, E2F-1 is a key TF for EZH2 expression[178,186-188], which upregulates the EZH2 levels in a dose-dependent manner but is not influenced by E2F4 or E2F6 overexpression[188].

To confirm whether EZH2 is involved in the classic E2F1-Rb signal pathway, we focused on the relationship between EZH2 and E2F1. First, we assessed the expression level of EZH2 and E2F1 in human PCa profiled by TCGA through bioinformatic analyses, which presented the co-expressed and positively correlation for EZH2 and E2F1 (Figure 33a). Then, we found

that EZH2 levels were significantly down-regulated after silencing E2F1 by E2F1 siRNA transfection in SU.86.86 cells (Figure 33 b). We next evaluated E2F1 recruitment to the EZH2 promoter by ChIP-PCR in SU.86.86 cell line after the presence or absence of E2F1 knockdown, E2F1 knockdown notably reduced E2F1 enrichment at the EZH2 promoter region (Figure 33c), three pairs of primers were performed to search the E2F1 binding sites located at EZH2 promoter from hTFtarget dataset(Figure 33d).

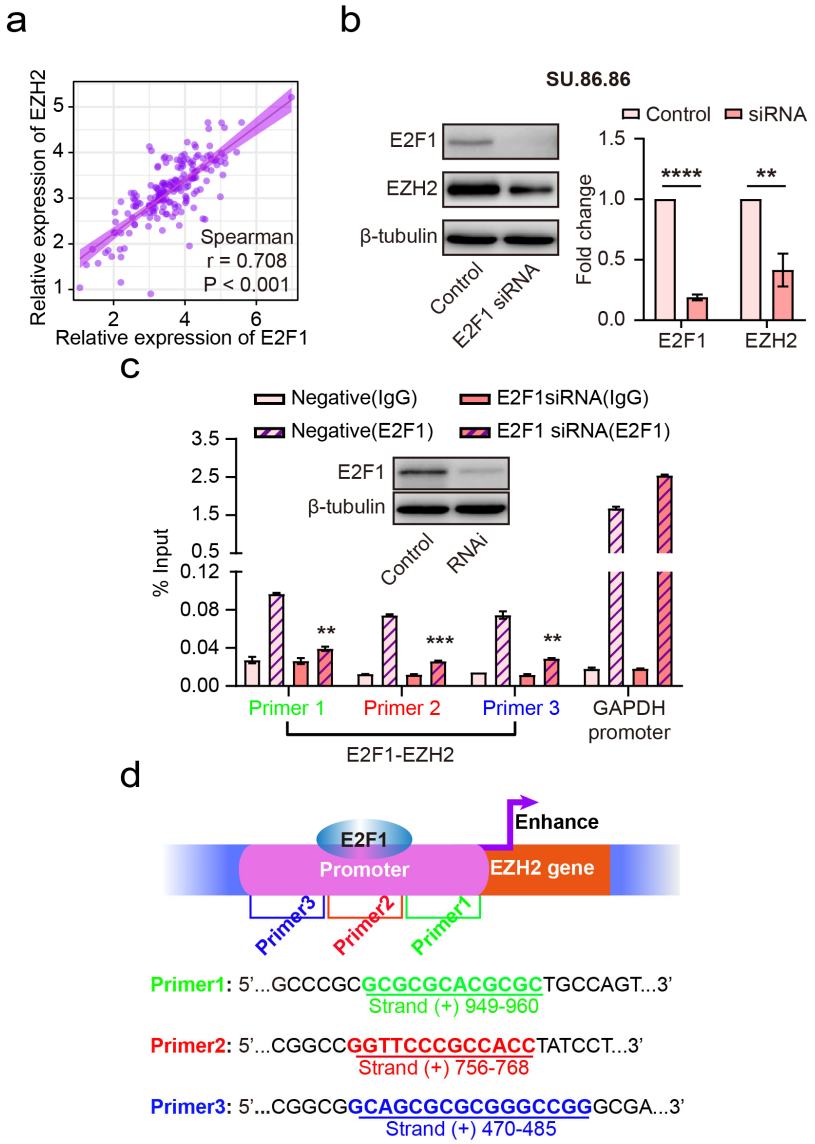

Figure 33. E2F1 as the transcription factor regulating EZH2 expression. (a) Comparison of mRNA co-expression among EZH2 and E2F1 by TCGA in human pancreatic cancer. P-values were computed using Spearman. (b) The relative expression levels of EZH2 in Su.86.86 cell line were performed by western blotting after the silencing E2F1 by E2F1 siRNA. (c) ChIP-PCR assays showed E2F1 binding to the EZH2 gene promoter in SU.86.86 cell line, IgG was used as a negative control,

GAPDH was used as a positive control which was bound by Anti-RNA Polymerase II Antibody from the manufacturer's instructions. (d) The binding site of E2F1 to EZH2 gene. P-value was determined by unpaired t-test. n = 3 independent experiments.

Combined the above mentioned results, this hypothesized EZH2-E2F-1-Rb signaling pathway can thus be involved in the regulatory mechanism upstream of GRIN2D (Figure 34a). Here, we first analyzed the synchronous gene-level changes in cardinal signaling molecules, including EZH2, E2F-1, CDKN2A and CDK4, belonging to the potential EZH2-E2F-1-Rb signaling pathway in neuroinvasive (SU.86.86) and non-neuroinvasive (Capan-1) cells after treatment with L-glutamate. The major signaling molecules EZH2, E2F-1, CDK4, and CDKN2A of this classic E2F-1-Rb pathway were primarily upregulated and downregulated respectively in SU.86.86 cells after stimulation with L-glutamate, in line with the pattern shown in the schematic illustration (Figure 34a), but did not exhibit any changes in the Capan-1 cell line (Figure 34b). To further investigate the probability of this pathway being involved in mediating the mechanisms upstream of GRIN2D in NI, SU.86.86 and Capan-1 cells were treated with L-glutamate, and the expression of the signaling molecules involved in the EZH2-E2F-1-Rb pathway was checked by western blotting. Here, we found that the protein levels of EZH2, E2F-1, CyclinD1, and CDK4 were markedly increased in SU.86.86 cells after treatment with L-glutamate, whereas CDKN2A (P16) was notably reduced. However, no changes were detected in the Capan-1 cell line (Figure 34c).

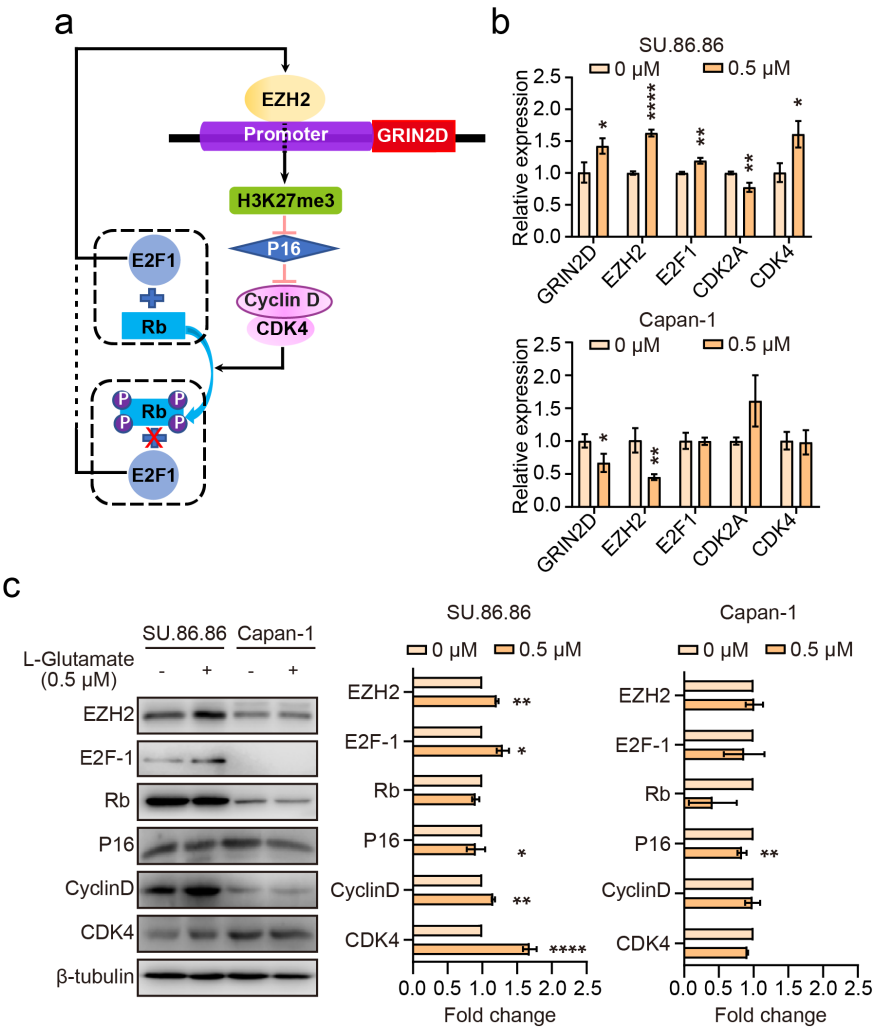

Figure 34. EZH2-E2F-1-Rb signaling pathway for the upstream mechanisms of GRIN2D. (a) Schematic diagram of the EZH2-E2F-1-Rb signal pathway. (b) The relative expression of GRIN2D, EZH2, E2F-1, CDKN2A and CDK4 in the potential EZH2- E2F-1-Rb signaling pathway in SU.86.86 and Capan-1 cells after treating with L-glutamate by quantitative real-time PCR. (c) After treatment with L-glutamate, the expression of the signal molecules in the EZH2- E2F-1-Rb signaling pathway in SU.86.86 and Capan-1 by western blotting. P-value was determined by unpaired t-test. n = 3 independent experiments.

Compared with the acetylation of H3K27, the expression levels of the trimethylation of H3K27 were significantly increased in the neuroinvasive SU.86.86 cancer cells after treatment with L-glutamate, but no marked changes were detected in the non-neuroinvasive Capan-1 cancer cells (Figure 35a). Similarly, compared with the level of Rb and the phosphorylation of Ser807 in Rb, the phosphorylation of Rb at Ser780 was unusually upregulated in the SU.86.86

cell line after L-glutamate treatment, and this finding was not detected in the Capan-1 cell line (Figure 35b).

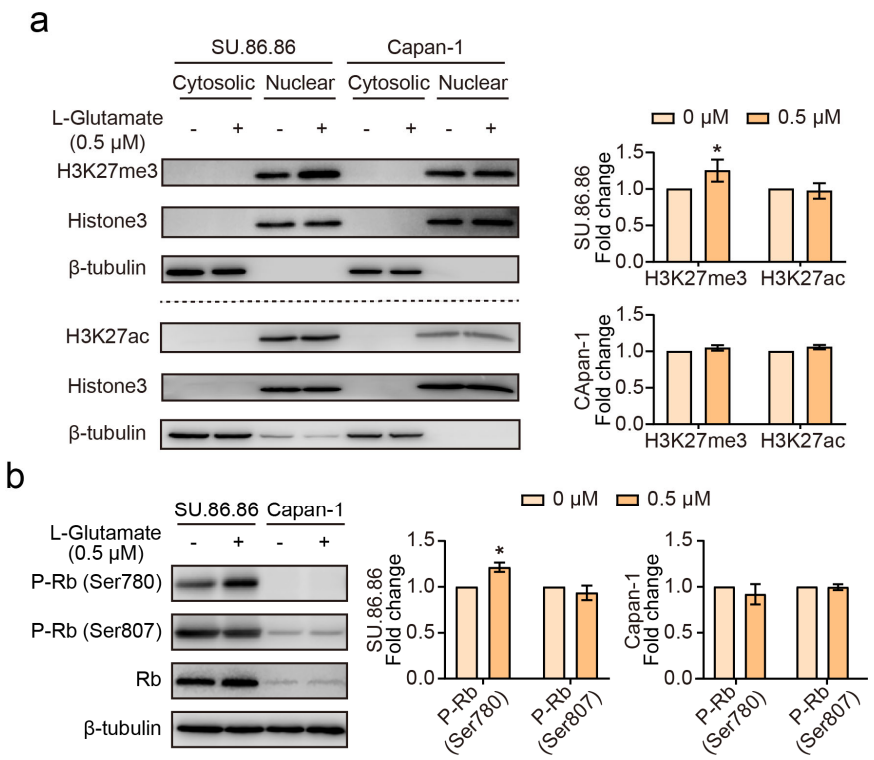

Figure 35. The trimethylation of H3K27 and phosphorylation of Rb in EZH2-E2F-1-Rb signaling pathway for the upstream mechanisms of GRIN2D. After treatment with 0.5 μl of L-glutamate, the expression level of H3K27me3 (a) and P-Rb (ser780) (b) was upregulated in neuroinvasive SU.86.86 cancer cells in comparison to non-neuroinvasive Capan-1 cancer cells, as detected via western blotting. P-value was determined by unpaired t-test. n = 3 independent experiments.

Based on the above mentioned findings regarding the signaling pathway induced by 0.5 μM L-glutamate treatment in SU.86.86 and Capan-1 cells, we also verified whether DRG CM treatment exerted a homologic effect on this hypothetical signaling pathway in these two cell lines. Our results with DRG CM treatment were the same as those obtained with L-glutamate (Figure 36a). It has been reported that EZH2 is required for Rb phosphorylation[178], and the phosphorylation of Rb (Ser780) can promote the dissociation of E2F from Rb-E2F complexes [189,190]. Based on the consistent effects of L-glutamate and DRG CM on this EZH2-E2F1-Rb signaling pathway in SU.86.86 and Capan-1 cells, to further confirm the relationship of EZH2 with E2F1 and RB, we performed a western blotting analysis and confirmed that the expression

levels of E2F1 and P-Rb (Ser780) were also significantly downregulated in the L-glutamate- and DRG CM-treated groups after the silencing of EZH2 by EZH2 siRNA transfection in SU.86.86 cells, but no variations in the Rb and P-Rb (Ser807) levels were detected (Figure 36b).

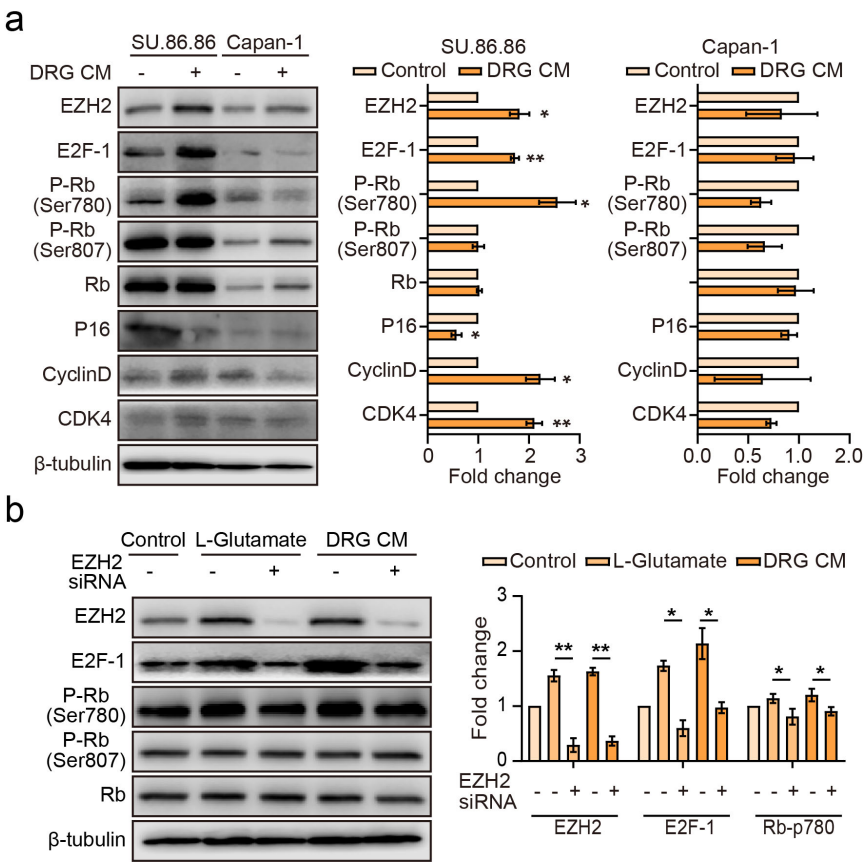

Figure 36. The hypothesized pathway signalling after the DRG CM treatment . a. After treatment with DRG CM, the expression of the signal molecules in the EZH2- E2F-1-Rb signaling pathway in SU.86.86 and Capan-1 by western blotting; b. The levels of EZH2, E2F1, and Rb after EZH2 siRNA transfection in SU.86.86. by western blotting. P-value was determined by unpaired t-test. n = 3 independent experiments.

In summary, our findings indicate that the above-described EZH2-E2F-1-Rb signaling pathway is closely linked to the mechanisms upstream of GRIN2D in neuroinvasive but not non-neuroinvasive PCa cells.

5.0 Discussion

The present study investigated the involvement of glutamatergic receptor signaling in NI in PCa and focused on the role of GluN2D-containing NMDARs. In this study, we found that GRIN2D could be involved in the migration and invasion of neuroinvasive but not non-neuroinvasive PCa cells mediated by L-glutamate or DRG CM, and these phenotypic features were completely reversed after GluN2D antagonist treatment and GRIN2D siRNA transfection in neuroinvasive but not non-neuroinvasive PCa cells. The signal-transduction molecules involved in glutamate-GluN2D-NMDAR signaling could be activated and upregulated by DRG or DRG CM.

GRIN2D, the members of whose family mainly function in neuronal synaptic transduction in the central nervous system[191-193], represents a promising immunologically target of colorectal cancer (CRC) therapies, as demonstrated by the finding that the vaccination of murine models against GRIN2D inhibited CRC tumor growth and impaired angiogenesis[194]. GRIN2D has also been identified as a candidate cancer gene with somatic mutations that potentially impact protein function in human breast cancer and strengthen the progression of breast cancer[195]. Inspired by these studies, we performed a bioinformatics analysis and found that GRIN2D is the receptor gene showing the strongest relationship to PCa among the members of the glutamatergic receptor gene family, and the elevated level of only GRIN2D among NMDARs was particularly significantly related to PCa, particularly the T and N stages

of the TNM status of PCa, which represent the progressive and invasive features of human cancer, respectively. GluN1, as the mandatory subunit of functional heterotetrameric NMDA receptors, is encoded by GRIN1, which showed a particularly significant and positive correlation with GRIN2D in human PCa based on our bioinformatics results. However, human PCa reportedly displays a nearly 100% frequency of NI[153,196], which indicates an association between the GluN1/GluN2D-containing heterotetrameric NMDA receptor and NI in PCa.

Previous studies have shown that the upregulation of glutamatergic receptors is continually detected, particularly in cancer cells, and the upregulation of these receptors can mediate the specific phenotypic features of cancer cells, which included uncontrollable proliferation, invasion and migration. The autocrine and/or paracrine secretion of L-glutamate can promote PCa cell growth via the KRAS metabolic pathway[197] and can also accelerate cell invasion and migration via glutamatergic receptor activation stimulated by L-glutamate. mGluR1 has been proposed as a target gene in therapy for metastatic melanoma, the growth and invasion of which are promoted by L-glutamate through activation of the mGlu1 receptor[198]. L-glutamate also increases the invasion and migration of PCa cells by activating AMPA receptors, including GRIA2[86] and GRIA3[199], and this activation can enhance K-ras-MAPK activity and further downstream phosphorylation of p38 and p44/42. Pancreatic neuroendocrine tumors (PNETs) can hijack neuronal GluN2B to mediate the

glutamate-NMDAR signaling circuit to facilitate cancer growth and invasion, and this circuit is induced by autocrine L-glutamate secretion evidently activated by pressure drop and fluid flow and is accompanied by the transport of L-glutamate to the GluN2 ligand site of the cancer cell surface, NMDAR phosphorylation and subsequently the activation of downstream signaling[80]. Consistently, breast-to-brain metastasis (B2BM) cells are also involved in the autocrine glutamate-NMDAR signaling pathway[161]. These studies have uncovered the essentiality of glutamatergic receptors in the migration and invasion of a variety of cancer cells, but the roles of glutamatergic receptors in NI in PCa remain elusive.

In our study, we found that the levels of GluN2D (encoded by GRIN2D) are changed by L-glutamate, the level of which can be gradually upregulated and then downregulated, or exhibit an increasing tendency at both the RNA and protein levels in neuroinvasive cell lines but not in non-neuroinvasive cell lines. Moreover, the corresponding changes in the GRIN1 levels were concomitant with the changes in the GRIN2D levels, and differences in the expression levels were obtained with an L-glutamate concentration of approximately 0.5 μM, which is generally consistently with the EC50 of L-glutamate to GluN2D receptors[89,120]. Our results then showed that the improved migration and invasion capabilities stimulated or chemoattracted by L-glutamate and DRG CM were clearly reversed in neuroinvasive cancer cells after pretreatment with the GluN2D antagonist UBP145 or transfection with GRIN2D siRNA,

but this finding was not found in non-neuroinvasive cancer cells. These results demonstrated that GluN2D-containing NMDARs were involved in and play a vital role in the migration and invasion of neuroinvasive PCa cells.

NMDARs are clustered at postsynaptic membranes by PSD-95, and this clustering is mediated by the common motif of L-glutamate serine (aspartate/L-glutamate) valine (ES(D/E)V)[200] of all NR2 subunit C-termini and then propagates the L-glutamate responses intracellularly via the interactions between L-glutamate receptors and downstream signaling molecules[150]. The key postsynaptic signal-transducing protein PSD-95 was highly expressed in B2BM cells packing brain metastases, which is in agreement with active NMDAR signaling[161]. We obtained consistent results showing that the PSD-95 level was significantly positive related to GluN1/GluN2D-containing NMDARs in not only PCa tissues with NI but also neuroinvasive cancer cells activated by DRG CM or L-glutamate via the GluN2 receptor. We also found that the presynaptic neuron marker vGlut2 and the presynaptic vesicle marker Syb 1 were strikingly associated in invaded nerves in PCa. The former is preferentially expressed in DRG neurons and is considered the most reliable marker for labeling glutamatergic neurons[122,127], and the latter is essential for synaptic vesicle exocytosis[137,140]. However, our results revealed that the vGlut2 and Syb 1 levels were downregulated after transfection with GRIN2D siRNA in neuroinvasive cancer cells but not in non-neuroinvasive cancer cells, which confirmed that the potential signal-

transduction molecules of the glutamate-NMDAR signaling pathway that were mainly present at the neural synaptic level are involved in NI in PCa.

NMDAR activation represents autocrine signaling in some primary tumors, but autocrine L-glutamate from cancer cells is not sufficient to induce signaling[161]. However, occasional NMDAR activation has been observed by paracrine L-glutamate released by nearby cells[201]. Our results demonstrated the elevated L-glutamate level in the cell lysates from the coculture of neuroinvasive cancer cells and DRG was higher than the sum of the levels found with the two corresponding monocultures. Zeng *et al*[161] found that B2BM cells can form pseudotripartite synapses with neuron synapses to fuel themselves with L-glutamate. The formation of these pseudotripartite synapses was revealed by vGlut2+ (presynaptic neurons) puncta and Syb 1+ (presynaptic neurons) bouton chains in close proximity to GluN2B+ puncta (B2BM cells) via STED superresolution microscopy. This pseudotripartite synapse might serve in NI in PCa, which encouraged further investigation.

An increasing number of reports have demonstrated that EZH2 can increase tumor angiogenesis to promote tumor metastasis by methylating and silencing vasohibin1[202] and is related to the long-distance metastasis and local invasion of many cancer types, including renal clear cell carcinoma[203], gastric cancer[204], breast cancer[205] and endometrial carcinoma[206]. As a TF, EZH2 was enriched on the GRIN2D promoter after L-glutamate treatment in PCa cells and exhibited synchronous changes with

GluN2D in neuroinvasive PCa cells but not in non-neuroinvasive cancer cells. However, E2F-1, as the critical factor in the classical E2F1-Rb signaling pathway, is a key TF for EZH2 expression[188]; EZH2 and E2F-1 exhibited a significant positive association in which E2F1 can bind the proximal EZH2 promoter to promote transcription; and the overexpression of both EZH2 and E2F-1 can enhance cancer cell colony formation, migration, and invasion in bladder tumors[187], which is completely consistent with our result that E2F-1 exerts a positive effect on EZH2 level and acts as a TF to EZH2 in SU.86.86 cell line. Consistently, our results also revealed that the expression levels of EZH2 and E2F-1 showed positive synchronous changes after treatment with L-glutamate. H3K27me3 catalyzed by EZH2 mainly suppresses the transcription of the CDKN2A (p16) gene, which is one of the most common tumor-suppressor genes in PCa and a canonical Polycomb target gene[178,179]; the enrichment of H3K27me3 is an early event after the steady silencing of p16 in mouse hepatocellular carcinoma cells; and the epigenetic silencing pattern can expedite tumor initiation and progression[180]. Mohammad F *et al*[181] demonstrated that the high levels of H3K27 trimethylation at the P16INK4a promoter could reduce p16INK4a expression, but EZH2 inhibitors could reverse the high H3K27me3 levels at the P16INK4a promoter and induce a corresponding marked increase in the p16INK4A levels. Our studies have shown that treatment with L-glutamate increases and decreases the expression levels of H3K27me3 and P16, respectively, in neuroinvasive pancreatic SU.86.86 cancer cells,

but no changes were observed in non-neuroinvasive pancreatic Capan-1 cancer cells. In this classical E2F1-Rb pathway, the blocking of the interaction between CDKs and RB maintained by P16[207] can reduce the level of phosphorylated Rb, which can promote binding to E2F1 and suppress E2F1 activity[208]; in contrast, hyperphosphorylated Rb can release and activate E2F1, which can induce the expression of EZH2[178]. Consistent with this finding, we demonstrated that P-Rb (Ser780) has emerged the synchronous upregulation with EZH2, H3K27me3 and E2F1 after treatment with L-glutamate. Altogether, our results clarify that EZH2 is involved in the regulatory mechanism upstream of GRIN2D in the NI of PCa cells through the EZH2-E2F1-Rb pathway.

6.0 Summary and Conclusion

In summary, this study investigated the mechanism underlying the involvement of glutamatergic receptors in NI in PCa. The results for the glutamatergic receptor family demonstrated that GluN2D-containing NMDARs play a critical role in the NI of PCa cells and participate in the migration and invasion of neuroinvasive PCa cells. Moreover, we found that the elevated L-glutamate levels in the culture of neuroinvasive cancer cells and DRG might predict the presence of pseudotripartite synapses in the frequent interaction between PCa cells and perineurons, which might fuel themselves with L-glutamate during NI. We then ascertained that the potential signal-transduction molecules of the glutamate-NMDAR signaling pathway mainly present at the neural synaptic level are involved in the NI of PCa cells. This formation of pseudotripartite synapses and the activation of GluN2D-mediated glutamate-NMDAR signaling can be involved in neuroinvasion and/or invasive growth in PCa, and these results can facilitate the development of innovative translational therapies for cancer and NI. These findings provide further support and encouragement for potential therapeutic strategies against NI, which merit further study.

7.0 Literature

1 Storz, P. & Crawford, H. C. Carcinogenesis of Pancreatic Ductal Adenocarcinoma. *Gastroenterology* 158, 2072-2081, doi:10.1053/j.gastro.2020.02.059 (2020).

2 Christenson, E. S., Jaffee, E. & Azad, N. S. Current and emerging therapies for patients with advanced pancreatic ductal adenocarcinoma: a bright future. *Lancet Oncol* 21, e135-e145, doi:10.1016/S1470-2045(19)30795-8 (2020).

3 Siegel, R. L., Miller, K. D. & Jemal, A. Cancer statistics, 2019. *CA Cancer J Clin* 69, 7-34, doi:10.3322/caac.21551 (2019).

4 Siegel, R. L., Miller, K. D. & Jemal, A. Cancer Statistics, 2017. *CA Cancer J Clin* 67, 7-30, doi:10.3322/caac.21387 (2017).

5 Scheufele, F., Hartmann, D. & Friess, H. Treatment of pancreatic cancer-neoadjuvant treatment in borderline resectable/locally advanced pancreatic cancer. *Transl Gastroenterol Hepatol* 4, 32, doi:10.21037/tgh.2019.04.09 (2019).

6 Rahib, L. *et al.* Projecting cancer incidence and deaths to 2030: the unexpected burden of thyroid, liver, and pancreas cancers in the United States. *Cancer Res* 74, 2913-2921, doi:10.1158/0008-5472.CAN-14-0155 (2014).

7 Fan, J. Q. *et al.* Current advances and outlooks in immunotherapy for pancreatic ductal adenocarcinoma. *Mol Cancer* 19, 32, doi:10.1186/s12943-020-01151-3 (2020).

8 Rawla, P., Sunkara, T. & Gaduputi, V. Epidemiology of Pancreatic Cancer: Global Trends, Etiology and Risk Factors. *World J Oncol* 10, 10-27, doi:10.14740/wjon1166 (2019).

9 Siegel, R. L., Miller, K. D., Fuchs, H. E. & Jemal, A. Cancer Statistics, 2021. *CA Cancer J Clin* 71, 7-33, doi:10.3322/caac.21654 (2021).

10 Jang, J. Y. *et al.* A prospective randomized controlled study comparing outcomes of standard resection and extended resection, including dissection of the nerve plexus and various lymph nodes, in patients with pancreatic head cancer. *Ann Surg* 259, 656-664, doi:10.1097/SLA.0000000000000384 (2014).

11 Gillen, S., Schuster, T., Meyer Zum Buschenfelde, C., Friess, H. & Kleeff, J. Preoperative/neoadjuvant therapy in pancreatic cancer: a systematic review and meta-analysis of response and resection percentages. *PLoS Med* 7, e1000267, doi:10.1371/journal.pmed.1000267 (2010).

12 Nitecki, S. S., Sarr, M. G., Colby, T. V. & van Heerden, J. A. Long-term survival after resection for ductal adenocarcinoma of the pancreas. Is it really improving? *Ann Surg* 221, 59-66, doi:10.1097/00000658-199501000-00007 (1995).

13 Pelosi, E., Castelli, G. & Testa, U. Pancreatic Cancer: Molecular Characterization, Clonal Evolution and Cancer Stem Cells. *Biomedicines* 5, doi:10.3390/biomedicines5040065 (2017).

14 Pan, S., Brentnall, T. A. & Chen, R. Proteome alterations in pancreatic ductal adenocarcinoma. *Cancer Lett* 469, 429-436, doi:10.1016/j.canlet.2019.11.020 (2020).

15 Andea, A., Sarkar, F. & Adsay, V. N. Clinicopathological correlates of pancreatic intraepithelial neoplasia: a comparative analysis of 82 cases with and 152 cases without pancreatic ductal adenocarcinoma. *Mod Pathol* 16, 996-1006, doi:10.1097/01.MP.0000087422.24733.62 (2003).

16 Vincent, A., Herman, J., Schulick, R., Hruban, R. H. & Goggins, M. Pancreatic cancer. *Lancet*

378, 607-620, doi:10.1016/S0140-6736(10)62307-0 (2011).
17 Kim, S. T. *et al.* Impact of KRAS mutations on clinical outcomes in pancreatic cancer patients treated with first-line gemcitabine-based chemotherapy. *Mol Cancer Ther* 10, 1993-1999, doi:10.1158/1535-7163.MCT-11-0269 (2011).
18 Schutte, M. *et al.* Abrogation of the Rb/p16 tumor-suppressive pathway in virtually all pancreatic carcinomas. *Cancer Res* 57, 3126-3130 (1997).
19 Hwang, R. F., Gordon, E. M., Anderson, W. F. & Parekh, D. Gene therapy for primary and metastatic pancreatic cancer with intraperitoneal retroviral vector bearing the wild-type p53 gene. *Surgery* 124, 143-150; discussion 150-141 (1998).
20 Blackford, A. *et al.* SMAD4 gene mutations are associated with poor prognosis in pancreatic cancer. *Clin Cancer Res* 15, 4674-4679, doi:10.1158/1078-0432.CCR-09-0227 (2009).
21 Roe, J. S. *et al.* Enhancer Reprogramming Promotes Pancreatic Cancer Metastasis. *Cell* 170, 875-+, doi:ARTN 888.e20 10.1016/j.cell.2017.07.007 (2017).
22 Collins, M. A. *et al.* Oncogenic Kras is required for both the initiation and maintenance of pancreatic cancer in mice. *J Clin Invest* 122, 639-653, doi:10.1172/Jci59227 (2012).
23 Hruban, R. H. *et al.* Tumor-suppressor genes in pancreatic cancer. *J Hepatobiliary Pancreat Surg* 5, 383-391 (1998).
24 Kim, W. Y. & Sharpless, N. E. The regulation of INK4/ARF in cancer and aging. *Cell* 127, 265-275, doi:10.1016/j.cell.2006.10.003 (2006).
25 Makohon-Moore, A. & Iacobuzio-Donahue, C. A. Pancreatic cancer biology and genetics from an evolutionary perspective. *Nat Rev Cancer* 16, 553-565, doi:10.1038/nrc.2016.66 (2016).
26 Stolzenberg-Solomon, R. Z., Schairer, C., Moore, S., Hollenbeck, A. & Silverman, D. T. Lifetime adiposity and risk of pancreatic cancer in the NIH-AARP Diet and Health Study cohort. *Am J Clin Nutr* 98, 1057-1065, doi:10.3945/ajcn.113.058123 (2013).
27 Andersen, D. K. *et al.* Diabetes, Pancreatogenic Diabetes, and Pancreatic Cancer. *Diabetes* 66, 1103-1110, doi:10.2337/db16-1477 (2017).
28 Pereira, S. P. *et al.* Early detection of pancreatic cancer. *Lancet Gastroenterol Hepatol* 5, 698-710, doi:10.1016/S2468-1253(19)30416-9 (2020).
29 Korc, M. *et al.* Tobacco and alcohol as risk factors for pancreatic cancer. *Best Pract Res Clin Gastroenterol* 31, 529-536, doi:10.1016/j.bpg.2017.09.001 (2017).
30 Mizrahi, J. D., Surana, R., Valle, J. W. & Shroff, R. T. Pancreatic cancer. *Lancet* 395, 2008-2020, doi:10.1016/S0140-6736(20)30974-0 (2020).
31 Rebours, V. *et al.* Obesity and Fatty Pancreatic Infiltration Are Risk Factors for Pancreatic Precancerous Lesions (PanIN). *Clin Cancer Res* 21, 3522-3528, doi:10.1158/1078-0432.CCR-14-2385 (2015).
32 Sung, H., Siegel, R. L., Rosenberg, P. S. & Jemal, A. Emerging cancer trends among young adults in the USA: analysis of a population-based cancer registry. *The Lancet Public Health* 4, e137-e147, doi:10.1016/s2468-2667(18)30267-6 (2019).
33 Blackford, A. *et al.* Genetic mutations associated with cigarette smoking in pancreatic cancer. *Cancer Res* 69, 3681-3688, doi:10.1158/0008-5472.CAN-09-0015 (2009).
34 Naudin, S. *et al.* Healthy lifestyle and the risk of pancreatic cancer in the EPIC study. *Eur J Epidemiol* 35, 975-986, doi:10.1007/s10654-019-00559-6 (2020).

35 Jiao, L. *et al.* A combined healthy lifestyle score and risk of pancreatic cancer in a large cohort study. *Arch Intern Med* 169, 764-770, doi:10.1001/archinternmed.2009.46 (2009).

36 Rabow, M. W., Petzel, M. Q. B. & Adkins, S. H. Symptom Management and Palliative Care in Pancreatic Cancer. *Cancer J* 23, 362-373, doi:10.1097/PPO.0000000000000293 (2017).

37 Sahni, S. *et al.* Identification of Novel Biomarkers in Pancreatic Tumor Tissue to Predict Response to Neoadjuvant Chemotherapy. *Front Oncol* 10, 237, doi:10.3389/fonc.2020.00237 (2020).

38 Kamisawa, T., Wood, L. D., Itoi, T. & Takaori, K. Pancreatic cancer. *Lancet* 388, 73-85, doi:10.1016/S0140-6736(16)00141-0 (2016).

39 Hartwig, W., Werner, J., Jager, D., Debus, J. & Buchler, M. W. Improvement of surgical results for pancreatic cancer. *Lancet Oncol* 14, e476-e485, doi:10.1016/S1470-2045(13)70172-4 (2013).

40 Kleeff, J. *et al.* Pancreatic cancer. *Nat Rev Dis Primers* 2, 16022, doi:10.1038/nrdp.2016.22 (2016).

41 Ren, L., Mota Reyes, C., Friess, H. & Demir, I. E. Neoadjuvant therapy in pancreatic cancer: what is the true oncological benefit? *Langenbecks Arch Surg* 405, 879-887, doi:10.1007/s00423-020-01946-4 (2020).

42 Jurcak, N. & Zheng, L. Signaling in the microenvironment of pancreatic cancer: Transmitting along the nerve. *Pharmacol Ther* 200, 126-134, doi:10.1016/j.pharmthera.2019.04.010 (2019).

43 Bapat, A. A., Hostetter, G., Von Hoff, D. D. & Han, H. Perineural invasion and associated pain in pancreatic cancer. *Nat Rev Cancer* 11, 695-707, doi:10.1038/nrc3131 (2011).

44 Liang, D. *et al.* New insights into perineural invasion of pancreatic cancer: More than pain. *Biochim Biophys Acta* 1865, 111-122, doi:10.1016/j.bbcan.2016.01.002 (2016).

45 Yang, Y. H., Liu, J. B., Gui, Y., Lei, L. L. & Zhang, S. J. Relationship between autophagy and perineural invasion, clinicopathological features, and prognosis in pancreatic cancer. *World J Gastroenterol* 23, 7232-7241, doi:10.3748/wjg.v23.i40.7232 (2017).

46 Liebig, C., Ayala, G., Wilks, J. A., Berger, D. H. & Albo, D. Perineural invasion in cancer: a review of the literature. *Cancer* 115, 3379-3391, doi:10.1002/cncr.24396 (2009).

47 Dobosz, L., Kaczor, M. & Stefaniak, T. J. Pain in pancreatic cancer: review of medical and surgical remedies. *ANZ J Surg* 86, 756-761, doi:10.1111/ans.13609 (2016).

48 Ceyhan, G. O., Michalski, C. W., Demir, I. E., Muller, M. W. & Friess, H. Pancreatic pain. *Best Pract Res Clin Gastroenterol* 22, 31-44, doi:10.1016/j.bpg.2007.10.016 (2008).

49 di Mola, F. F. & di Sebastiano, P. Pain and pain generation in pancreatic cancer. *Langenbecks Arch Surg* 393, 919-922, doi:10.1007/s00423-007-0277-z (2008).

50 Demir, I. E., Friess, H. & Ceyhan, G. O. Neural plasticity in pancreatitis and pancreatic cancer. *Nat Rev Gastroenterol Hepatol* 12, 649-659, doi:10.1038/nrgastro.2015.166 (2015).

51 Chang, A., Kim-Fuchs, C., Le, C. P., Hollande, F. & Sloan, E. K. Neural Regulation of Pancreatic Cancer: A Novel Target for Intervention. *Cancers (Basel)* 7, 1292-1312, doi:10.3390/cancers7030838 (2015).

52 Ceyhan, G. O. *et al.* Pancreatic neuropathy and neuropathic pain--a comprehensive pathomorphological study of 546 cases. *Gastroenterology* 136, 177-186 e171, doi:10.1053/j.gastro.2008.09.029 (2009).

53 Demir, I. E., Tieftrunk, E., Maak, M., Friess, H. & Ceyhan, G. O. Pain mechanisms in chronic pancreatitis: of a master and his fire. *Langenbecks Arch Surg* 396, 151-160, doi:10.1007/s00423-010-0731-1 (2011).

54 Demir, I. E., Friess, H. & Ceyhan, G. O. Nerve-cancer interactions in the stromal biology of pancreatic cancer. *Front Physiol* 3, 97, doi:10.3389/fphys.2012.00097 (2012).

55 Schorn, S. *et al.* The influence of neural invasion on survival and tumor recurrence in pancreatic ductal adenocarcinoma - A systematic review and meta-analysis. *Surg Oncol* 26, 105-115, doi:10.1016/j.suronc.2017.01.007 (2017).

56 Badger, S. A. *et al.* The role of surgery for pancreatic cancer: a 12-year review of patient outcome. *Ulster Med J* 79, 70-75 (2010).

57 Chen, J. W. *et al.* Predicting patient survival after pancreaticoduodenectomy for malignancy: histopathological criteria based on perineural infiltration and lymphovascular invasion. *HPB (Oxford)* 12, 101-108, doi:10.1111/j.1477-2574.2009.00140.x (2010).

58 Chatterjee, D. *et al.* Perineural and intraneural invasion in posttherapy pancreaticoduodenectomy specimens predicts poor prognosis in patients with pancreatic ductal adenocarcinoma. *Am J Surg Pathol* 36, 409-417, doi:10.1097/PAS.0b013e31824104c5 (2012).

59 Cervero, F. Sensory innervation of the viscera: peripheral basis of visceral pain. *Physiol Rev* 74, 95-138, doi:10.1152/physrev.1994.74.1.95 (1994).

60 Gebhart, G. F. It's chickens and eggs all over again: is central reorganization the result or cause of persistent visceral pain? *Gastroenterology* 132, 1618-1620, doi:10.1053/j.gastro.2007.02.060 (2007).

61 Randich, A. & Gebhart, G. F. Vagal afferent modulation of nociception. *Brain Res Brain Res Rev* 17, 77-99, doi:10.1016/0165-0173(92)90009-b (1992).

62 Zhu, Z. *et al.* Nerve growth factor expression correlates with perineural invasion and pain in human pancreatic cancer. *J Clin Oncol* 17, 2419-2428, doi:10.1200/JCO.1999.17.8.2419 (1999).

63 Schneider, M. B. *et al.* Expression of nerve growth factors in pancreatic neural tissue and pancreatic cancer. *J Histochem Cytochem* 49, 1205-1210, doi:10.1177/002215540104901002 (2001).

64 Amit, M., Na'ara, S. & Gil, Z. Mechanisms of cancer dissemination along nerves. *Nat Rev Cancer* 16, 399-408, doi:10.1038/nrc.2016.38 (2016).

65 Jobling, P. *et al.* Nerve-Cancer Cell Cross-talk: A Novel Promoter of Tumor Progression. *Cancer Res* 75, 1777-1781, doi:10.1158/0008-5472.CAN-14-3180 (2015).

66 Stopczynski, R. E. *et al.* Neuroplastic changes occur early in the development of pancreatic ductal adenocarcinoma. *Cancer Res* 74, 1718-1727, doi:10.1158/0008-5472.CAN-13-2050 (2014).

67 Demir, I. E. *et al.* Investigation of Schwann cells at neoplastic cell sites before the onset of cancer invasion. *J Natl Cancer Inst* 106, doi:10.1093/jnci/dju184 (2014).

68 Liebl, F. *et al.* The severity of neural invasion is associated with shortened survival in colon cancer. *Clin Cancer Res* 19, 50-61, doi:10.1158/1078-0432.CCR-12-2392 (2013).

69 Saloman, J. L. *et al.* Ablation of sensory neurons in a genetic model of pancreatic ductal adenocarcinoma slows initiation and progression of cancer. *Proc Natl Acad Sci U S A* 113, 3078-3083, doi:10.1073/pnas.1512603113 (2016).

70 Bapat, A. A., Hostetter, G., Von Hoff, D. D. & Han, H. Y. Perineural invasion and associated pain in pancreatic cancer. *Nat Rev Cancer* 11, 695-707, doi:10.1038/nrc3131 (2011).

71 Demir, I. E. *et al.* The microenvironment in chronic pancreatitis and pancreatic cancer induces neuronal plasticity. *Neurogastroenterol Motil* 22, 480-490, e112-483, doi:10.1111/j.1365-2982.2009.01428.x (2010).

72 Friess, H. *et al.* Neural alterations in surgical stage chronic pancreatitis are independent of the underlying aetiology. *Gut* 50, 682-686 (2002).

73 Demir, I. E., Friess, H. & Ceyhan, G. O. Neural plasticity in pancreatitis and pancreatic cancer. *Nat Rev Gastro Hepat* 12, 649-659, doi:10.1038/nrgastro.2015.166 (2015).

74 Scanlon, C. S. *et al.* Galanin modulates the neural niche to favour perineural invasion in head and neck cancer. *Nat Commun* 6, 6885, doi:10.1038/ncomms7885 (2015).

75 Danbolt, N. C. Glutamate uptake. *Prog Neurobiol* 65, 1-105, doi:10.1016/s0301-0082(00)00067-8 (2001).

76 MacDonald, M. J. & Fahien, L. A. Glutamate is not a messenger in insulin secretion. *J Biol Chem* 275, 34025-34027, doi:10.1074/jbc.C000411200 (2000).

77 Miller, K. E., Hoffman, E. M., Sutharshan, M. & Schechter, R. Glutamate pharmacology and metabolism in peripheral primary afferents: physiological and pathophysiological mechanisms. *Pharmacol Ther* 130, 283-309, doi:10.1016/j.pharmthera.2011.01.005 (2011).

78 Hoffman, E. M., Schechter, R. & Miller, K. E. Fixative composition alters distributions of immunoreactivity for glutaminase and two markers of nociceptive neurons, Nav1.8 and TRPV1, in the rat dorsal root ganglion. *J Histochem Cytochem* 58, 329-344, doi:10.1369/jhc.2009.954008 (2010).

79 Miller, K. E., Douglas, V. D. & Kaneko, T. Glutaminase immunoreactive neurons in the rat dorsal root ganglion contain calcitonin gene-related peptide (CGRP). *Neurosci Lett* 160, 113-116, doi:10.1016/0304-3940(93)90926-c (1993).

80 Li, L. & Hanahan, D. Hijacking the neuronal NMDAR signaling circuit to promote tumor growth and invasion. *Cell* 153, 86-100, doi:10.1016/j.cell.2013.02.051 (2013).

81 Rzeski, W., Turski, L. & Ikonomidou, C. Glutamate antagonists limit tumor growth. *Proc Natl Acad Sci U S A* 98, 6372-6377, doi:10.1073/pnas.091113598 (2001).

82 Takano, T. *et al.* Glutamate release promotes growth of malignant gliomas. *Nat Med* 7, 1010-1015, doi:10.1038/nm0901-1010 (2001).

83 Seidlitz, E. P., Sharma, M. K., Saikali, Z., Ghert, M. & Singh, G. Cancer cell lines release glutamate into the extracellular environment. *Clin Exp Metastasis* 26, 781-787, doi:10.1007/s10585-009-9277-4 (2009).

84 Sharma, M. K., Seidlitz, E. P. & Singh, G. Cancer cells release glutamate via the cystine/glutamate antiporter. *Biochem Biophys Res Commun* 391, 91-95, doi:10.1016/j.bbrc.2009.10.168 (2010).

85 Nicoletti, F. *et al.* Metabotropic glutamate receptors: new targets for the control of tumor growth? *Trends Pharmacol Sci* 28, 206-213, doi:10.1016/j.tips.2007.03.008 (2007).

86 Herner, A. *et al.* Glutamate increases pancreatic cancer cell invasion and migration via AMPA receptor activation and Kras-MAPK signaling. *Int J Cancer* 129, 2349-2359, doi:10.1002/ijc.25898 (2011).

87 Stansley, B. J. & Conn, P. J. Neuropharmacological Insight from Allosteric Modulation of mGlu Receptors. *Trends Pharmacol Sci* 40, 240-252, doi:10.1016/j.tips.2019.02.006 (2019).

88 Gladding, C. M. & Raymond, L. A. Mechanisms underlying NMDA receptor synaptic/extrasynaptic distribution and function. *Mol Cell Neurosci* 48, 308-320, doi:10.1016/j.mcn.2011.05.001 (2011).

89 Traynelis, S. F. *et al.* Glutamate receptor ion channels: structure, regulation, and function. *Pharmacol Rev* 62, 405-496, doi:10.1124/pr.109.002451 (2010).

90 Wang, J. X. *et al.* Structural basis of subtype-selective competitive antagonism for GluN2C/2D-containing NMDA receptors. *Nat Commun* 11, 423, doi:10.1038/s41467-020-14321-0 (2020).

91 Vyklicky, V. *et al.* Structure, function, and pharmacology of NMDA receptor channels. *Physiol Res* 63, S191-203, doi:10.33549/physiolres.932678 (2014).

92 Hansen, K. B. *et al.* Structure, function, and allosteric modulation of NMDA receptors. *J Gen Physiol* 150, 1081-1105, doi:10.1085/jgp.201812032 (2018).

93 Baj, A. *et al.* Glutamatergic Signaling Along The Microbiota-Gut-Brain Axis. *Int J Mol Sci* 20, doi:10.3390/ijms20061482 (2019).

94 Luo, T., Wu, W. H. & Chen, B. S. NMDA receptor signaling: death or survival? *Front Biol (Beijing)* 6, 468-476, doi:10.1007/s11515-011-1187-6 (2011).

95 Bell, K. F. & Hardingham, G. E. The influence of synaptic activity on neuronal health. *Curr Opin Neurobiol* 21, 299-305, doi:10.1016/j.conb.2011.01.002 (2011).

96 Paoletti, P., Bellone, C. & Zhou, Q. NMDA receptor subunit diversity: impact on receptor properties, synaptic plasticity and disease. *Nat Rev Neurosci* 14, 383-400, doi:10.1038/nrn3504 (2013).

97 Hardingham, G. NMDA receptor C-terminal signaling in development, plasticity, and disease. *F1000Res* 8, doi:10.12688/f1000research.19925.1 (2019).

98 Sun, Y. *et al.* The Functional and Molecular Properties, Physiological Functions, and Pathophysiological Roles of GluN2A in the Central Nervous System. *Mol Neurobiol* 54, 1008-1021, doi:10.1007/s12035-016-9715-7 (2017).

99 Franchini, L., Carrano, N., Di Luca, M. & Gardoni, F. Synaptic GluN2A-Containing NMDA Receptors: From Physiology to Pathological Synaptic Plasticity. *Int J Mol Sci* 21, doi:10.3390/ijms21041538 (2020).

100 Sheng, M., Cummings, J., Roldan, L. A., Jan, Y. N. & Jan, L. Y. Changing subunit composition of heteromeric NMDA receptors during development of rat cortex. *Nature* 368, 144-147, doi:10.1038/368144a0 (1994).

101 Monyer, H., Burnashev, N., Laurie, D. J., Sakmann, B. & Seeburg, P. H. Developmental and regional expression in the rat brain and functional properties of four NMDA receptors. *Neuron* 12, 529-540, doi:10.1016/0896-6273(94)90210-0 (1994).

102 Akazawa, C., Shigemoto, R., Bessho, Y., Nakanishi, S. & Mizuno, N. Differential expression of five N-methyl-D-aspartate receptor subunit mRNAs in the cerebellum of developing and adult rats. *J Comp Neurol* 347, 150-160, doi:10.1002/cne.903470112 (1994).

103 Neagoe, I. *et al.* The GluN2B subunit represents a major functional determinant of NMDA receptors in human induced pluripotent stem cell-derived cortical neurons. *Stem Cell Res* 28, 105-114, doi:10.1016/j.scr.2018.02.002 (2018).

104 Lind, G. E. *et al.* Structural basis of subunit selectivity for competitive NMDA receptor antagonists with preference for GluN2A over GluN2B subunits. *Proc Natl Acad Sci U S A* 114, E6942-E6951, doi:10.1073/pnas.1707752114 (2017).

105 Naaz, S. *et al.* Association of SAPAP3 allelic variants with symptom dimensions and pharmacological treatment response in obsessive-compulsive disorder. *Exp Clin Psychopharmacol*, doi:10.1037/pha0000422 (2020).

106 Mayer, M. L. & Armstrong, N. Structure and function of glutamate receptor ion channels. *Annu Rev Physiol* 66, 161-181, doi:10.1146/annurev.physiol.66.050802.084104 (2004).

107 Monyer, H. *et al.* Heteromeric NMDA receptors: molecular and functional distinction of subtypes. *Science* 256, 1217-1221, doi:10.1126/science.256.5060.1217 (1992).

108 Vicini, S. *et al.* Functional and pharmacological differences between recombinant N-methyl-D-aspartate receptors. *J Neurophysiol* 79, 555-566, doi:10.1152/jn.1998.79.2.555 (1998).

109 Ishii, T. *et al.* Molecular characterization of the family of the N-methyl-D-aspartate receptor subunits. *J Biol Chem* 268, 2836-2843 (1993).

110 Bloomfield, C., O'Donnell, P., French, S. J. & Totterdell, S. Cholinergic neurons of the adult rat striatum are immunoreactive for glutamatergic N-methyl-d-aspartate 2D but not N-methyl-d-aspartate 2C receptor subunits. *Neuroscience* 150, 639-646, doi:10.1016/j.neuroscience.2007.09.035 (2007).

111 Landwehrmeyer, G. B., Standaert, D. G., Testa, C. M., Penney, J. B., Jr. & Young, A. B. NMDA receptor subunit mRNA expression by projection neurons and interneurons in rat striatum. *J Neurosci* 15, 5297-5307 (1995).

112 Standaert, D. G., Landwehrmeyer, G. B., Kerner, J. A., Penney, J. B., Jr. & Young, A. B. Expression of NMDAR2D glutamate receptor subunit mRNA in neurochemically identified interneurons in the rat neostriatum, neocortex and hippocampus. *Brain Res Mol Brain Res* 42, 89-102, doi:10.1016/s0169-328x(96)00117-9 (1996).

113 Zhang, X. & Chergui, K. Dopamine depletion of the striatum causes a cell-type specific reorganization of GluN2B- and GluN2D-containing NMDA receptors. *Neuropharmacology* 92, 108-115, doi:10.1016/j.neuropharm.2015.01.007 (2015).

114 Li, S. X. *et al.* Uncoupling DAPK1 from NMDA receptor GluN2B subunit exerts rapid antidepressant-like effects. *Mol Psychiatry* 23, 597-608, doi:10.1038/mp.2017.85 (2018).

115 Chatterton, J. E. *et al.* Excitatory glycine receptors containing the NR3 family of NMDA receptor subunits. *Nature* 415, 793-798, doi:10.1038/nature715 (2002).

116 Wrighton, D. C., Baker, E. J., Chen, P. E. & Wyllie, D. J. Mg2+ and memantine block of rat recombinant NMDA receptors containing chimeric NR2A/2D subunits expressed in Xenopus laevis oocytes. *J Physiol* 586, 211-225, doi:10.1113/jphysiol.2007.143164 (2008).

117 Cull-Candy, S., Brickley, S. & Farrant, M. NMDA receptor subunits: diversity, development and disease. *Curr Opin Neurobiol* 11, 327-335, doi:10.1016/s0959-4388(00)00215-4 (2001).

118 Misra, C., Brickley, S. G., Wyllie, D. J. & Cull-Candy, S. G. Slow deactivation kinetics of NMDA receptors containing NR1 and NR2D subunits in rat cerebellar Purkinje cells. *J Physiol* 525 Pt 2, 299-305, doi:10.1111/j.1469-7793.2000.t01-1-00299.x (2000).

119 Siegler Retchless, B., Gao, W. & Johnson, J. W. A single GluN2 subunit residue controls NMDA receptor channel properties via intersubunit interaction. *Nat Neurosci* 15, 406-413, S401-402, doi:10.1038/nn.3025 (2012).

120 Camp, C. R. & Yuan, H. GRIN2D/GluN2D NMDA receptor: Unique features and its contribution to pediatric developmental and epileptic encephalopathy. *Eur J Paediatr*

Neurol 24, 89-99, doi:10.1016/j.ejpn.2019.12.007 (2020).

121 Barria, A. Dangerous liaisons as tumour cells form synapses with neurons. *Nature* 573, 499-501, doi:10.1038/d41586-019-02746-7 (2019).

122 Zhang, F. X. *et al.* Vesicular glutamate transporter isoforms: The essential players in the somatosensory systems. *Prog Neurobiol* 171, 72-89, doi:10.1016/j.pneurobio.2018.09.006 (2018).

123 Brumovsky, P. R. *et al.* Expression of vesicular glutamate transporters type 1 and 2 in sensory and autonomic neurons innervating the mouse colorectum. *J Comp Neurol* 519, 3346-3366, doi:10.1002/cne.22730 (2011).

124 Oliveira, A. L. *et al.* Cellular localization of three vesicular glutamate transporter mRNAs and proteins in rat spinal cord and dorsal root ganglia. *Synapse* 50, 117-129, doi:10.1002/syn.10249 (2003).

125 Moechars, D. *et al.* Vesicular glutamate transporter VGLUT2 expression levels control quantal size and neuropathic pain. *J Neurosci* 26, 12055-12066, doi:10.1523/JNEUROSCI.2556-06.2006 (2006).

126 Brumovsky, P., Watanabe, M. & Hokfelt, T. Expression of the vesicular glutamate transporters-1 and -2 in adult mouse dorsal root ganglia and spinal cord and their regulation by nerve injury. *Neuroscience* 147, 469-490, doi:10.1016/j.neuroscience.2007.02.068 (2007).

127 Malet, M. *et al.* Transcript expression of vesicular glutamate transporters in lumbar dorsal root ganglia and the spinal cord of mice - effects of peripheral axotomy or hindpaw inflammation. *Neuroscience* 248, 95-111, doi:10.1016/j.neuroscience.2013.05.044 (2013).

128 Seal, R. P. *et al.* Injury-induced mechanical hypersensitivity requires C-low threshold mechanoreceptors. *Nature* 462, 651-655, doi:10.1038/nature08505 (2009).

129 El Mestikawy, S., Wallen-Mackenzie, A., Fortin, G. M., Descarries, L. & Trudeau, L. E. From glutamate co-release to vesicular synergy: vesicular glutamate transporters. *Nat Rev Neurosci* 12, 204-216, doi:10.1038/nrn2969 (2011).

130 Fremeau, R. T., Jr. *et al.* The identification of vesicular glutamate transporter 3 suggests novel modes of signaling by glutamate. *Proc Natl Acad Sci U S A* 99, 14488-14493, doi:10.1073/pnas.222546799 (2002).

131 Gras, C. *et al.* A third vesicular glutamate transporter expressed by cholinergic and serotoninergic neurons. *J Neurosci* 22, 5442-5451 (2002).

132 Schafer, M. K., Varoqui, H., Defamie, N., Weihe, E. & Erickson, J. D. Molecular cloning and functional identification of mouse vesicular glutamate transporter 3 and its expression in subsets of novel excitatory neurons. *J Biol Chem* 277, 50734-50748, doi:10.1074/jbc.M206738200 (2002).

133 Liguz-Lecznar, M. & Skangiel-Kramska, J. Vesicular glutamate transporters VGLUT1 and VGLUT2 in the developing mouse barrel cortex. *Int J Dev Neurosci* 25, 107-114, doi:10.1016/j.ijdevneu.2006.12.005 (2007).

134 Wang, L. *et al.* Regulating nociceptive transmission by VGluT2-expressing spinal dorsal horn neurons. *J Neurochem* 147, 526-540, doi:10.1111/jnc.14588 (2018).

135 Duan, B. *et al.* Identification of spinal circuits transmitting and gating mechanical pain. *Cell* 159, 1417-1432, doi:10.1016/j.cell.2014.11.003 (2014).

136 Raptis, A., Torrejon-Escribano, B., Gomez de Aranda, I. & Blasi, J. Distribution of

synaptobrevin/VAMP 1 and 2 in rat brain. *J Chem Neuroanat* 30, 201-211, doi:10.1016/j.jchemneu.2005.08.002 (2005).

137 Gu, Y. & Huganir, R. L. Identification of the SNARE complex mediating the exocytosis of NMDA receptors. *Proc Natl Acad Sci U S A* 113, 12280-12285, doi:10.1073/pnas.1614042113 (2016).

138 Liu, Y., Sugiura, Y. & Lin, W. The role of synaptobrevin1/VAMP1 in Ca2+-triggered neurotransmitter release at the mouse neuromuscular junction. *J Physiol* 589, 1603-1618, doi:10.1113/jphysiol.2010.201939 (2011).

139 Sudhof, T. C. & Rothman, J. E. Membrane fusion: grappling with SNARE and SM proteins. *Science* 323, 474-477, doi:10.1126/science.1161748 (2009).

140 Engel, A. G. Congenital Myasthenic Syndromes in 2018. *Curr Neurol Neurosci Rep* 18, 46, doi:10.1007/s11910-018-0852-4 (2018).

141 Manca, P., Mameli, O., Caria, M. A., Torrejon-Escribano, B. & Blasi, J. Distribution of SNAP25, VAMP1 and VAMP2 in mature and developing deep cerebellar nuclei after estrogen administration. *Neuroscience* 266, 102-115, doi:10.1016/j.neuroscience.2014.02.008 (2014).

142 Feng, W. & Zhang, M. Organization and dynamics of PDZ-domain-related supramodules in the postsynaptic density. *Nat Rev Neurosci* 10, 87-99, doi:10.1038/nrn2540 (2009).

143 Kim, E. & Sheng, M. PDZ domain proteins of synapses. *Nat Rev Neurosci* 5, 771-781, doi:10.1038/nrn1517 (2004).

144 Liang H, W. H., Wang S, Francis R, Paxinos G, Huang X. . *3D imaging of PSD-95 in the mouse brain using the advanced CUBIC method*. Vol. 11 (Mol Brain, 2018).

145 Cheng D, H. C., Rush J, Ramm E, Schlager MA, Duong DM, Xu P, Wijayawardana SR, Hanfelt J, Nakagawa T, Sheng M, Peng J. . *Relative and absolute quantification of postsynaptic density proteome isolated from rat forebrain and cerebellum*. Vol. 5 1158-70 (Mol Cell Proteomics, 2006).

146 Won, S., Incontro, S., Nicoll, R. A. & Roche, K. W. PSD-95 stabilizes NMDA receptors by inducing the degradation of STEP61. *Proc Natl Acad Sci U S A* 113, E4736-4744, doi:10.1073/pnas.1609702113 (2016).

147 Wang, D., Li, B., Wu, Y. & Li, B. The Effects of Maternal Atrazine Exposure and Swimming Training on Spatial Learning Memory and Hippocampal Morphology in Offspring Male Rats via PSD95/NR2B Signaling Pathway. *Cell Mol Neurobiol* 39, 1003-1015, doi:10.1007/s10571-019-00695-3 (2019).

148 Vieira, M., Yong, X. L. H., Roche, K. W. & Anggono, V. Regulation of NMDA glutamate receptor functions by the GluN2 subunits. *J Neurochem* 154, 121-143, doi:10.1111/jnc.14970 (2020).

149 Kornau, H. C., Schenker, L. T., Kennedy, M. B. & Seeburg, P. H. Domain interaction between NMDA receptor subunits and the postsynaptic density protein PSD-95. *Science* 269, 1737-1740, doi:10.1126/science.7569905 (1995).

150 Polgar, E., Watanabe, M., Hartmann, B., Grant, S. G. & Todd, A. J. Expression of AMPA receptor subunits at synapses in laminae I-III of the rodent spinal dorsal horn. *Mol Pain* 4, 5, doi:10.1186/1744-8069-4-5 (2008).

151 Kim, E. & Sheng, M. Differential K+ channel clustering activity of PSD-95 and SAP97, two related membrane-associated putative guanylate kinases. *Neuropharmacology* 35, 993-

1000, doi:10.1016/0028-3908(96)00093-7 (1996).

152 Jeyifous, O. *et al.* Palmitoylation regulates glutamate receptor distributions in postsynaptic densities through control of PSD95 conformation and orientation. *Proc Natl Acad Sci U S A* 113, E8482-E8491, doi:10.1073/pnas.1612963113 (2016).

153 Demir, I. E. *et al.* Neural invasion in pancreatic cancer: the past, present and future. *Cancers (Basel)* 2, 1513-1527, doi:10.3390/cancers2031513 (2010).

154 Kayahara, M., Nakagawara, H., Kitagawa, H. & Ohta, T. The nature of neural invasion by pancreatic cancer. *Pancreas* 35, 218-223, doi:10.1097/mpa.0b013e3180619677 (2007).

155 Ryschich, E. *et al.* Promotion of tumor cell migration by extracellular matrix proteins in human pancreatic cancer. *Pancreas* 38, 804-810, doi:10.1097/MPA.0b013e3181b9dfda (2009).

156 Stepulak, A. *et al.* Expression of glutamate receptor subunits in human cancers. *Histochem Cell Biol* 132, 435-445, doi:10.1007/s00418-009-0613-1 (2009).

157 North, W. G., Gao, G., Jensen, A., Memoli, V. A. & Du, J. NMDA receptors are expressed by small-cell lung cancer and are potential targets for effective treatment. *Clin Pharmacol* 2, 31-40, doi:10.2147/CPAA.S6262 (2010).

158 North, W. G., Gao, G., Memoli, V. A., Pang, R. H. & Lynch, L. Breast cancer expresses functional NMDA receptors. *Breast Cancer Res Treat* 122, 307-314, doi:10.1007/s10549-009-0556-1 (2010).

159 Abdul, M. & Hoosein, N. N-methyl-D-aspartate receptor in human prostate cancer. *J Membr Biol* 205, 125-128, doi:10.1007/s00232-005-0777-0 (2005).

160 North, W. G., Liu, F., Lin, L. Z., Tian, R. & Akerman, B. NMDA receptors are important regulators of pancreatic cancer and are potential targets for treatment. *Clin Pharmacol* 9, 79-86, doi:10.2147/CPAA.S140057 (2017).

161 Zeng, Q. *et al.* Synaptic proximity enables NMDAR signalling to promote brain metastasis. *Nature* 573, 526-531, doi:10.1038/s41586-019-1576-6 (2019).

162 Venkataramani, V. *et al.* Glutamatergic synaptic input to glioma cells drives brain tumour progression. *Nature* 573, 532-538, doi:10.1038/s41586-019-1564-x (2019).

163 Venkatesh, H. S. *et al.* Electrical and synaptic integration of glioma into neural circuits. *Nature* 573, 539-545, doi:10.1038/s41586-019-1563-y (2019).

164 Ceyhan, G. O. *et al.* Neural invasion in pancreatic cancer: a mutual tropism between neurons and cancer cells. *Biochem Biophys Res Commun* 374, 442-447, doi:10.1016/j.bbrc.2008.07.035 (2008).

165 Vivian, J. *et al.* Toil enables reproducible, open source, big biomedical data analyses. *Nat Biotechnol* 35, 314-316, doi:10.1038/nbt.3772 (2017).

166 Demir, I. E. Transcriptional and functional characterization of the first neuro-invasive genetically engineered mouse model of pancreatic cancer *University library of the Technical University of Munich*, 116 (2016).

167 Volianskis, A. *et al.* Different NMDA receptor subtypes mediate induction of long-term potentiation and two forms of short-term potentiation at CA1 synapses in rat hippocampus in vitro. *J Physiol* 591, 955-972, doi:10.1113/jphysiol.2012.247296 (2013).

168 Rimbault, C. *et al.* Engineering selective competitors for the discrimination of highly conserved protein-protein interaction modules. *Nat Commun* 10, 4521, doi:10.1038/s41467-019-12528-4 (2019).

169 Liang, H. *et al.* 3D imaging of PSD-95 in the mouse brain using the advanced CUBIC method. *Mol Brain* 11, 50, doi:10.1186/s13041-018-0393-4 (2018).

170 Yoo, K. S. *et al.* Postsynaptic density protein 95 (PSD-95) is transported by KIF5 to dendritic regions. *Mol Brain* 12, 97, doi:10.1186/s13041-019-0520-x (2019).

171 Beique, J. C. & Andrade, R. PSD-95 regulates synaptic transmission and plasticity in rat cerebral cortex. *J Physiol* 546, 859-867, doi:10.1113/jphysiol.2002.031369 (2003).

172 Migaud, M. *et al.* Enhanced long-term potentiation and impaired learning in mice with mutant postsynaptic density-95 protein. *Nature* 396, 433-439, doi:10.1038/24790 (1998).

173 Roche, K. W. *et al.* Molecular determinants of NMDA receptor internalization. *Nat Neurosci* 4, 794-802, doi:10.1038/90498 (2001).

174 Chung, H. J., Huang, Y. H., Lau, L. F. & Huganir, R. L. Regulation of the NMDA receptor complex and trafficking by activity-dependent phosphorylation of the NR2B subunit PDZ ligand. *J Neurosci* 24, 10248-10259, doi:10.1523/JNEUROSCI.0546-04.2004 (2004).

175 Yang, C., Zhang, X., Gao, J., Wang, M. & Yang, Z. Arginine vasopressin ameliorates spatial learning impairments in chronic cerebral hypoperfusion via V1a receptor and autophagy signaling partially. *Transl Psychiatry* 7, e1174, doi:10.1038/tp.2017.121 (2017).

176 Chen, I. *et al.* Glutamate transporters have a chloride channel with two hydrophobic gates. *Nature* 591, 327-331, doi:10.1038/s41586-021-03240-9 (2021).

177 Gregory, K. J. & Goudet, C. International Union of Basic and Clinical Pharmacology. CXI. Pharmacology, Signaling, and Physiology of Metabotropic Glutamate Receptors. *Pharmacol Rev* 73, 521-569, doi:10.1124/pr.119.019133 (2021).

178 Beguelin, W. *et al.* EZH2 enables germinal centre formation through epigenetic silencing of CDKN1A and an Rb-E2F1 feedback loop. *Nat Commun* 8, 877, doi:10.1038/s41467-017-01029-x (2017).

179 Kim, K. H. & Roberts, C. W. Targeting EZH2 in cancer. *Nat Med* 22, 128-134, doi:10.1038/nm.4036 (2016).

180 Yao, J. Y. *et al.* H3K27 trimethylation is an early epigenetic event of p16INK4a silencing for regaining tumorigenesis in fusion reprogrammed hepatoma cells. *J Biol Chem* 285, 18828-18837, doi:10.1074/jbc.M109.077974 (2010).

181 Mohammad, F. *et al.* EZH2 is a potential therapeutic target for H3K27M-mutant pediatric gliomas. *Nat Med* 23, 483-492, doi:10.1038/nm.4293 (2017).

182 Malinkova, V., Vylicil, J. & Krystof, V. Cyclin-dependent kinase inhibitors for cancer therapy: a patent review (2009 - 2014). *Expert Opin Ther Pat* 25, 953-970, doi:10.1517/13543776.2015.1045414 (2015).

183 Matsushime, H. *et al.* Identification and properties of an atypical catalytic subunit (p34PSK-J3/cdk4) for mammalian D type G1 cyclins. *Cell* 71, 323-334, doi:10.1016/0092-8674(92)90360-o (1992).

184 Sherr, C. J., Beach, D. & Shapiro, G. I. Targeting CDK4 and CDK6: From Discovery to Therapy. *Cancer Discov* 6, 353-367, doi:10.1158/2159-8290.CD-15-0894 (2016).

185 Sherr, C. J. & Roberts, J. M. Living with or without cyclins and cyclin-dependent kinases. *Genes Dev* 18, 2699-2711, doi:10.1101/gad.1256504 (2004).

186 Bracken, A. P. *et al.* EZH2 is downstream of the pRB-E2F pathway, essential for proliferation and amplified in cancer. *EMBO J* 22, 5323-5335, doi:10.1093/emboj/cdg542 (2003).

187 Lee, S. R. *et al.* Activation of EZH2 and SUZ12 Regulated by E2F1 Predicts the Disease Progression and Aggressive Characteristics of Bladder Cancer. *Clin Cancer Res* 21, 5391-5403, doi:10.1158/1078-0432.CCR-14-2680 (2015).

188 Du, L., Fakih, M. G., Rosen, S. T. & Chen, Y. SUMOylation of E2F1 Regulates Expression of EZH2. *Cancer Res* 80, 4212-4223, doi:10.1158/0008-5472.CAN-20-1259 (2020).

189 Kitagawa, M. *et al.* The consensus motif for phosphorylation by cyclin D1-Cdk4 is different from that for phosphorylation by cyclin A/E-Cdk2. *EMBO J* 15, 7060-7069 (1996).

190 Lundberg, A. S. & Weinberg, R. A. Functional inactivation of the retinoblastoma protein requires sequential modification by at least two distinct cyclin-cdk complexes. *Mol Cell Biol* 18, 753-761, doi:10.1128/MCB.18.2.753 (1998).

191 Wang, H. Y. *et al.* mGluR5 hypofunction is integral to glutamatergic dysregulation in schizophrenia. *Mol Psychiatry* 25, 750-760, doi:10.1038/s41380-018-0234-y (2020).

192 Reiner, A. & Levitz, J. Glutamatergic Signaling in the Central Nervous System: Ionotropic and Metabotropic Receptors in Concert. *Neuron* 98, 1080-1098, doi:10.1016/j.neuron.2018.05.018 (2018).

193 Compans, B. *et al.* NMDAR-dependent long-term depression is associated with increased short term plasticity through autophagy mediated loss of PSD-95. *Nat Commun* 12, 2849, doi:10.1038/s41467-021-23133-9 (2021).

194 Ferguson, H. J. *et al.* Glutamate dependent NMDA receptor 2D is a novel angiogenic tumour endothelial marker in colorectal cancer. *Oncotarget* 7, 20440-20454, doi:10.18632/oncotarget.7812 (2016).

195 Jiao, X. *et al.* Somatic mutations in the Notch, NF-KB, PIK3CA, and Hedgehog pathways in human breast cancers. *Genes Chromosomes Cancer* 51, 480-489, doi:10.1002/gcc.21935 (2012).

196 Liu, B. & Lu, K. Y. Neural invasion in pancreatic carcinoma. *Hepatobiliary Pancreat Dis Int* 1, 469-476 (2002).

197 Son, J. *et al.* Glutamine supports pancreatic cancer growth through a KRAS-regulated metabolic pathway. *Nature* 496, 101-105, doi:10.1038/nature12040 (2013).

198 Gelb, T. *et al.* Metabotropic glutamate receptor 1 acts as a dependence receptor creating a requirement for glutamate to sustain the viability and growth of human melanomas. *Oncogene* 34, 2711-2720, doi:10.1038/onc.2014.231 (2015).

199 Ripka, S. *et al.* Glutamate receptor GRIA3--target of CUX1 and mediator of tumor progression in pancreatic cancer. *Neoplasia* 12, 659-667, doi:10.1593/neo.10486 (2010).

200 Cousins, S. L., Papadakis, M., Rutter, A. R. & Stephenson, F. A. Differential interaction of NMDA receptor subtypes with the post-synaptic density-95 family of membrane associated guanylate kinase proteins. *J Neurochem* 104, 903-913, doi:10.1111/j.1471-4159.2007.05067.x (2008).

201 Robinson, H. P. C. & Li, L. Autocrine, paracrine and necrotic NMDA receptor signalling in mouse pancreatic neuroendocrine tumour cells. *Open Biol* 7, doi:10.1098/rsob.170221 (2017).

202 Lu, C. *et al.* Regulation of tumor angiogenesis by EZH2. *Cancer Cell* 18, 185-197, doi:10.1016/j.ccr.2010.06.016 (2010).

203 Sun, C. *et al.* EZH2 Expression is increased in BAP1-mutant renal clear cell carcinoma and is related to poor prognosis. *J Cancer* 9, 3787-3796, doi:10.7150/jca.26275 (2018).

204 Gan, L. *et al.* The polycomb group protein EZH2 induces epithelial-mesenchymal transition and pluripotent phenotype of gastric cancer cells by binding to PTEN promoter. *J Hematol Oncol* 11, 9, doi:10.1186/s13045-017-0547-3 (2018).

205 Bachmann, I. M. *et al.* EZH2 expression is associated with high proliferation rate and aggressive tumor subgroups in cutaneous melanoma and cancers of the endometrium, prostate, and breast. *J Clin Oncol* 24, 268-273, doi:10.1200/JCO.2005.01.5180 (2006).

206 Krill, L. *et al.* Overexpression of enhance of Zeste homolog 2 (EZH2) in endometrial carcinoma: An NRG Oncology/Gynecologic Oncology Group Study. *Gynecol Oncol* 156, 423-429, doi:10.1016/j.ygyno.2019.12.003 (2020).

207 Serrano, M. The tumor suppressor protein p16INK4a. *Exp Cell Res* 237, 7-13, doi:10.1006/excr.1997.3824 (1997).

208 Luo, Q. *et al.* ARID1A prevents squamous cell carcinoma initiation and chemoresistance by antagonizing pRb/E2F1/c-Myc-mediated cancer stemness. *Cell Death Differ* 27, 1981-1997, doi:10.1038/s41418-019-0475-6 (2020).

8.0 Acknowledgments

I have complicated emotions when I am writing these acknowledgment parts. Retrospecting the most memorable and happiest 3 years here in my past 36-year life, I am grateful to all people who have given me great help and support at Technische Universität München.

Firstly, I especially would like to thank my supervisor Prof. PD. Dr. med Ihsan Ekin Demir for the opportunity, scientific supervision, instruction, and support of this project, and the preparation of my dissertation. Prof. PD. Dr. med Ihsan Ekin Demir has a modest, amiable and noble personality, encyclopedic knowledge, and rigorous scientific attitude which benefit us tremendously. He also sets a perfect model to be a scientific researcher and surgeon for me. Without his brilliant and valuable ideas and patient guidance, I cannot finish this dissertation successfully. Many thanks to him from my depth heart.

Then, Many thanks to our postdoc, Dr. Rouzanna Istvánffy, who discussed the project, provided excellent ideas; Many thanks to our technician, Dr. Enkhtsetseg Munkhbaatar, Mrs. Altmayr Felicitas, for her intensive scientific and tireless technical assistance, which is crucial to keep the lab in perfect order.

Many thanks to Linhan Ye to go the airports to pick up me and share his living experiences here and accompany me to search for the apartment. I would like to appreciate Dr. Xiaobo Wang for teaching me research techniques. Many thanks to my

other colleagues including Dr. med Okan Safak, Dr. Sergey Tokalov, Dr. H. Erdinç Beşikcioğlu, Dr. Carmen Mota Reyes, Dr. Pavel Stupakov, for their generous supports during these years.

I would like to thank my domestic hospital for supporting and funding my studies and living here.

Finally, I would like to thank my beloved parents (Botang Ren and Cuiying Xu), my wife (Chunfeng Liu), and my son (Haorui Ren), who are my motivation source and the beacon of life. Especially my wife, who is devoted and exhausted herself to taking care of my family, encouraging and comforting me when I was missing in the scientific sea each time, and accompanying me to conquer each difficult moment. Many thanks for their continuous and endless spiritual support.

Many thanks to everybody here, thank you all.